

Master's thesis

NTNU
Norwegian University of Science and Technology

Furkan Kaya

Fabrication of conductive graphene thin films for opto-electronic use

Master's thesis in MTNANO

Supervisor: Solon Economopoulos

July 2020



Norwegian University of
Science and Technology

Furkan Kaya

Fabrication of conductive graphene thin films for opto-electronic use

Master's thesis in MTNANO
Supervisor: Solon Economopoulos
July 2020

Norwegian University of Science and Technology



Norwegian University of
Science and Technology

Dedicated to my parents

Preface

This thesis for the master's degree in Nanotechnology at NTNU was written in the Spring of 2020. Sadly, the Covid-19 virus pandemic hampered the scheduled work of this project. 44 work days were lost during the national lock-down. My diabetic condition also put me in the risk group and extra precaution had to be taken. Regardless, through perseverance and sheer hard work the bulk of the project was carried out in time.

I would like to express my gratitude towards my supervisor, Solon Economopoulos, for giving me the assignment. Nanotechnology is an interdisciplinary field and perhaps is it too complex for one single individual to comprehend all facets of it. However, we did our best by implementing both the chemistry, physics and even some computation. I would also like to thank the following people for helping me during this work; Yingda Yu for help on the SEM, Astrid Bjørkøy for help on the AFM, Sigmund Mordal Lucasen for providing me with an introduction to the sonicator, Surendra Kumar Yadav for help on the four-point probe, David Moe Almenning for manufacturing the Solar Cells and Maria Psarrou for giving me an introduction to the UV-Vis equipment.

I also want to send warm regards to my parents and my two sisters for encouragement during the work.

Table of Contents

Preface	iii
Table of Contents	vi
List of Tables	viii
List of Figures	xi
Abbreviations	xii
abstract	i
Sammendrag	i
1 Introduction	1
2 Graphene	3
2.1 Conductivity of graphene	4
2.2 Production of graphene	6
2.2.1 Graphene oxide and reduced graphene oxide	8
2.2.2 Graphene from exfoliation of graphite in solvents	9
2.2.3 Micromechanical exfoliation	14
2.2.4 Chemical Vapor Deposition (CVD)	14
2.2.5 Chemical synthesis	16
2.2.6 Epitaxial graphene	16
2.2.7 Pulsed Laser Deposition (PLD)	17
2.3 Hindrances preventing further commercialization of graphene	18
2.3.1 Narrowing of the gap to pristine graphene	19
2.3.2 Standardization of the production process	19
2.3.3 Problem of low fabrication rate	19
2.3.4 Financial feasibility of graphene-based products	20

3	Transparent Conducting Electrodes	21
3.1	The basics of Solar Cell	24
3.2	Dye-Sensitized Solar Cell (DSSC)	25
3.3	Light-emitting Diode (LED)	27
3.4	Liquid Crystal Display and Touch screens	30
4	Aim of thesis	33
5	Results and Discussion	35
5.1	Electrodeposition results	35
5.1.1	The role of electrolytes/salts	37
5.1.2	Solvent comparison	38
5.2	Doctor Blade, Drop Casting and Langmuir-Blodgett results	40
5.2.1	Doctor Blade	40
5.2.2	Drop Casting	40
5.2.3	Langmuir-Blodgett	41
5.3	Morphological characterization	43
5.3.1	Deposition on simple glass plates	43
5.3.2	Deposition on conductive glass plates	46
5.4	Implementation of the graphene thin films in a DSSC	53
5.5	The absorbance of the graphene thin films	55
6	Conclusion and Future Work	57
7	Experimental section	59
7.1	Chemicals and Materials	59
7.2	Production of exfoliated graphene	59
7.3	Methods used to fabricate the films	60
7.3.1	Electrodeposition experimental procedure	60
7.3.2	Langmuir-Blodgett experimental procedure	60
7.3.3	Drop Casting experimental procedure	60
7.3.4	Doctor Blade experimental procedure	60
7.4	Characterization Methods	60
7.5	Fabrication of the Solar Cell	61
8	Appendix	73
8.1	Multimeter measurements of the Electrodeposition samples	73
8.2	The failure of the Spin Coating method	74
8.3	Doctor Blade parameters and samples	75
8.4	Absorbance of other samples	76
8.5	SEM image of bare FTO	77
8.6	50000x magnification SEM images	78

List of Tables

2.1	Table shows different production methods of graphene with classification	7
2.2	Table of organic solvents used to exfoliate graphite[52, 58, 59, 60]	12
5.1	Table shows the sheet resistance, resistivity and conductivity of the 5 FTO samples coated with graphene and P16ED (a simple glass plate coated with graphene by the use of Electrodeposition) and a reference glass plate.	36
5.2	Table of samples and the parameters applied in producing the film on the samples. Columns represent amount of graphene and NMP in ml, TBAPF ₆ and NMP mixture in molarity and amount in ml and voltage applied.	38
5.3	Table of the samples chosen out from table 6.4 and their conductivity	40
5.4	Table of the current measurements obtained on graphene films on simple glass deposited with the Drop Casting method	41
5.5	Table shows the parameters used in the G30 Langmuir-Blodgett experiment and the values of resistance obtained. The R in the names of the materials stands for resistance.	41
5.6	Table shows the parameters used in the G60 Langmuir-Blodgett experiment and the values of resistance obtained. The R in the names of the materials stands for resistance.	42
5.7	Table shows the different values obtained for the different parameters when the DSSC was tested with a graphene counter electrode and a Pt counter electrode.	55
8.1	Table of the measured conductivity with a multimeter.	73
8.2	Shows the parameters for SCP1	74
8.3	Shows the parameters for SCP2	75
8.4	Shows the parameters used in SCP3	75

List of Figures

2.1	Schematic of the Honeycomb lattice of graphene[9]	3
2.2	a) Shows the honeycomb lattice with the vectors δ_1 , δ_2 and δ_3 connecting the nn carbon atoms, separated by a distance $a = 0.142$ nm. Vectors a_1 and a_2 are the basis vectors of the triangular Bravais lattice and b) Shows the reciprocal lattice[7].	5
2.3	Illustration of the process of graphene transferred to a glass substrate and becoming a conductive film.	7
2.4	Image of the bottom-up and top-down approaches in synthesis of carbon based nanomaterials[44].	8
2.5	Schematic of an AFM image (a)[2] and structural model (b)[49] of graphene oxide sheets.	9
2.6	Schematic diagram of the process of graphite to exfoliated graphene with the use of the solvent NMP[55]	10
2.7	Schematic representation of the liquid-phase exfoliation process of graphite in the absence (top-right) and presence (bottom-right) of surfactant/intercalator molecules[54].	11
2.8	Concentration of graphene in NMP after centrifugation as a function of sonication time[57].	11
2.9	Schematic diagram of production of graphene in LPE[42].	13
2.10	Schematic of the working procedure of micromechanical exfoliation process[63]. The process is also known as micromechanical cleavage.	14
2.11	Schematic diagram of Thermal CVD a) and Plasma Assisted CVD b) process: case of graphene from CH_4/H_2 mixtures[71].	15
2.12	Schematic of the solvothermal reaction followed by a pyrolysis resulting in graphene[79].	16
2.13	Schematic depiction of the formation process of epitaxial graphene via sublimation of Si from the SiC surface[83].	17
2.14	Schematic diagram of PLD process[90].	18

3.1	Schematic illustration of three types of general organic photovoltaic (OPV) and organic light-emitting diode (OLED) device architectures: (a) superstrate type OPV and bottom-emitting OLED, where light transfers into or out of the device through bottom substrates and transparent electrodes; (b) substrate type OPV and top-emitting OLED, where light travels through top transparent electrodes (TE); and (c) transparent OPV and OLED, where light travels through both bottom and top transparent electrodes[120]. RE is an abbreviation for reflective electrode.	21
3.2	Transmission (T) and reflection (R) spectra of FTO with different F-doping concentration. The crossover between the T and R curves shows the position of the plasma wavelength which shifts towards the visible range with increasing F-doping[122].	22
3.3	Metal grid/graphene hybrid transparent electrode. The yellow lines in the figure represent the metal grid. The grid size and gridline width in the figure are only illustrative and are not scaled with the graphene molecular structure[134].	23
3.4	Schematic of an J-V plot[142]. The plot exponentially growing represents the diode equation. Blue box is the fill factor (FF).	25
3.5	Schematic shows the construction and working principle of a DSSC[143].	26
3.6	Schematic diagram of how a real DSSC deviates from ideality. Figure provided at the courtesy of David A. Moe	27
3.7	The LED materials and range of wavelength of the emission associated with them[149]. The color band indicates the visible region of the spectrum.	28
3.8	Schematic representation of a LED where ITO replaces the ohmic metal contact[149].	29
3.9	Schematic diagram of RGO based LED illumination on the left[152]. When a suitable bias voltage (V) is applied, luminescent spots appear on the device. On the right, a schematic of a graphene bulb.	29
3.10	Image of the 4-pentyl-4'-cyanobiphenyl molecule widely used in LCD[155].	30
3.11	Schematic shows the build of tablets and smartphones. All smartphones and tablets use some form of “decorated covering” (rows 1 and 2) to protect the LCD (rows 6 to 11) from damage. When a projected capacitive touchscreen is added, most commonly, the electrodes are located on a fourth piece of glass (rows 3 to 5). In the figure TFT is an abbreviation for thin film transistor[163]	31
5.1	Box and whisker plot of the conductivity distribution of the samples. Top and bottom of the box indicate 75th and 25th percentile, respectively. The line in the box indicates media. Vertical line above and below the box extend to high and low values.	36
5.2	Schematic of the plots for the different electrolyte concentration when + 20 V Voltage was the input and all had the deposition time of one hour	37
5.3	Plot of the difference in conductivity between 13 ml solution of Benzylamine + NMP + salt (red) and 9 ml of the same solution (blue).	39

5.4	Image of the images taken with a SEM of the film obtained with the Doctor Blade method. The image on the upper left shows the 22x magnification, upper right shows the 1000x magnification, down left shows the 5000x magnification and down right shows the 10000x magnification	43
5.5	AFM image of the Doctor Blade sample	44
5.6	Image of the characterization done with the SEM tool on the films obtained by using the Drop Casting method. The upper left side shows the 100x magnification, the upper right side shows the 1000x magnification. While the two lower rows show the 5000x and 10000x magnifications respectively	44
5.7	AFM image of the films obtained with the Drop Casting method. Both images show a film thickness of 0.25 μm . A aggregation of graphene layers can also be seen.	45
5.8	Shows the SEM images of sample P13ED at the magnifications 200x (upper left), 500x (upper right), 1000x (down left) and 2000x (down right)	46
5.9	Shows the SEM images of sample P14ED at the magnifications 500x, 1000x, 2000x and 10000x	47
5.10	Image shows (a) P13ED with 70x magnification and (b) P14ED with 70x magnification	48
5.11	SEM image of two different areas on the P18ED sample with the 100x magnification	48
5.12	Recording of SEM images of the P18ED sample at the area denoted as area (I)	49
5.13	Recording of SEM images of the P18ED sample at the area denoted as area (II)	49
5.14	Recording of two SEM images of the surface of the P22ED taken with the 70x and 200x magnifications	50
5.15	SEM recordings of four images of the P22ED sample. They show two different areas on the surface at two magnifications, 500x and 1000x. The upper image is 500x and the image immediately below it, represents the 1000x magnification	51
5.16	Recordings of the AFM of (a) P22ED and (b) P13ED	51
5.17	Four SEM images of a sample where negative current was applied. Upper left is 100x magnification, the upper right is 500x, the down left is 1000x and the down right is 5000x	52
5.18	The J-V plot for the DSSC with graphene used as a counter-electrode	53
5.19	Plot of the EQE vs wavelength for the DSSC.	54
5.20	Plot of the absorbance spectrum for the P13ED sample.	56
8.1	Plot of the absorbance spectrum for the P14ED sample.	76
8.2	Plot of the absorbance spectrum for the P22ED sample	77
8.3	SEM image of a bare FTO glass plate[185].	77
8.4	Image of the 50000x magnification of Drop Casting film	78
8.5	Image of the 50000x magnification of the sample on figure 5.17	78

Abbreviations

AFM	=	Atomic Force Microscopy
CH ₄	=	Methane
CNT	=	Carbon Nanotubes
CVD	=	Chemical Vapor Deposition
DMF	=	Dimethylformamide
DMSO	=	Dimethyl sulfoxide
DSSC	=	Dye-Sensitized Solar Cell
FTO	=	Flourine-doped Tin Oxide
F:SnO ₂	=	Flourine-doped Tin Oxide
GO	=	Graphene oxide
HI-AcOH	=	Hydriodic acid with acetic acid
LCD	=	Liquid Crystal Device
LED	=	Light-Emitting Diode
LPE	=	Liquid-phase exfoliation
NMP	=	N-methyl-2-pyrrolidone
ODCB	=	1,2-Dichlorobenzene
OPV	=	Organic Photovoltaics
PLD	=	Pulsed Laser Deposition
QED	=	Quantum Electrodynamics
QHE	=	Quantum Hall Effect
RGO	=	Reduced graphene oxide
RPM	=	Revolutions per minute
SiC	=	Silicon Carbide
SGP	=	Simple Glass Plate
SEM	=	Scanning Electron Microscope
TCE	=	Transparent Conducting Electrodes
TCO	=	Transparent Conducting Oxide
UHV	=	Ultra-High Vacuum

Abstract

A method of depositing graphene thin films on conductive and non-conductive glass substrates is presented. A comprehensive study of several deposition methods was carried out including Spin Coating, Doctor Blading, Electrodeposition, Drop Casting and Layer-by-Layer (Langmuir-Blodgett). The resulting films were extensively characterized morphologically, using AFM and SEM, as well as towards their electrical conductivity using Four-point probe. The Electrodeposition proved to be the most efficient method for depositing graphene on conductive glass plates. With this method single layers of graphene form at nucleation sites at the grain boundaries of the FTO glass plate. The growth then follows this pattern if there is enough conductivity applied. The characterization showed an increase of conductivity over pristine FTO. Absorption measurements using UV-Vis Spectrophotometer showed excellent transparency for the deposited films, in accordance to literature values. The graphene thin films were tried as a catalyst, replacing the more expensive Pt, in a counter electrode of a DSSC with limited success. The other methods to deposit graphene thin films proved to be not options, with the small exception of the Langmuir-Blodgett method.

Sammendrag

En metode for å lage tynnfilmer av grafen deponert på konduktive og ikke-konduktive glass substrater blir presentert her. En omfattende studie av flere deponeringsmetoder som Spin Coating, Doctor Blading, Elektrodeponering, Drop Casting og Langmuir-Blodgett ble utført. Filmene produsert ble karakterisert morfologisk med AFM og SEM, samt at deres elektriske konduktivitet ble målt ved bruk av en Fire-punkts probe. Elektrodeponering viste seg å være den mest effektive metoden for deponering av grafen på konduktive glass plater. Med denne metoden dannet enkeltlag av grafen seg ved nukleasjonsplasser langs korngrensene på FTO glass platene. Veksten til filmene følger så dette mønsteret om nok konduktivitet blir anvendt. Karakteriseringen viste en økning av konduktivitet i forhold til pristine FTO. Absorpsjonmålinger ved bruk av UV-Vis Spectrophotometer viste utmerket gjennomsiktighet for de deponerte filmer, og med verdier sammenlignbart med kjente litteraturverdier. Grafen tynnfilmene ble brukt som katalyst, for å erstatte det langt dytere Pt, som en motelektrode i en DSSC med begrenset suksess. De andre metoder for å deponere grafen tynnfilmer viste seg å ikke fungere, med et unntak for Langmuir-Blodgett metoden.

Introduction

Much interest has been dedicated to the allotrope of carbon called graphene in recent years. Graphene was first isolated in 2004 by Geim and Novoselov. Since 2004, the number of graphene-related academic publications has increased exponentially[1]. While the material is known to have remarkable properties, there are still some problems associated with it that prevents its widespread use. Some of the questions, such as the production methods[2], are well known and widely discussed in the scientific community. The question posed in this project is of equal importance but is a less prominent feature in the above-mentioned discussions.

With the previous paragraph functioning as an impetus, the aim of the work done in this project is to present a method of fabrication of conductive graphene thin film for optoelectronic applications. The graphene films were deposited through five different methods: Spin Coating, Doctor Blade, Drop Casting, Electrodeposition and the Langmuir-Blodgett method. The films were then characterized by a wide array of instruments. The scope of the characterization was meant to target vital aspects of graphene thin films deposition like conductivity, morphology and absorbance.

The best way to quantify the quality of the produced films is perhaps to utilize the films in an actual device. With that in mind, it was decided to use the graphene thin films in a Dye-Sensitized Solar Cell (DSSC), as one of the available in-house optoelectronic application. In the device the films were opted to be used to replace Pt as the catalyst in the counter electrode.

The structure of the thesis follows the format of presenting. Graphene, its properties and the methods to produce it chapter 2. Chapter 3 deals with the prominent target application of this project as Transparent conducting electrodes. Chapter 4 includes the results and discussion from the project followed by a conclusion and then an experimental section. In the experimental section, the entire procedure from producing the graphene to deposition of film precursors to post-production processes is presented.

Chapter 2

Graphene

Graphene is in many ways an extraordinary material with properties not seen in other materials[3]. Until graphene was successfully isolated, it was widely believed that an extended sheet of graphene would be unable to withstand the effects of thermal fluctuations[4]. Furthermore, it was thought that even if the sheet were stable they would be impossible to isolate[5]. Andre Geim and Konstantin Novoselov proved in 2004 these beliefs were false[6]. The team used a technique called micromechanical cleavage to extract a monolayer of atoms[2]. In layman terms, they managed to isolate a single layer of graphene on silicon oxide substrate by peeling the graphite by scotch tape. Graphite is a common allotrope of carbon and it consists of sp^2 hybridized layers of carbon which are stacked together and held in that "formation" by van der Waals forces. These single layers of carbon were the graphene layers Geim *et al.* were interested in[7]. They are pulled together into a 2D honeycomb lattice[7] arranged in a hexagonal pattern with a carbon to carbon bond distance of 0.142 nm. The single layer of graphene is comparable to a polycyclic aromatic hydrocarbon of quasi-infinite size[8].

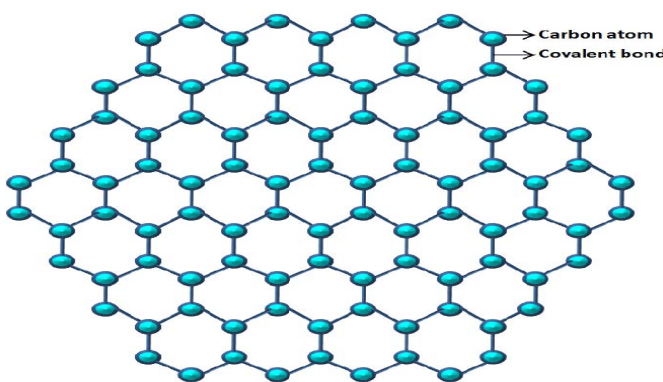


Figure 2.1: Schematic of the Honeycomb lattice of graphene[9]

Landau[10] and Peierls[11] argued that strictly 2D crystals could not exist. For over 7 decades this belief was predominant in the scientific world. The Mermin-Wagner theorem formalized this thought and the theorem stated that there should be no long-range order in 2D[12]. Meaning that dislocations would appear in 2D crystals and therefore would make crystalline materials into non-crystalline. Mermin's hypothesis was supported by a whole omnibus of experimental observations[5]. Katsnelson explains how Geim *et al.* managed to get past this conundrum posed by the Mermin-Wagner theorem[4]. This was done by describing thermodynamics of solids by using a picture of an ideal gas of phonons[13]. In 2D crystals, the number of wavelength diverges at low temperatures. This is important for graphene because it has been demonstrated theoretically divergent long-wavelength fluctuations can be suppressed by nonlinear coupling between bending and stretching modes[14, 15]. This important aspect makes single-crystalline membranes possible, but they should be "rippled"[4]. In order to clarify the meaning of an important term, the definition of a rippled graphene sheet is a sheet that is not flat[16].

The upsurge in interest in graphene can be contributed to two factors: the properties of the material[7] and its potential as a possible replacement for more expensive and less abundant materials[17]. Graphene is interesting property-wise because the one-atom-thick fabric of carbon uniquely combines extreme mechanical strength, exceptionally high electronic and thermal conductivities, as well as impermeability to gases[3] and ambipolar field effect[18]. In addition to this, some research has shown that decoupled monolayer and bilayer exhibit Landau quantization of massless and massive Dirac fermions respectively[19]. The single layer of graphene absorbs only 2.3 percent of incident light[18], and can therefore be considered almost fully transparent. Furthermore, some reports suggest a very high carrier mobility at over $15000 \text{ cm}^2/\text{Vs}$ at ambient conditions[20]. The by now famous Quantum Hall Effect (QHE) can in graphene be seen at room temperature[21]. This is because the temperature range for QHE for graphene is 10 times broader than that of other 2D materials[18].

2.1 Conductivity of graphene

The highly interesting properties of graphene makes it stand out among other common metals and semiconductors[18]. They are the reason why more focus has been put on graphene compared to other 2D materials[22]. Structure-wise, graphene is made out of carbon atoms in hexagonal structure as shown in Figure 2.2[7]. Although not a Bravais lattice[13], it can be seen as a triangular lattice with a basis of two atoms per cell[23]. Because A and B are not equivalent, it is impossible to denote the structure as a Bravais lattice. The lattice vectors can be written as:

$$a_1 = \frac{a}{2}(3, \sqrt{3}), \quad a_2 = \frac{a}{2}(3, -\sqrt{3}) \quad (2.1)$$

where $a = 0.142 \text{ nm}$ is the carbon-carbon distance. The reciprocal lattice vectors are given by the relations:

$$b_1 = \frac{2\pi}{2a}(1, \sqrt{3}), \quad b_2 = \frac{2\pi}{3a}(1, -\sqrt{3}) \quad (2.2)$$

The corresponding Brillouin Zone, with the two corners K and K', is therefore written as:

$$K = \left(\frac{2\pi}{3a}, \frac{2\pi}{3\sqrt{3}a} \right), K' = \left(\frac{2\pi}{3a}, -\frac{2\pi}{3\sqrt{3}a} \right) \quad (2.3)$$

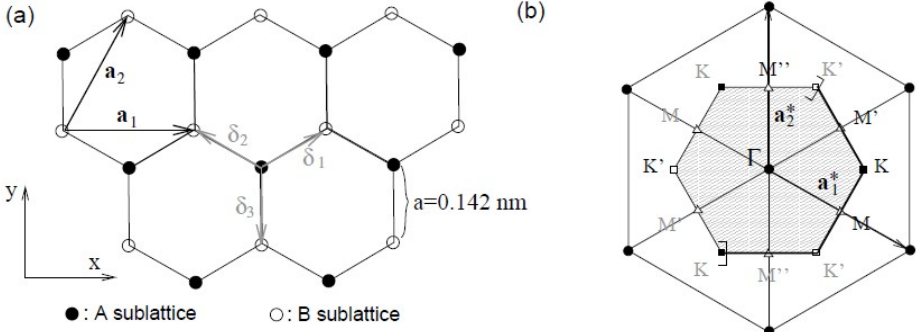


Figure 2.2: a) Shows the honeycomb lattice with the vectors δ_1 , δ_2 and δ_3 connecting the nn carbon atoms, separated by a distance $a = 0.142 \text{ nm}$. Vectors \mathbf{a}_1 and \mathbf{a}_2 are the basis vectors of the triangular Bravais lattice and b) Shows the reciprocal lattice[7].

The nearest neighbor vectors are given by:

$$\delta_1 = \frac{a}{2}(1, \sqrt{3}), \delta_2 = \frac{a}{2}(1, -\sqrt{3}), \delta_3 = -a(1, 0) \quad (2.4)$$

By finding the vectors \mathbf{a}_i and δ_i , it is possible to use the tight-bonding approximation[23, 7] to find the energy band of graphene. This is done by only considering the nearest neighbor interactions[7, 23, 24]. The energy bands derived from the tight-binding approach on the Hamiltonian for graphene are given as[7, 24, 25]:

$$E_{\pm} = \pm t \sqrt{1 + 4 \cos\left(\frac{3}{2}k_x a\right) \cos\left(\frac{3}{2}k_y a\right) + 4 \cos^2\left(\frac{\sqrt{3}}{2}k_y a\right)} \quad (2.5)$$

where the plus sign applies to the upper (conduction) and the minus sign the lower (valence) band.

The effective Hamiltonian around K' and K is made of two copies of the massless Dirac-like Hamiltonian, one holding for p around K and other for p around K'[7]. Geim *et al.* point out that in the first quantized formalism, the two-component electron wavefunction, $\psi(r)$, close to the K-point obeys the 2D Dirac equation given by:

$$-iv_F \sigma * \nabla \psi(r) = E \psi(r) \quad (2.6)$$

It is therefore inferred that electrons in graphene obey a linear dispersion relation[26]. This means that as electrons propagate through the lattice of graphene, they effectively

lose their mass, producing quasi-particles that are described by a 2D analogue of equation (2.6) instead of the Schrodinger's equation. This results in several consequences of notice: an anomalous QHE, absence of localization and a bridge between condensed matter physics and QED[4]. But perhaps the most important feature of the Dirac spectrum is that it can be used to explain the existence of anti-particles[27].

The states at positive and negative energies (representing electron and positron) are conjugated, implying that they are described by different components of the spinor wavefunction. This is known as the charge-conjugation symmetry[28]. Katsnelson writes that when it comes to Dirac particles with mass m , there is a gap between minimal electron energy given by: $E_0 = mc^2$ and maximal positron energy given by $-E_0$ [4]. At limits when the electron energy $E \gg E_0$, the energy becomes linearly dependent on the wavevector k , meaning that $E = c\hbar k$. When there is no mass Dirac fermions, the gap is zero[29]. Charge carriers in graphene can be described by the Dirac equation rather than Schrodinger's equation because of the material's crystal structure. Quantum mechanical hopping between the two sublattices leads to the formation of two energy bands. Their interaction near the edges of the BZ yields the conical energy spectrum[4]. This rather than the parabolic energy spectrum seen for metals and other materials[30].

Graphene's electrical conductivity is known to decrease when the number of layers and interlayer hopping increase[31]. The thermal conductivity of single-layer graphene wildly outperforms competitors like carbon nanotubes[32]. Min Tian *et al.* fabricated a graphene nanoplatelets-based temperature sensor[33]. They found a non-linear variation resistance. The sheet resistance of single-layer graphene has been found to be 30-35 Ohm/square[34] and under 50 Ohm/square[35]. It has been observed that suspended graphene sheets that are not perfectly flat show ripples. These ripples generate band gaps in graphene by developing spatially varying potential or effective magnetic fields[16, 36] Generally, the value of the energy band gaps increases as the height of the ripples increase, while it decreases as the range of ripples enlarge. A rippled graphene therefore can be a good semiconductor depending on the size of the band gap. The perhaps most remarkable property found in graphene, however, is the ambipolar electric field effect in single layer graphene[18, 37]. The term ambipolar means that the charge carriers (with mobilities, μ , at over 15000 cm²/Vs at ambient condition) can be continually switched between electrons and holes. This at concentrations, n , over 10^{13} cm⁻².

2.2 Production of graphene

The once elusive graphene single layer that nobody could isolate with any method, can be produced today via several methods with good quality[38]. An illustration of the process of graphene transferred to a glass substrate and becoming a conductive film can be seen in figure 2.3.

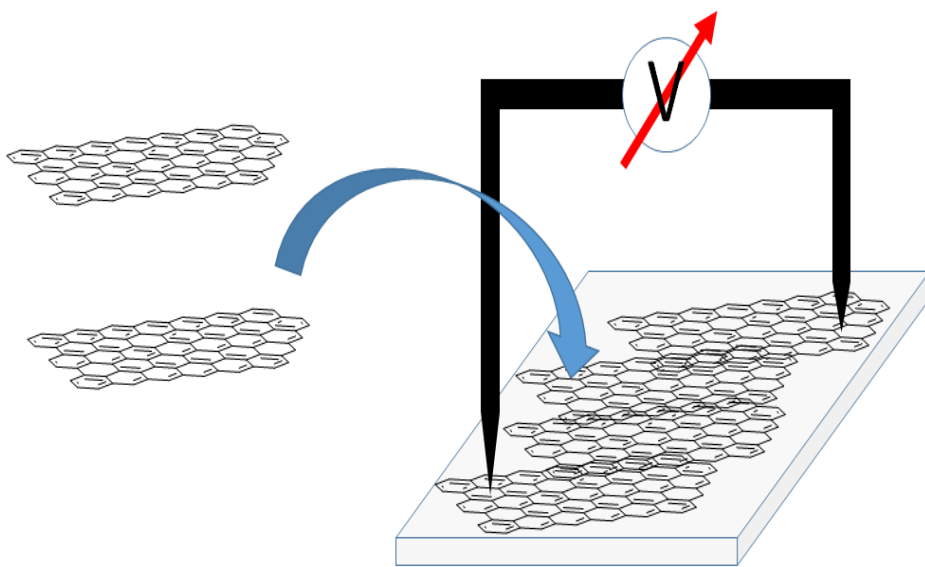


Figure 2.3: Illustration of the process of graphene transferred to a glass substrate and becoming a conductive film.

The methods vary in working principle and mechanism, but because the material produced is a nanomaterial[39], they are divided in two groups: Top-down approach and bottom-up approach[40]. Bottom-up approach[41], also known as self-assembly, is the process where basic units at the nanoscale assemble into larger structures. In the top-down[41] approach the process start at a larger structure and the structure during the process becomes smaller. The production methods presented in this section are classified according to table 2.1

Top-down	Bottom-up
Reduced graphene oxide	Chemical Vapor Deposition
Exfoliated graphite via solvent	Chemical synthesis
Micromechanical exfoliation	Epitaxial graphene
	Pulsed Laser Deposition

Table 2.1: Table shows different production methods of graphene with classification

Fabrication methodology of graphene has to take into account several factors. The methodology has to consider the desire for producing a material in high-quality, high yield, defect-free and cost-effectively[42]. While in some instances and applications the bottom-up method is preferable, in others the ability to scale up leads to liquid exfoliation as the production method of choice[43].

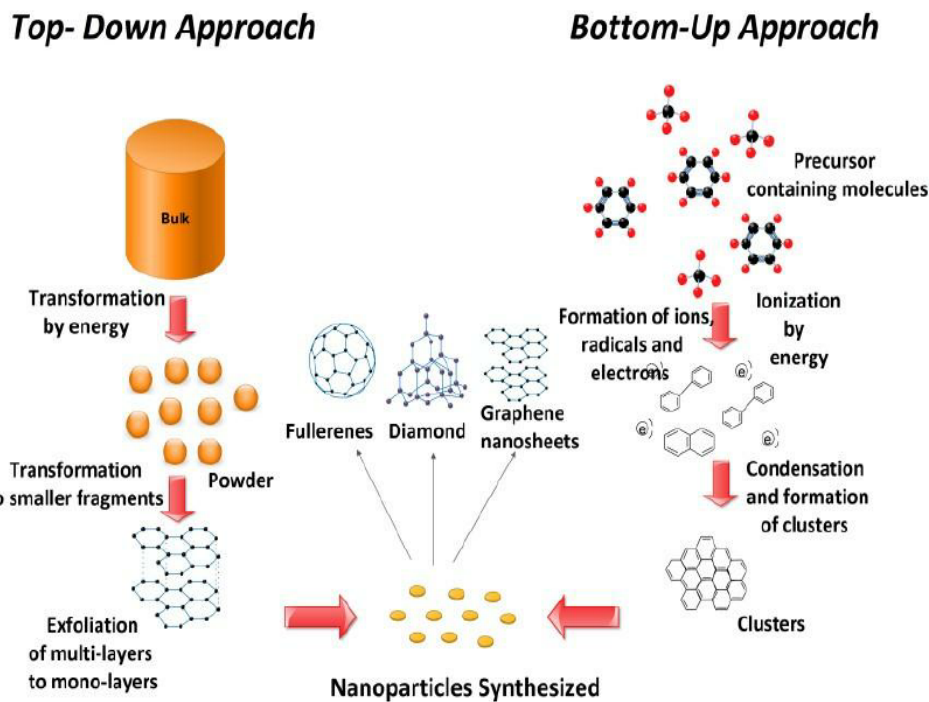


Figure 2.4: Image of the bottom-up and top-down approaches in synthesis of carbon based nanomaterials[44].

2.2.1 Graphene oxide and reduced graphene oxide

After pristine graphene first was isolated, it was concluded that the method developed by Hummers and Offeman[45] was capable of producing exfoliated oxidized single graphene layers by the dispersion of graphite oxide in water[2]. The monolayers of GO (referencing figure 2.5) are precursors for the production of graphene by the removal of the oxygen group[2]. Until 2010, the most widely used reducing agent was hydrazine hydrate[46, 47]. That year Ruoff *et al.* reported of the synthesis of high-quality RGO by the use of a new reducing agent, HI-AcOH[47]. Since then, several reducing agents have been applied, but none have achieved full reduction of the GO monolayers into graphene[2]. Boukhvalov and Katsnelson did a modelling of this particular posed question, and it was concluded by their work that a reduction of GO from 75 percent to 6.25 percent was easy to do, but further reduction was seemingly a much harder task[48].

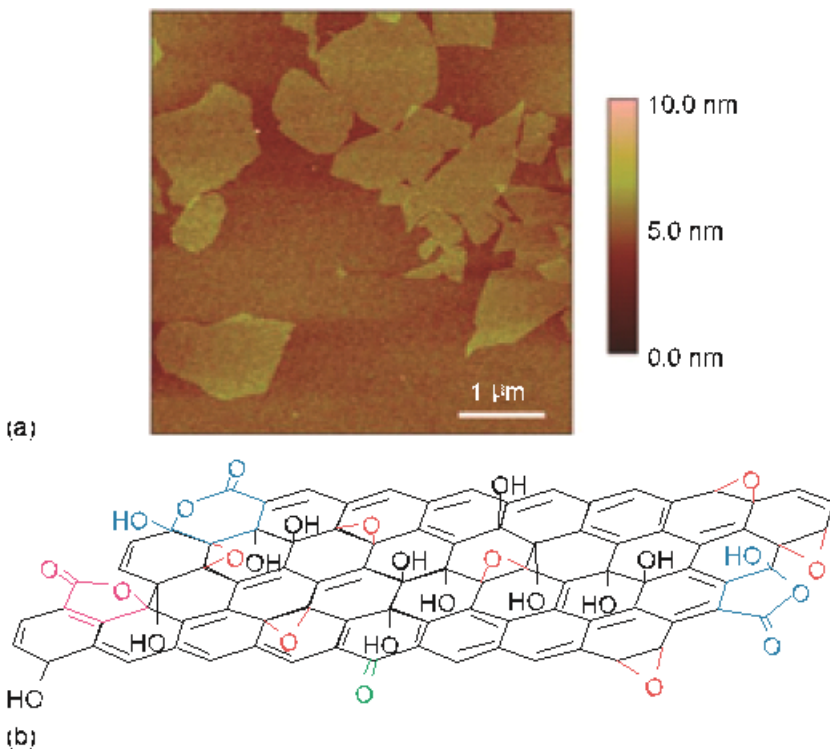


Figure 2.5: Schematic of an AFM image (a)[2] and structural model (b)[49] of graphene oxide sheets.

Furthermore, in research done by Hidayah *et al.*[50], graphite, GO and RGO were compared and were shown to have different morphologies, quality, functional groups, absorption peaks and crystallinity. This is important because it indicates different properties associated with the respective compounds[39, 51]. The GO was prepared by using Hummer's method, and the produced GO was chemically reduced to RGO by the use of hydrazine hydrate.

2.2.2 Graphene from exfoliation of graphite in solvents

This section concerns a process formally known as Liquid-Phase Exfoliation, abbreviated as LPE. Of the top-down methods, reduction of graphene oxide is perhaps the most widely used[52]. However, doughty chemical oxidation associated with it severely damages electronic structure of graphene[52], thereby making the case for LPE as an attractive alternative top-down method. LPE makes it possible to obtain a stable dispersion of single layer graphene or few-layered graphene. The process has few process steps with the method only involving the exfoliation of natural graphite via sonication[52]. Graphite consists of stacked graphene layers in vertical direction[53]. Where the stacked layers are held together by van der Waals forces[54]. By immersing the graphite in a suitable liquid the

strength of the van der Waal forces can be reduced and overcome. This makes it possible to apply sonication to prepare graphene[52]. This is illustrated in figure 2.6 where NMP is used as solvent.

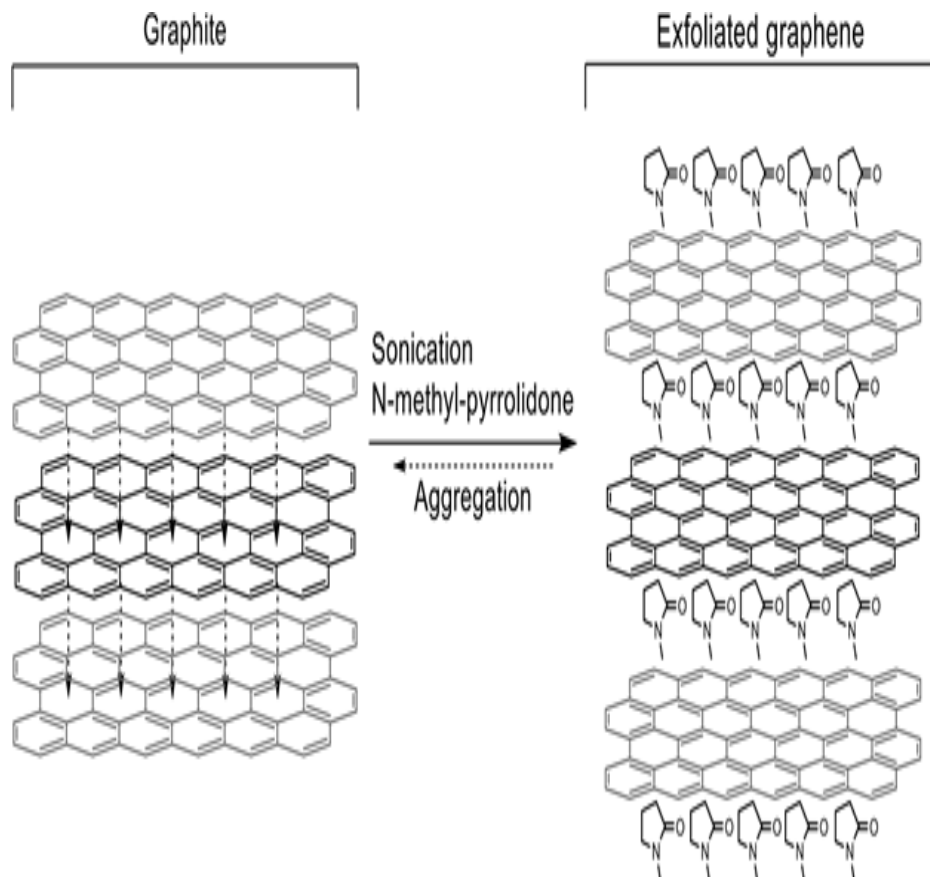


Figure 2.6: Schematic diagram of the process of graphite to exfoliated graphene with the use of the solvent NMP[55]

Although LPE is a straightforward procedure with high potential for the mass production of graphene[52], large-scale application of sonication-assisted LPE is still some steps away because of the low concentration of graphene and the high energy consumption during the production process. Exfoliated graphene can also be suspended in surfactants. The benefit of this method is using the surface tension of these solvents to make graphite to split in thinner platelets[53], as seen on figure 2.7.

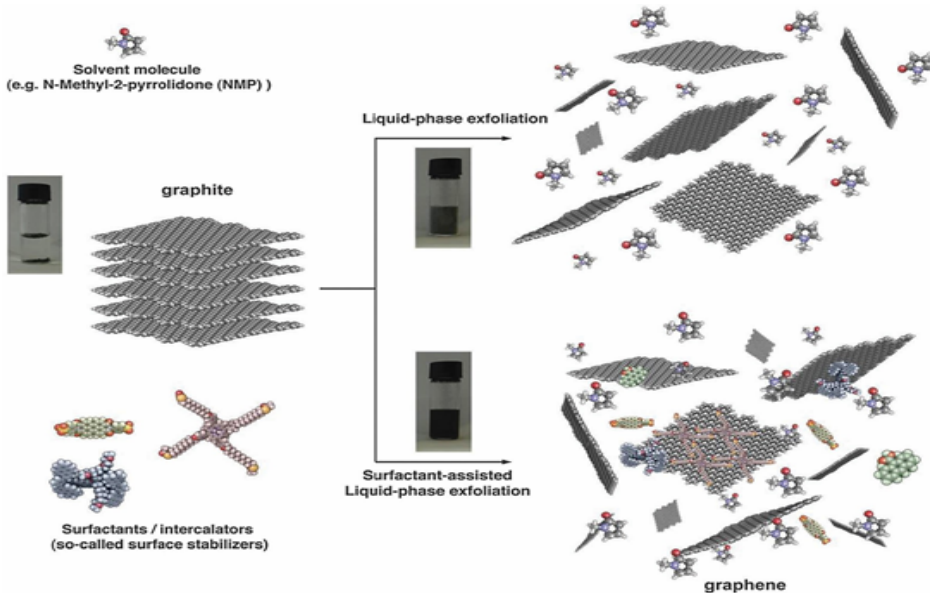


Figure 2.7: Schematic representation of the liquid-phase exfoliation process of graphite in the absence (top-right) and presence (bottom-right) of surfactant/intercalator molecules[54].

Some work has been done on increasing the concentration of graphene. Bhoria *et al.* addressed the problem of low concentration of graphene (<0.01 mg/ml) obtained by LPE by employing various techniques for enhancing the graphene concentration in organic solvents[56]. Specifically, it was found that by adding anthracene in NMP solvent, graphene concentration increased up to 0.04 mg/ml.

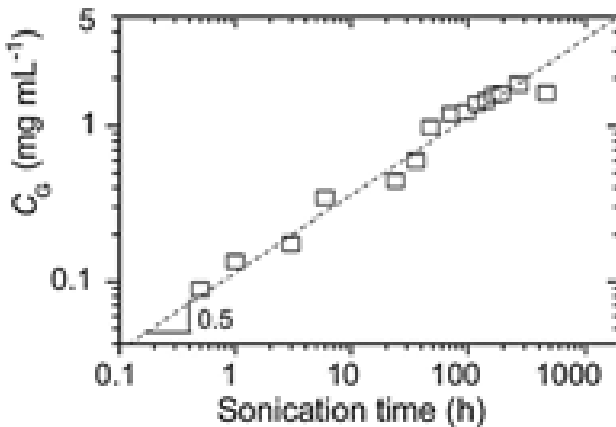


Figure 2.8: Concentration of graphene in NMP after centrifugation as a function of sonication time[57].

Coleman *et al.* demonstrated a method to prepare graphene dispersion of high concentrations up to 1.2 mg/ml, with yields up to 4 wt% monolayers[57]. The process relies on low-power sonication for durations of up to 460 hours (Figure 2.8). Coleman *et al.* tried other parameters as well, and found that the graphene flakes centrifuged at 3000 RPM were much smaller than those centrifuged at 500 RPM[54, 57]. The main use for centrifugation is to remove the large, unexfoliated and unstable dispersed graphite particles or aggregates[52], but as shown by Coleman *et al.*'s work it can also be used to create graphene flakes more suited to particular tasks.

When choosing a solvent, the most important factor to consider is the surface tension of the solvent[54]. The surface energy of graphite must be in close proximity to the surface tension of the solvent. This in order to minimize the interfacial tension between graphite and solvent. For graphite, the solvent must have a surface tension at around 40-50 mJ/m⁻². A list of solvents appropriate for LPE of graphite can be found in table 2.2.

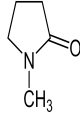
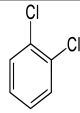
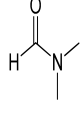
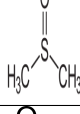
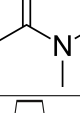
Organic Solvents	Surface Tension (mJ/m ⁻²)	Boiling Point (°C)	Chemical Structure	Concentration (mg/ml)
NMP	40	203		1
Benzylamine	38.8	185		0.5
ODCB	37	181		0.03
DMF	37.1	154		0.0045
DMSO	42.9	189		0.0041
DMAC	36.7	165		0.01
γ-butyrolactone	46.5	204		0.01

Table 2.2: Table of organic solvents used to exfoliate graphite[52, 58, 59, 60]

As is common in the scientific world, several research teams have attempted to establish new procedures for the production of graphene with a basis in LPE. Perhaps the most impressive of those was done by Ayela *et al*[61]. Ayela *et al.* presented in 2018 LPE of graphite into graphene nanosheets in a hydrocavitating "lab-on-a-chip". Characterization showed the presence of monolayer graphene with a lateral size around 300 nm. Other LPE-related research progress in recent years worth mentioning is the breakthrough Hamaker constant theory in exfoliation and the equally innovative Hansen solubility coefficient theory in stable dispersion mechanism[62].

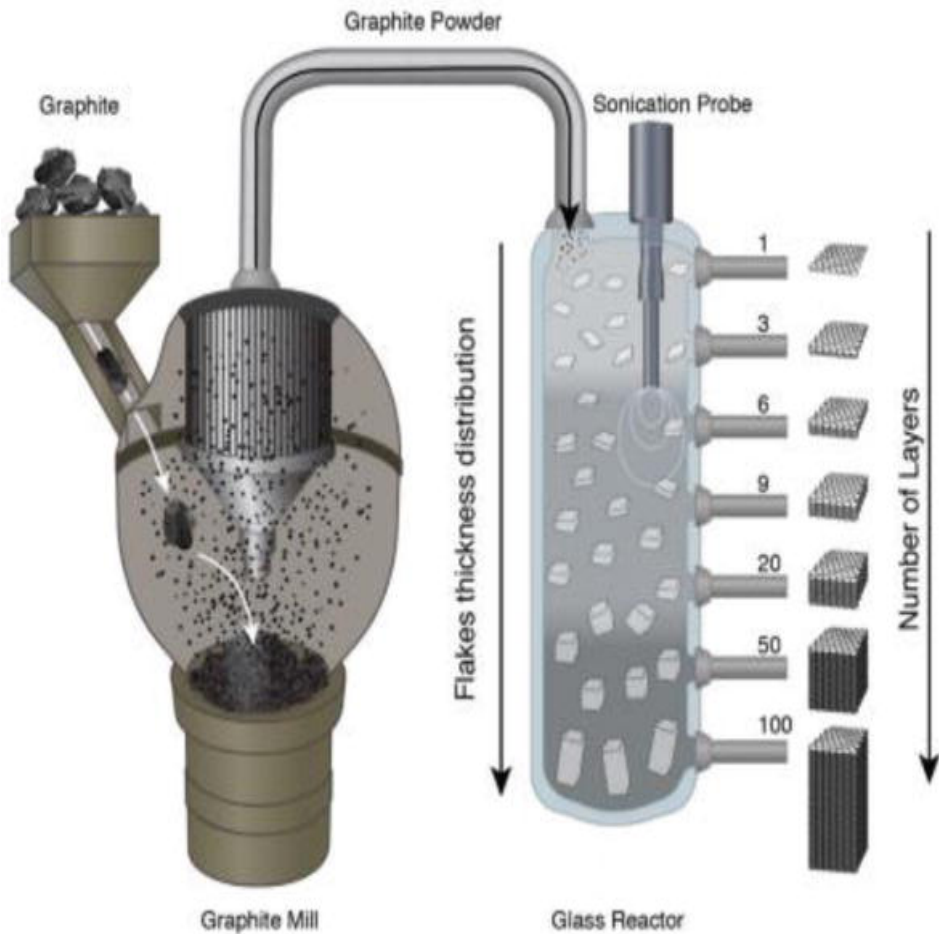


Figure 2.9: Schematic diagram of production of graphene in LPE[42].

Figure 2.9 is a schematic diagram of production of graphene in LPE. The entire process from the processing of natural graphite in a graphite mill to graphite powder to layers of

graphene produced by LPE is illustrated. An important aspect of the figure worth noticing is the number of layers and their vertical position in the glass reactor.

2.2.3 Micromechanical exfoliation

Micromechanical exfoliation was the first method that successfully managed to isolate a single layer of graphene[4]. The method involves repeated peeling of ordered pyrolytic graphite with the use of adhesive tape[42] (Figure 2.10).

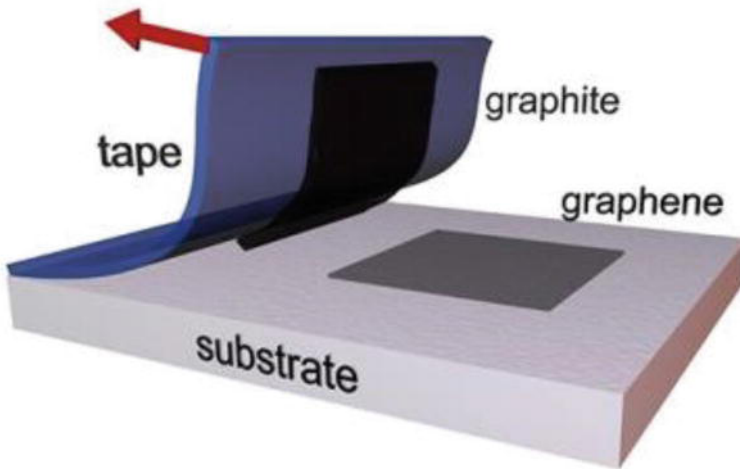


Figure 2.10: Schematic of the working procedure of micromechanical exfoliation process[63]. The process is also known as micromechanical cleavage.

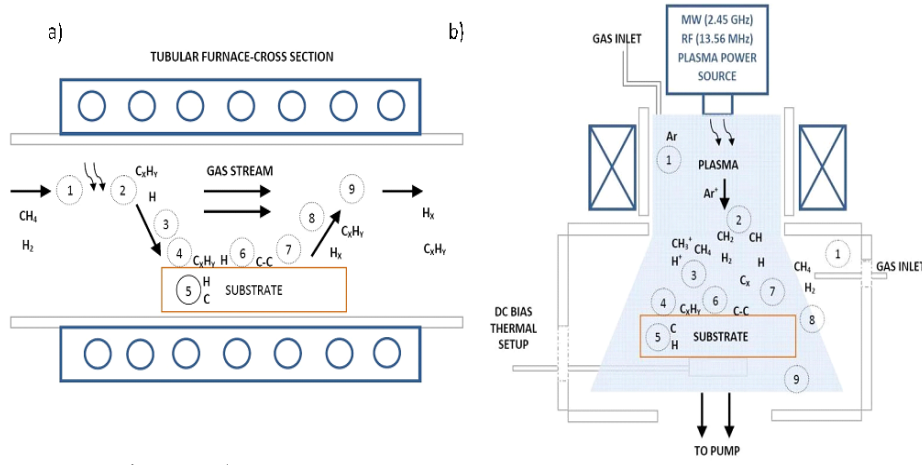
The working principle is to detach graphene from an already existing graphite crystal[64]. After the peeling, multiple layers of graphene remains on the tape. By repeated peeling, the multiple layer graphene is cleaved into various flakes of few-layer graphene[64]. Then the tape is attached to the substrate and then removed by dissolving in acetone.

Micromechanical exfoliation yields high quality layers, with size limited by the single crystal grains in the precursor graphite[43, 65]. But a major drawback is that it is very poorly suited for large scale production[65] and the obtained flakes differ considerably in various parameters[64]. da Costa *et al.* developed a fabrication method inspired by micromechanical exfoliation method to compensate for these problems by using a hot-press machine called polymeric stamp[66]. Although, there is still some way to go before it can be applied to large scale production.

2.2.4 Chemical Vapor Deposition (CVD)

CVD is a proven method frequently used in the semiconductor industry[67] and is a promising method for the production of large area, high-quality graphene[68, 42]. In

the CVD process a solid material is deposited from a vapor by a chemical reaction occurring on or in the close proximity of a normally heated substrate[69, 70]. The deposition process either results in a film or a powder[70] depending if whether it is a homogeneous gas phase reaction or heterogeneous chemical reaction. The former gives a powder, while the latter results in a thin film. On figure 2.11 a schematic diagram of two forms of CVD processes used to grow graphene can be seen[71]. The thermal CVD is more common, while the PECVD has the advantage of operating at far lower temperatures[72].



1. Transport of reactants by forced convection.
2. Thermal a) or plasma b) activation. Homogeneous gas reaction with particles and powder production should be avoided in graphene synthesis, controlling the kinetic parameters (P, T, n).
3. Transport of reactants by gas diffusion from the main gas stream through the boundary layer.
4. Adsorption of reactants on the substrate surface.
5. Dissolution and bulk diffusion of species depending on the solubility and physical properties of the substrate
6. Thermal activation mediated-surface processes, including chemical decomposition (catalytic), reaction, surface migration to attachment sites (such as atomic-level steps), incorporation and other heterogeneous surface reactions. Growth of the film.
7. Desorption of byproducts from the surface.
8. Transport of byproducts by diffusion through the boundary layer and back to the main gas stream.
9. Transport of byproducts by forced convection away from the deposition region.

Figure 2.11: Schematic diagram of Thermal CVD a) and Plasma Assisted CVD b) process: case of graphene from CH_4/H_2 mixtures[71].

The CVD process has been explored extensively to synthesize large areas of single layer graphene[73]. Much progress has been made, but CVD graphene is still a polycrystalline film made of micrometer to millimeter size domain[70] posing a major disadvantage. Another challenge is the extreme sensitivity, of multiple aspects, to the catalyst substrate as e.g. the process does not yield uniform monolayers of graphene when grown on Ni, whereas Cu looks to have more potential in this regard[70, 74]. It should be added that the nucleation and growth mechanism of graphene is enhanced on the catalytic substrate. In fact the catalytic substrate play the fundamental role on the control growth of layers and domain[70].

2.2.5 Chemical synthesis

With researchers always in a quest to improve the fabrication methods for single layer graphene, it is natural that they also investigate the prospects of chemical synthesis of the material. In fact, the chemical synthesis method has proven to be effective enough to be responsible for 7 percent of the total synthesis of graphene[75]. Applying the method of chemical synthesis on graphene is slightly more difficult than to applying it to produce fullerenes and CNT[76]. The reason for this is that graphene is, in contrast to them, a flat and strain free system whose plane can be attacked from both sides when dispersed in a solvent[76].

Simpson *et al.* developed in 2002 a method for producing large nanographene sheets[77]. A suitable 3D oligophenylenne precursor molecule was built up by a sequence of Diels-Alder and cyclotrimerization reactions, followed subsequently by planarization by oxidative cyclodehydrogenation to a graphene sheet with a diameter of 3.2 nm. A team led by Chouair introduced in 2009 an approach based on solvothermal synthesis[78]. In this approach laboratory-grade ethanol and sodium were used as starting material to synthesize sodium ethoxide. A second process step of pyrolyzation yielded a fused array of graphene sheets. The process was scalable and low-temperature. Speyer *et al.* contributed further to the method by proposing a method where commercial sodium ethoxide was applied[79].

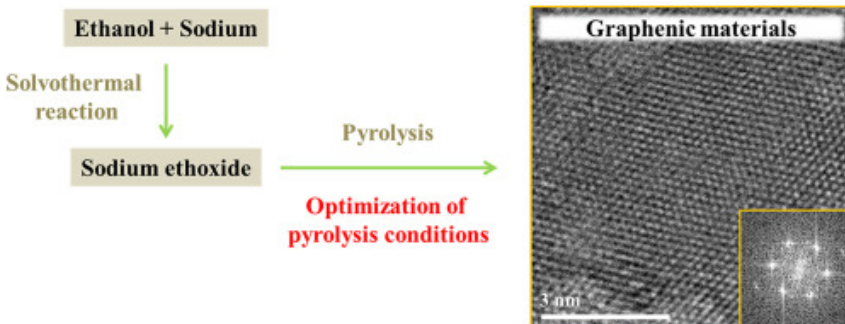


Figure 2.12: Schematic of the solvothermal reaction followed by a pyrolysis resulting in graphene[79].

Figure 2.12 depicts the two-folded process where a solvothermal reaction is followed by a pyrolysis. The good quality of the resulting graphene material indicates a high potential for the synthesis if commercial sodium ethoxide can be applied.

2.2.6 Epitaxial graphene

The word epitaxy comes from Greek and refers to the process of growth of a crystalline layer on a crystalline substrate which follows the structure of the substrate[80]. The method involves CVD growth on epitaxially matched surfaces[38]. Graphene grown epitaxially on silicon carbide substrates has proven to be exceptionally well suited as a platform for graphene-based electronics[81]. This is because the graphene is grown on a semi-

conductor and the graphene sheets are oriented with respect to the semiconductor[81]. Also included in the analysis is the high temperature involved in the process. The high temperature guarantee few defects[81]. Furthermore, the graphene films fabricated on the carbon-terminated face show signs of being rotationally stacked[81], and thereby giving origin to a whole new set of properties[82]. A common formation process of epitaxial graphene is via sublimination of Si from the SiC surface (Figure 2.13).

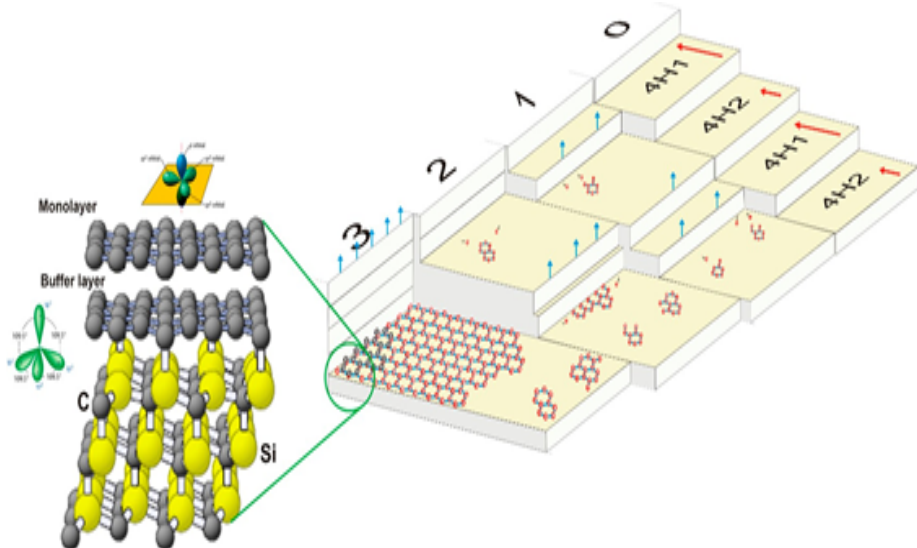


Figure 2.13: Schematic depiction of the formation process of epitaxial graphene via sublimation of Si from the SiC surface[83].

Recent studies have shown that large-area growth on SiC wafer surfaces by temperatures above 1300 °C in UHV makes it possible to prepare wafer-sized graphene with carrier mobilities at over 2000 cm²/Vs[38, 84]. Other studies show that large area monolayer graphene has been achieved on Cu[85, 86]. The method shows no apparent limitation in lateral or vertical size growth.

2.2.7 Pulsed Laser Deposition (PLD)

The PLD technique was first used in 1965[87]. It is a technique considered to be technologically more sophisticated than the previous one presented. PLD is a thin-film[88, 89] deposition technique using high-energy laser pulses to vaporize the surface of a solid target inside a vacuum chamber and condensing the vapor on a substrate to form a thin film up to a few micrometers in thickness, as seen on figure 2.14[90].

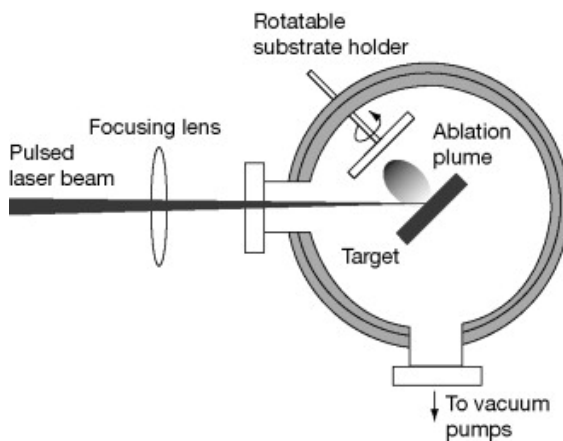


Figure 2.14: Schematic diagram of PLD process[90].

The main characteristics of PLD is the stoichiometry transfer between target and deposited film, high deposition rates of about 0.1 nm per pulse and droplets on the substrates[87]. The stoichiometric transfer makes it possible to fabricate a wide array of materials[90]. A synthesis performed by a pulsed mode makes it possible to grow small amount of matter in a timescale defined as microseconds[91]. The properties mentioned so far are all advantages. Disadvantages of the method are the presence of micrometer sized particulates and the narrow forward distribution that makes it difficult to do a large-area scale up[92].

Because of the advantages associated with the PLD method, several research groups have used it to grow single-layer graphene. The review from Bleu *et al.*[93] separates between PLD graphene growth with[94, 95] and without[96] a metal catalyst. The metal catalyst is used to improve the quality of graphene. In other big breakthroughs, Hemani *et al.* did a PLD to grow graphene on a silicon substrate[97]. This was done with a nickel metal as catalyst. Wang *et al.* presented in 2015 an epitaxial growth of graphene thin films by PLD[98].

2.3 Hindrances preventing further commercialization of graphene

With there being so many potential applications of graphene and something akin to unlimited funding[99, 100], the expectation of the consumer would be to see more graphene-based applications on the market[1]. However, several hindrances prevent the widespread commercialization of graphene. Primarily it is that despite the large number of production techniques, pure graphene is not yet available in mass scale[101]. The techniques used to isolate these 2D crystals in the laboratory are difficult to transfer to large scale manufacturing. Related to this are also the challenges with narrowing the gap of the properties obtained with commercial graphene compared to those of pristine graphene[102] and a required standardization of production as done with the industry standard silicone[67].

Other hindrances are low fabrication rates[101], integration into modern electronics[43] and high sales costs[102, 17]. Graphene commercialization has increased steadily since 2009[102]. Production of graphene was 14 tonnes in 2009, 120 tonnes in 2015 and will likely be 1200 tonnes this year[102]. Accompanying the increased production are newly started enterprises[103] pursuing development of graphene-related products[43]. But the challenges facing a full commercialization has largely persisted.

2.3.1 Narrowing of the gap to pristine graphene

Pristine graphene is defined as the pure, unoxidized form of graphene[104]. The headline of this subsection implies that there is a considerable gap between the graphene on the market and the quality associated with pristine graphene. A pure form of graphene is an atomic plane of carbon bonded with pure sp^2 -bonds[102]. But in reality the production method gives origin to differences in lateral size, material thickness and structural defects. Examples are conductivity decreasing by the number of layers[31], absorbance increasing by the layer[18] and the stiffness of graphene increasing with thickness[102]. Having a material that differs in property values from those of pristine graphene lead to devices with unsatisfactory performance[105, 106, 107] and process parameters that must be adjusted.

2.3.2 Standardization of the production process

A study by Kauling *et al.*[108] showed that the current classification of graphene flakes in the market is erroneous. The quality of the graphene is shown to be poor and can be considered to be graphite microplatelets[101] rather than single-layer graphene. The fundamental challenge of the graphene production is therefore the run-to-run variation in terms of graphene properties like thickness and defects[102]. There is therefore a need for characterization methods with large throughput. Sadly, the existing methods are not suitable for industrial adoption. Methods like SEM[109] and Raman Spectroscopy[110, 111] are very useful when used to detect defects like grain boundaries and vacancies. Especially Raman spectroscopy is highly sensitive to any disorders in the sp^2 -hybridized carbon bonds and can convey structural and electrical properties[102]. But there are questions as to whether it can be used for large-area detection with high throughput as needed in the industry. The same analogy can be made about the SEM tool. In Norway, the SEM with highest throughput can be found at SINTEF in Oslo with a throughput of 8 simultaneous samples.

2.3.3 Problem of low fabrication rate

The methods used to produce graphene today give a low fabrication rate[101, 43]. In 2019, after 15 years of research, only 1200 tonnes of graphene was produced the entire year[102]. In comparison, about 6.7 million tonnes of silicon was produced the same year[112]. For graphene to be a viable option for replacing silicon, the production of the material would have to reach the same level. The four primary ways of producing pristine graphene are nowhere near of achieving the same fabrication rate as the processes of silicon[38]. Zhu *et al.* defined four criteria the fabrication method had to meet before being able to be transferred to mass production[43]. The factors were given as: (i) the demands of attaining

the desired properties and form/morphology for target graphene products; (ii) the quality and applications of the graphene materials; (iii) the scalability from laboratory to industry; and (iv) the stability and controllability of manufacturing. The review concluded that exfoliation of graphite and CVD[113, 114] were the methods with highest potential to achieve mass production on industrial scale.

2.3.4 Financial feasibility of graphene-based products

In a free-market economy the law of supply and demand reign supreme[115]. Inferring that the relationship between supply and demand decides the prices of the goods. Applications based on graphene must therefore be able to compete in price in order to get on the market. The materials low fabrication rate has already been pointed in the previous subsection. An increase in production with current fabrication would mean greater production costs than financially feasible[102, 43]. The most likely fabrication method for industrial application, exfoliation of graphene[43], is the cheapest and best alternative. Graphite itself is cheap and abundant[116]. But a correct interpretation of the law of supply and demand would mean that with an industrial application of the exfoliation fabrication method, the increase on the demand side would require a steep rise in supply and as a result in price as well. Other methods of fabricating graphene like from eucalyptus bark are exciting, but several years from practical implementation[17].

Chapter 3

Transparent Conducting Electrodes

Transparent Conducting Electrodes, or TCEs, must as the name suggests, exhibit both electrical conductivity and optical transparency[117]. TCEs have been key components for opto-electronic devices such as Solar Cells, Light-emitting Diodes (LED), Liquid Crystal Displays (LCD) and touch screens[118, 119]. Figure 3.1 shows two opto-electronic devices where TCEs are used.

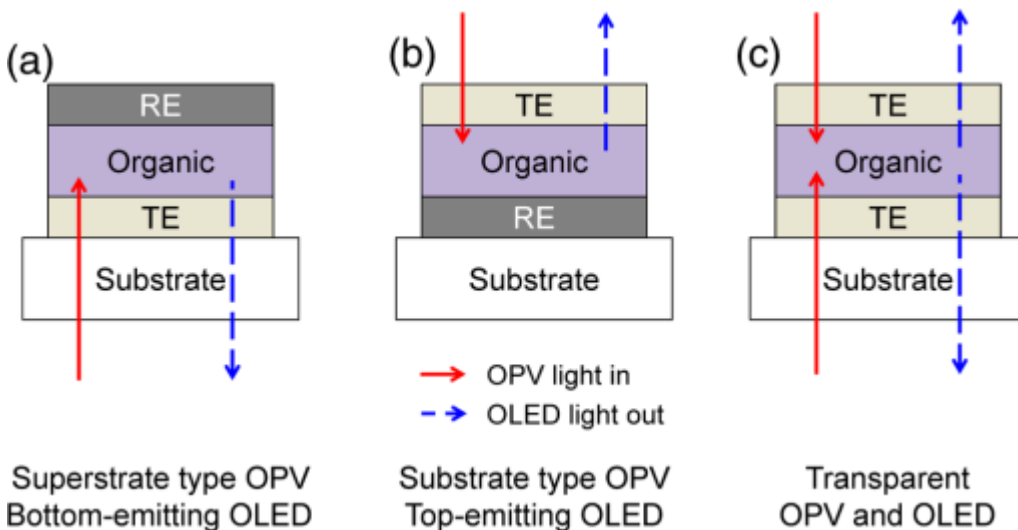


Figure 3.1: Schematic illustration of three types of general organic photovoltaic (OPV) and organic light-emitting diode (OLED) device architectures: (a) superstrate type OPV and bottom-emitting OLED, where light transfers into or out of the device through bottom substrates and transparent electrodes; (b) substrate type OPV and top-emitting OLED, where light travels through top transparent electrodes (TE); and (c) transparent OPV and OLED, where light travels through both bottom and top transparent electrodes[120]. RE is an abbreviation for reflective electrode.

Transparent Conductive Oxide (TCO) are a class of materials that have been predominantly used TCEs. Two widely known TCOs are ITO and FTO, which are Indium-doped and Fluorine-doped Tin Oxide [117] respectively. ITO currently has 97 percent of the market share[121] owing to its relatively high electrical conductivity and transparency[118, 120]. However, it's widespread use has increased exponentially the prices of Indium, inducing high cost of raw materials. Other disadvantages include poor mechanical flexibility and the high process temperatures involved and an alternative solution is much needed[118]. FTO (F:SnO_2) and graphene (either alone or in a hybrid) are considered to be likely potential replacements[119, 118].

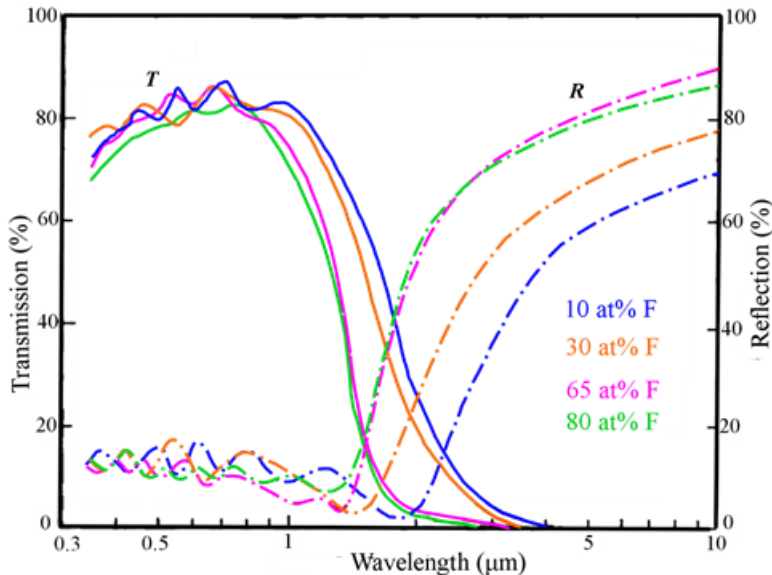


Figure 3.2: Transmission (T) and reflection (R) spectra of FTO with different F-doping concentration. The crossover between the T and R curves shows the position of the plasma wavelength which shifts towards the visible range with increasing F-doping[122].

Because the anionic radius of F is similar to O, the lattice distortion induced by F-doping is minimized compared to other cationic doping[117]. Resulting in FTO having the same crystal structure as pure SnO_2 . When F is the dopant and substitutes O, the electrical conductivity increases proportionally to the increase in free electron concentration. One side-effect by applying heavy doping is that it damages the film transparency[122], as can be seen on figure 3.2. Because of the heavy doping associated with TCOs, the conduction band becomes partially occupied[123]. This means that the photons need a larger energy than the original band gap to excite transitions from the valence band to the conduction band. A phenomena called the Burstein-Moss shift[124]. Mobility is important for the conductivity of a material. Rey *et al.* found that structural defects like grain boundaries are important for the mobility of thin film FTO, while for thicker films ionized impurity scattering becomes dominant in determining the conductivity[125].

Due to its properties, graphene shows promise as a possible material for use in TCE. The main disadvantage with graphene is the high sheet resistance compared to the metal-based transparent electrodes that exhibit the same level of transparency[118]. But some reports indicate that this can be negated by improving the performance of TCE by hybridizing graphene with materials like ITO[126] and PEDOT:PSS[127, 118]. Though, the research is still in its infancy and therefore limited in scope[118]. An another approach at hybridizing ITO and graphene was done by Lee *et al.* where CVD graphene is synthesize by immersing graphene into aqueous ITO sol-gel[128]. The resulting products show a decrease in sheet resistance, while maintaining the necessary transparency at over 80 percent[118].

Electrophoretic deposition was in 2010 used as a method for coating GO suspension with a film[129, 118]. The deposition was performed through the migration of GO sheets[129] in a suspension toward the positive electrode when a direct current voltage is applied[130, 131]. This method is limited by the fact that only conductive substrates are possible to use. There have been attempts at depositing graphene on simple glass, and thereby making the glass conductive in the process. Sun *et al.* used APCVD to grow large-area and uniform graphene films on glass[132]. Xiong *et al.* fabricated monolayers of graphene on various dielectric substrates via rapid thermal process[133]. The resulting exhibited a low sheet resistance of 50 Ohm/square at 95 % transparency. A downside with the process was the high process temperature of 1100 °C.

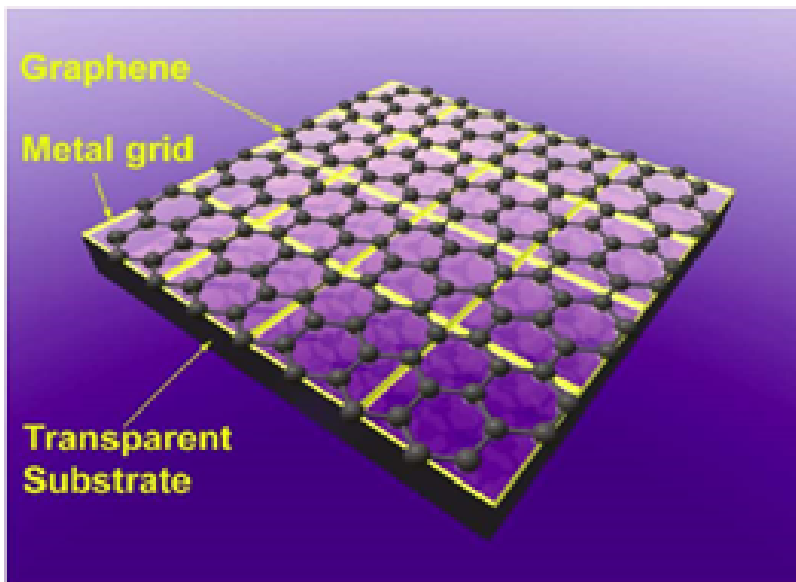


Figure 3.3: Metal grid/graphene hybrid transparent electrode. The yellow lines in the figure represent the metal grid. The grid size and gridline width in the figure are only illustrative and are not scaled with the graphene molecular structure[134].

Magdassi *et al.* suggest that when using a nanomaterial to pattern a transparent electrode, the morphology of the conductive pattern must provide high transparency[121]. It is therefore important that the pattern does not reduce the charge collection over the layer in question. A way to optimize the charge collection is by changing the geometry of the conductive lines to a honeycomb lattice[121, 135, 136]. For graphene this can be achieved as a natural consequence by depositing graphene on the conductive lines on the substrate. Figure 3.3 shows a metal grid/graphene hybrid transparent electrode[134].

3.1 The basics of Solar Cell

A Solar Cell is defined as any device that directly converts the energy in light into electrical energy by the process known as the Photovoltaic effect[88]. The Solar Cell is a renewable energy source with zero emission[137]. Due to this, it is widely seen as a source potentially capable of replacing fossil energy sources like oil and gas[138, 139]. TCOs are important in photovoltaics and often used as front and back electrodes[117]. And thereby playing an important role in determining the maximum attainable energy conversion efficiency. In practicality, the role of the TCO is to transmit light and collect charge carriers. Preferred parameters for a TCO is an optical transmission of 80 % and above, and a low resistivity below 10^{-3} Ohm cm[117]. The TCO must have the ability to absorb as much light as possible in the active layer and at the same time to efficiently collect charge carriers.

One fundamental principle behind Solar Cells is the photovoltaic energy conversion[88]. Incident photons with energies higher than the Solar Cell material's work function excite charge carriers to higher energy levels where they become mobile[140]. A net current occurs in the Solar Cell due to a built-in asymmetry in it[88]. Furthermore, the energy difference between the charge carriers extracted at the external generates a potential difference that is then used to drive a current through a load to do electrical work. The Solar Cell has two important characteristics, 1) it acts as a diode in the dark and 2) it generates photovoltage V and a photogenerated I_{SC} when illuminated[141]. The best way of evaluating the properties of a Solar Cell is by presenting them in an J-V plot, as done in figure 3.4. The key characteristic of a Solar Cell is its ability to convert light into electricity. This is measured with the power conversion efficiency (PCE). The PCE is given according to the equation:

$$PCE = \frac{P_{out}}{P_{in}} = \frac{J_{SC}V_{OC}FF}{P_{in}} \quad (3.1)$$

with all variables defined on figure 3.4.

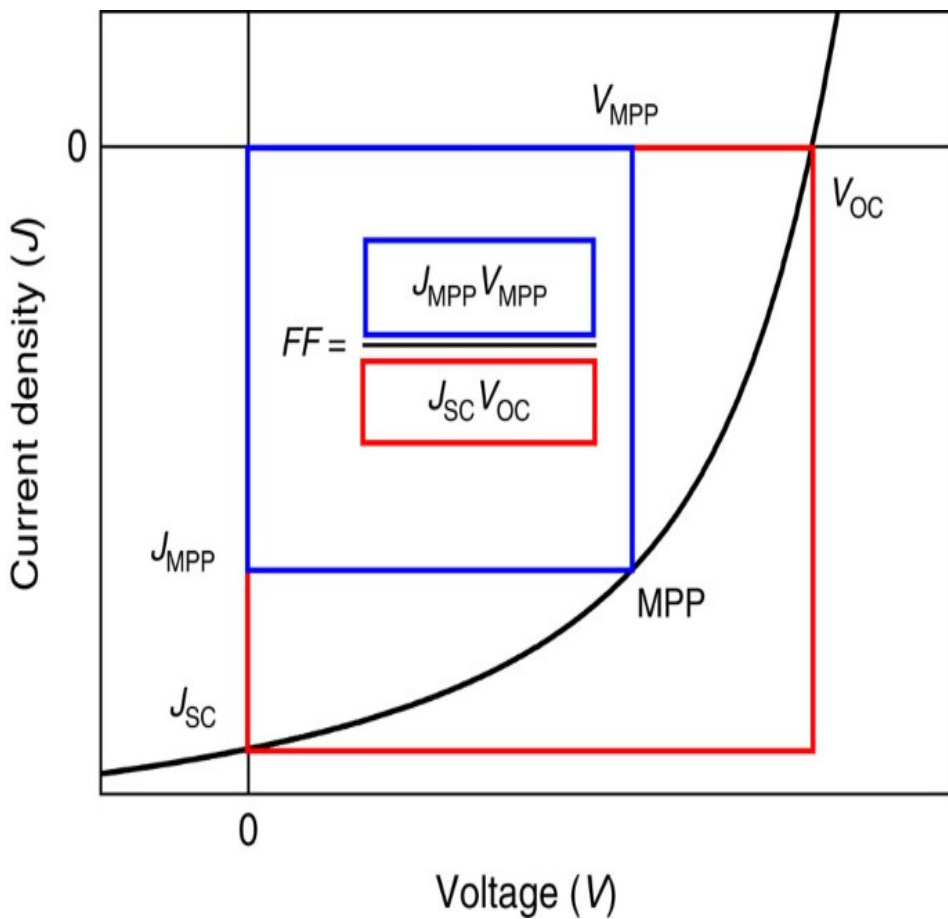


Figure 3.4: Schematic of an J-V plot[142]. The plot exponentially growing represents the diode equation. Blue box is the fill factor (FF).

3.2 Dye-Sensitized Solar Cell (DSSC)

One application of a repeatable fabrication process of a continuous layer of conductive graphene film is as a catalyst in a Dye-Sensitized Solar Cell. DSSC is a form of thin film photovoltaic cell that is easy to manufacture with traditional roll-printing techniques[143]. The four most important parameters of a DSSC are: Working Electrode (WE), Sensitizer (also known as a dye), redox-mediator (called electrolyte) and Counter Electrode (CE)[144]. A well-functioning TCE has the potential to replace the two electrode parts of the system. Sharma *et al.* define a DSSC as: "DSSC is an assembly of WE soaked with a sensitizer or a dye and sealed to a CE soaked with a thin layer of electrolyte with the help of a hot melt tape to prevent the leakage of the electrolyte"[143]. The materials a DSSC is made of are low cost materials, and this combined with its efficiency in converting solar

light to electricity makes it a viable alternative to the industry standard Si-based modules. Pt is the only part of the DSSC that is considered to be expensive[143].

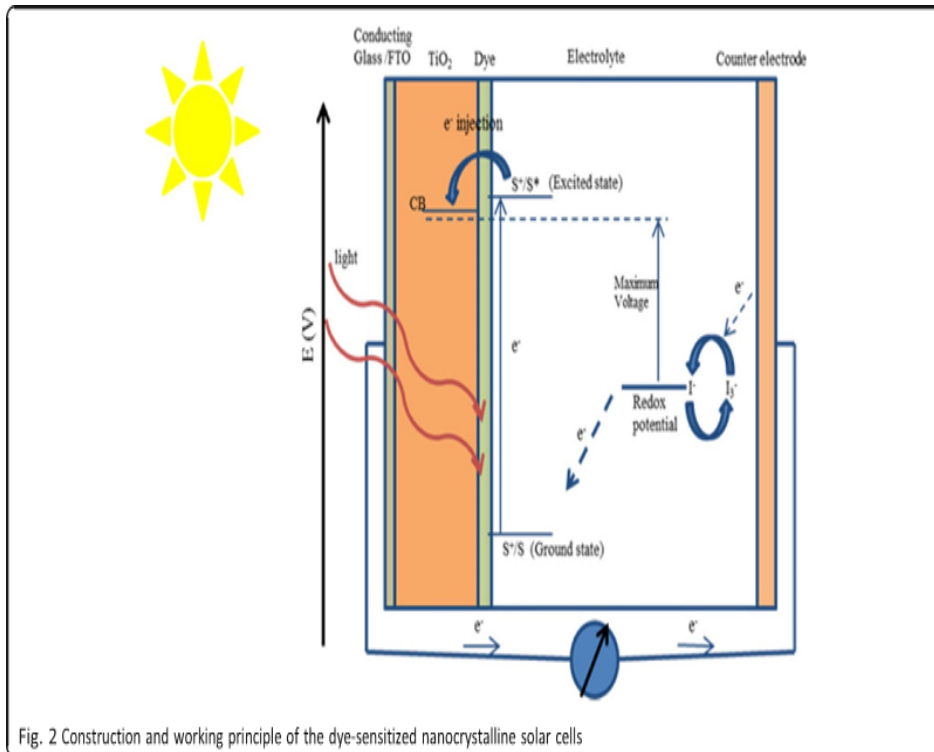


Figure 3.5: Schematic shows the construction and working principle of a DSSC[143].

Research suggests that graphene can be used effectively as catalysts in DSSC[145]. Hagfeldt *et al.* have done a comprehensive literature review of research where graphene has been used as a catalyst for the reduction of redox species. The first report of the application of graphene as a replacement for Pt catalyst in a CE was done in the 2010s by Roy-Mayhew *et al.* They managed to achieve a PCE of 4.99 percent with a device with graphene included in the CE with a control DSSC with Pt with a PCE of 5.48 percent[146]. The reasoning for this is that catalytic activity of graphene effectively reduced the electrolyte used in a DSSC. Other groups like Yen *et al.* observed a PCE of 2.89 percent for their attempt on a DSSC with graphene (with reduced Graphene oxide as the precursor material). Zhu *et al.* attempted an electrophoretic deposition to deposit graphene films for implementation in the CE of DSSC[147]. The research team managed a PCE of 3.63 percent.

It can therefore be seen that the method used to produce graphene films has an effect on the PCE of the DSSC and other Solar Cells. Hsien *et al.* for example found that by decreasing the Oxygen/Carbon ratio would induce an increase in the catalytic activity toward I_3^-/I^- redox reaction. Hagfeldt *et al.* also suggest that the catalytic activity of graphene is related

to amount of defects in the material[145]. By increasing the defects in the material one would get a higher catalytic activity and thereby most likely also a higher PCE for Solar Cells. On figure 3.6 a schematic diagram of how a real DSSC deviates from the ideal can be found. Physical barriers like alkyl chains, co-adsorbers and perpendicular orientation of dyes lead to deviations from ideal conditions. Recombination to oxidized dye and the electrolyte has to be taken into account as well.

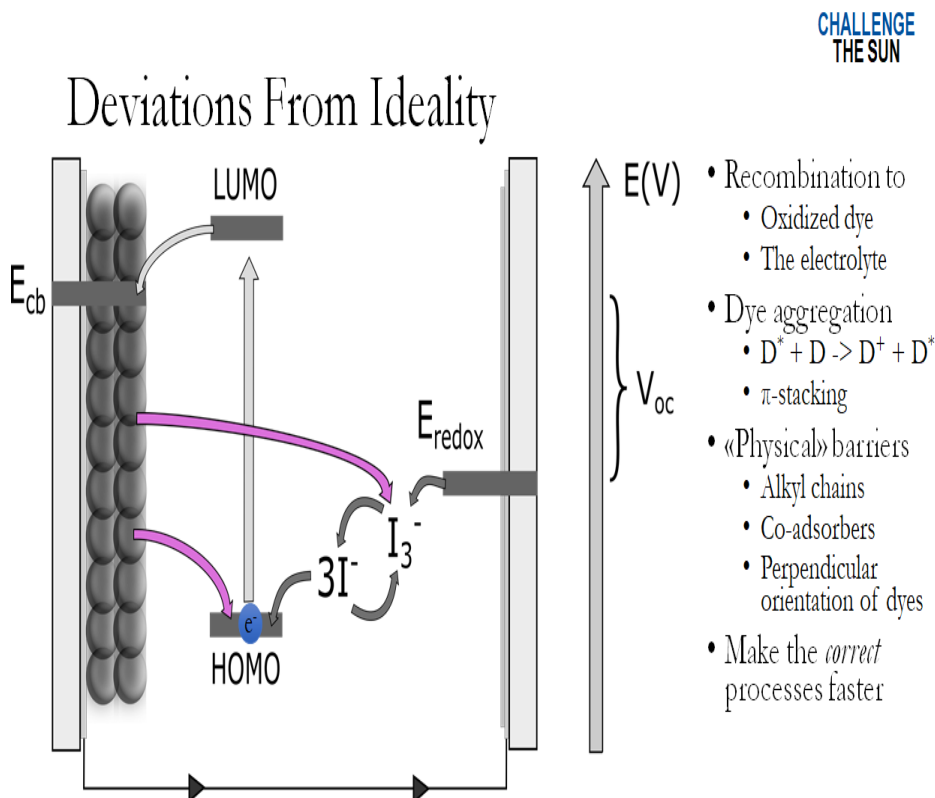


Figure 3.6: Schematic diagram of how a real DSSC deviates from ideality. Figure provided at the courtesy of David A. Moe

3.3 Light-emitting Diode (LED)

A LED is a solid-state semiconductor device with a single junction[148]. This single junction can be obtained by doping the semiconductor with different materials at different locations, thereby forming a junction between the two areas. LEDs produce light through spontaneous emission of radiation[149]. The wavelength of the light is determined by the materials used to form the semiconductor junction[148].

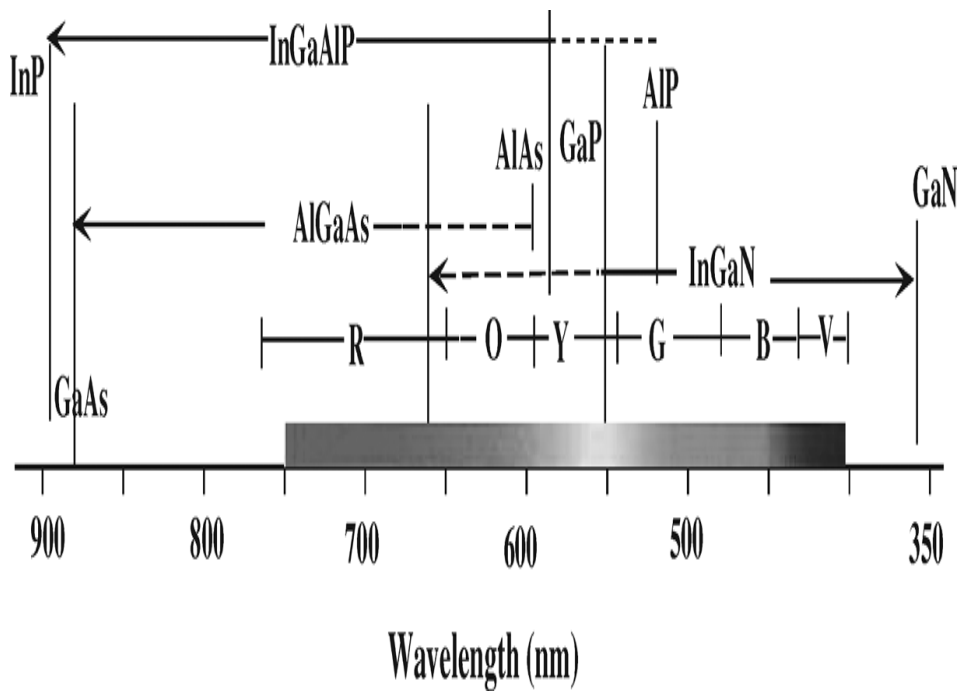


Figure 3.7: The LED materials and range of wavelength of the emission associated with them[149]. The color band indicates the visible region of the spectrum.

Figure 3.7 represents the binary, ternary and quaternary composition of materials deciding the wavelength of emitted radiation. Applications of LED are displays, indicator lights and illumination among others. The common theme is that the applications require emission in the visible part of the spectrum[149]. Originally, the function of a LED was limited to indicator lights, but as white light generating varieties of the LED became available, the role shifted to illumination as well. This transformation was mainly possible due to Nakamura *et al.*'s major breakthrough in 1992[150]. Nakamura *et al.* developed the blue LED, a feat deemed important because it enabled bright and energy-saving white light sources. The blue LED was manufactured as low-resistivity p-type GaN films, which were obtained by N₂-ambient thermal annealing or LEEBI treatment[150]. Uchida *et al.* built on Nakamura *et al.*'s invention and developed a near-UV based white LED lighting system linked with a semiconductor InGaN LED and compound phosphors for general lighting applications[151]. The new LED is a novel type of high-color rendering index white LED light source which is composed of near-UV LED and multiphosphors showing orange, yellow, green and blue emissions[151].

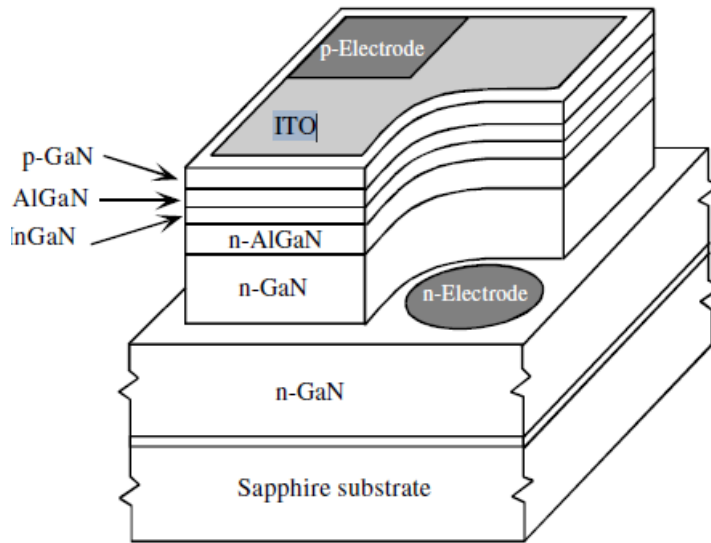


Figure 3.8: Schematic representation of a LED where ITO replaces the ohmic metal contact[149].

The primary use of a TCE is to replace the ohmic metal contact[149]. This can be done to reduce absorption from the metal contact. A schematic representation of how such a LED would look can be found on figure 3.8. OLED is an abbreviation for Organic LED and the basic device architecture of an OLED can be classified into three groups according to the position of the TCE[120], as seen on figure 3.1.

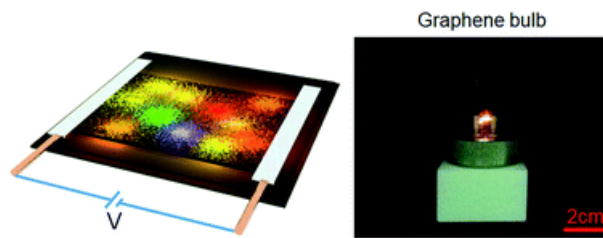


Figure 3.9: Schematic diagram of RGO based LED illumination on the left[152]. When a suitable bias voltage (V) is applied, luminescent spots appear on the device. On the right, a schematic of a graphene bulb.

The hype surrounding graphene as a potential part in a TCE has not gone unnoticed in the LED development community. Jiang *et al.* prepared a flexible LED by using laser-induced RGO[152]. The LED achieved a luminescence lifetime of over 60 hours. In addition to this, the luminous behaviour of the component was controlled by modifying the supply

voltage and laser reduction intensity. Figure 3.9 shows the schematic diagram of the RGO based LED illumination and the graphene bulb developed. Huang *et al.* demonstrated the gas phase encapsulation of graphene layer on superfine Cu nanowires network by CVD for highly transparent LED[153]. They also found that point discharge effect is found to produce locally high injection current through contact points and thereby forming ohmic contacts.

3.4 Liquid Crystal Display and Touch screens

The Liquid Crystal Display (LCD) was invented in 1964[154]. Liquid crystals are organic materials that are liquid, but that show a certain degree of positional ordering[155]. For use in LCD it is required that the liquid crystal are thermotropic. The LCD is an electronic display device operating by applying a varying electric voltage to a layer of liquid crystal, thereby inducing changes in its optical properties[156]. As partially already explained, the basic principle for a LCD is that by mixing pure nematic liquid crystalline compounds together, one can produce stable homogeneous crystal mixture which could operate along a broad temperature range. Especially important of the materials used are the cyanobiphenyl materials[157]. Figure 3.10 is of the widely used 4-pentyl-4'-cyanobiphenyl.

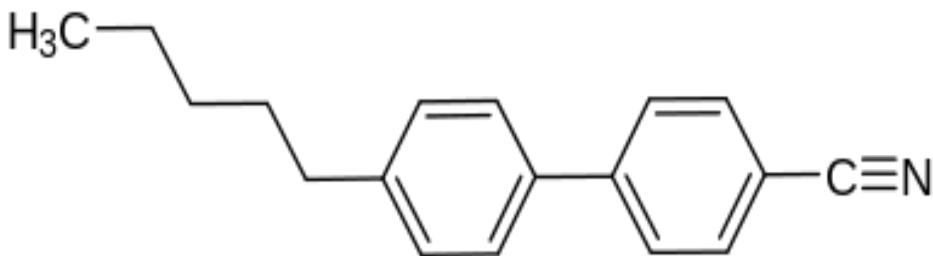


Figure 3.10: Image of the 4-pentyl-4'-cyanobiphenyl molecule widely used in LCD[155].

From 2007 and on, the interest in LCD increased rapidly. The reason was that the image quality of the LCD surpassed that of the traditional CRT TVs[158]. LCDs today are commonly used in applications like computer monitors, flat-panel televisions and screens for cellular phones[156]. Although it is dominating the multi-billion market for screens, it has a fierce competitor in the OLED technology[159]. Both technologies can be made transparent and flexible, but OLED has the advantage that it can produce its own light, while the LCDs are illuminated with a backlight[159].

A LCD can be improved by using a TCE[121]. A TCE proves it is useful since in a typical LCD device, the liquid crystals are aligned under an electrical potential generated between two electrodes. Because of the desire to see the colors, one of the electrodes must be transparent[121]. Chae defines two requirements that must be satisfied for the TCO before an eventual implementation in a LCD[160]. These are; 1) there must be no etch residue after TCO patterning and good etch selectivity against low electrical resistivity

metals and 2) there must be good chemical endurance of the TCO material to secure a good electrical signal that is transported from the controller to the TFT-LCD by way of contact between the TCO and the tape carrier package (TCP). Byeong-Yun *et al.* made an attempt with Al-doped Zinc Oxide, but saw only minor improvement[161]. Seok-Han *et al.* experimented with polymer-dispersed liquid crystal devices (PDLC) with graphene electrodes[162]. They found that PDLC exhibited higher contrast and faster response than ITO, but at the same time also experienced more haze.

Close to 13 touchscreen technologies have been identified with a total of 38 variations[163]. The touch screen is a combined input and output device found in many electronic applications today. The display's, based on either LCD or OLED, working principle follows projected capacitive or analog resistive mechanisms. The two mechanisms have for the last decade been firmly entrenched as the two dominant technologies for touch screens. Crucial parts of a functioning touch screen device are the controller and sensor. TCE is considered a potential replacement[121] because it eliminates the need for vacuum sputtering. Implying that a patterning of the TCE can be done in room temperature, which would be a major cost decrease[163]. Figure 3.11 presents the schematic of the build up of tablets and smartphones.

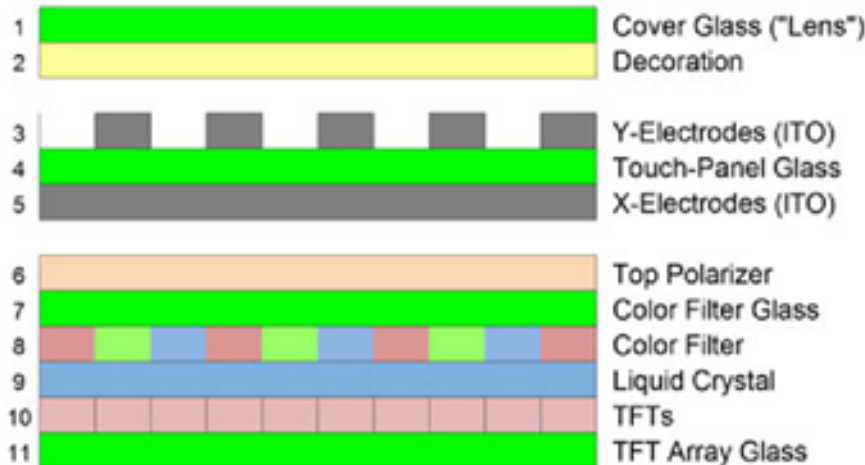


Figure 3.11: Schematic shows the build of tablets and smartphones. All smartphones and tablets use some form of “decorated covering” (rows 1 and 2) to protect the LCD (rows 6 to 11) from damage. When a projected capacitive touchscreen is added, most commonly, the electrodes are located on a fourth piece of glass (rows 3 to 5). In the figure TFT is an abbreviation for thin film transistor[163]

Chapter

4

Aim of thesis

The primary goal of this master thesis is to develop an experimental procedure for the reliable fabrication of a continuous layer of graphene. The intention is to deposit uniform thin films comprised of exfoliated graphene nanoparticles onto a given substrate using a variety of different techniques. The substrates used in this project are simple glass plates and conductive Fluorine doped Tin Oxide (FTO) glass plates. The project involves a comprehensive study of several deposition techniques, ranging from basic Drop Casting, to Spin Coating, Doctor Blading, layer-by-layer deposition and Electrodeposition.

As the most important part of a deposition method is the parent solution, two solvents will be examined: N-Methyl-2-pyrrolidone (NMP) and Benzylamine. Other important factors to consider are the qualities of exfoliated graphene depending on experimental details of producing the material and post-production processes like annealing.

The graphene layers produced will be investigated using several techniques like UV-Vis spectrometry for optical transparency, AFM and SEM for morphological characterization and a Four-point probe, along with a multimeter for the electrical conductivity characterization.

Towards the application area of our project, graphene as a constituent material is applicable to a wide variety of technologies. The focus in this thesis will be narrowed to Solar Cell research as an area of research interest.

After the deposition the thin films are characterized to understand the deposition mechanics and limitations of each method. Graphene deposited onto simple glass plates is examined towards its electrical conductivity, while graphene deposited onto FTO glass plates with graphene deposited on, the glass plates will be evaluated as Pt-replacement in counter electrodes in Dye-sensitized Solar Cells (DSSC). Meaning measuring the catalytic properties for the regeneration of the electrolyte in the solar cell.

Results and Discussion

Several experiments with different methods were tried out to find the best way of coating the glass substrates with graphene thin films. The results and discussion section reflects that in its layout. Included are also characterization of the morphology and absorbance. One of the graphene thin film samples was tried out as a counter electrode in a DSSC. This is presented in section 5.4.

5.1 Electrodeposition results

In the electrodepositon, ± 10 mA current and ± 20 V, as well as lower currents and voltages, were applied. Positive voltage and negative current gave a coating, while the two other parameters did not. It was concluded that the highest voltage possible on the Power supply gave the best process. For the deposition time, or the duration of the Electrodeposition process, several parameter values were tried. One hour proved to be close to optimal deposition time. Lower times gave insufficient coating because of the maximum value of the Power supply possible given at only +20 V. Higher deposition times led to unwanted effects. The sample held in the bath for two hours broke in two when pulled slowly out of the bath.

A Four-point probe was used to measure the conductivity and resistivity, in addition to the sheet resistance. The result was compared with ultraclean FTO glass. For achieving a successful coating it was deemed sufficient to prove a higher sheet resistance compared to the reference point. An abnormally high value in this aspect would hint at the formation of graphite rather than graphene[164]. Table 5.1 contains the experiments done with Electrodeposition of graphene and the values for the electrical conductivity obtained.

Sample name	S. Resistance (Ohm/square)	Resistivity (Ohm*m)	Conductivity (S/m)
Blank FTO	2.22	1.663e6	6.018e5
P10ED	7.48	3.738e6	2.678e6
P13ED	4.41	7.502e6	1.333e5
P14ED	10.76	1.829e5	5.47e4
P15ED	5.13	2.564e6	3.914e5
P23ED	6.37	4.781e6	2.095e5
P16ED	58.86	1.766e5	5.664e4

Table 5.1: Table shows the sheet resistance, resistivity and conductivity of the 5 FTO samples coated with graphene and P16ED (a simple glass plate coated with graphene by the use of Electrodeposition) and a reference glass plate.

P10ED was a sample where mixed negative and positive current was applied. With P13ED, +20 V was applied for an hour, and P14ED and P15ED had +12 V and +15V applied for an hour, respectively. P18ED had the parameters of +20 V for two hours. P19ED (not listed in table) used the same parameters as P18ED and was used for the DSSCs. P21ED had the parameters: Benzylamine + graphene and Benzylamine + TBAPF₆ as electrolyte and +20 V sent in for one hour. P23ED followed the same procedure as P21ED (considered not conductive enough), but a solvent mixture of Benzylamine and NMP + TBAPF₆ was used instead of Benzylamine + TBAPF₆ alone. Finally, the sample P16ED was a simple glass plate that was treated with drop-casted graphene in NMP. Subsequent annealing to remove residual solvent, yielded a glass substrate conducting enough to allow for the Electrodeposition process to take place. The values for sheet resistance were much higher than those of the pure FTO samples and indicate graphite rather than graphene. The box plot on figure 5.1 shows a conductivity in close proximity to each other.

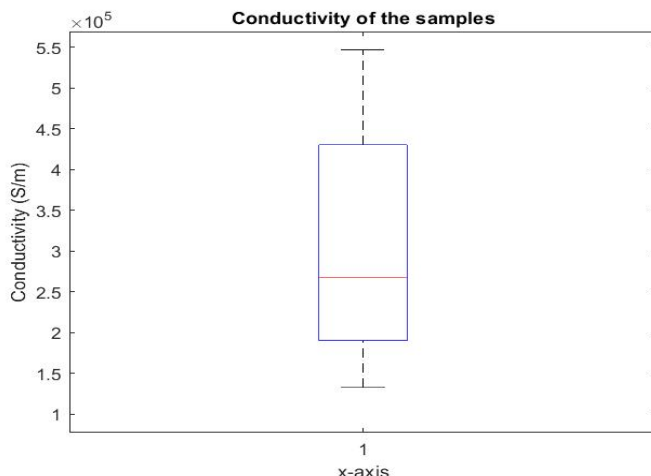


Figure 5.1: Box and whisker plot of the conductivity distribution of the samples. Top and bottom of the box indicate 75th and 25th percentile, respectively. The line in the box indicates media. Vertical line above and below the box extend to high and low values.

Despite the values of the graphene-coated samples being lower than FTOs, it furthers the hope for graphene possibly replacing FTO with time. Due to time constraints, only basic optimization took place focused mostly on instrument settings (applied voltages and currents). Possible optimization parameters that could be examined to improve the results are different solvents and electrolytes as well as solvent and electrolyte concentrations.

5.1.1 The role of electrolytes/salts

This subsection attempts to investigate how electrolytes affect the process of Electrodeposition. For the experiment the salt used was TBAPF₆. The molecular mass of TBAPF₆ is 387 g/mol. The solution comprised of TBAPF₆ in NMP. In general, the process would start with 10 ml NMP and the appropriate amount of electrolyte would be added in order to reach a concentration of 0.1 M to 1 M. This solution would then be added to the NMP + graphene solution to form the final mixture for the Electrodeposition. By varying the amount of electrolyte and NMP, changes were observed in the voltage/current measurements of the instrumentation (Figure 5.2).

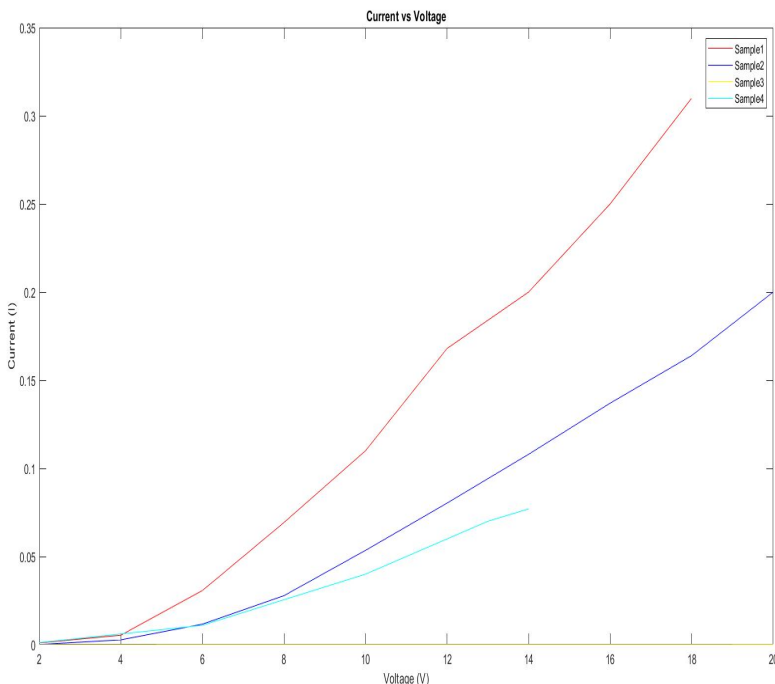


Figure 5.2: Schematic of the plots for the different electrolyte concentration when + 20 V Voltage was the input and all had the deposition time of one hour

On figure 5.2 there are four different samples given the names Sample1, Sample2, Sample3

and Sample4. Table 5.2 summarizes the parameters applied when the films were produced.

Sample No	Graphene in NMP (ml)	TBAPF ₆ in NMP	Voltage (V)
1	11	1 M and 9 ml	+20
2	13	1 M and 8 ml	+20
3	5	0.1 M and 5 ml	+20
4	7	1 M and 5 ml	+14

Table 5.2: Table of samples and the parameters applied in producing the film on the samples. Columns represent amount of graphene and NMP in ml, TBAPF₆ and NMP mixture in molarity and amount in ml and voltage applied.

It was concluded that there was a strong correlation between the molarity of the electrolyte and the current measured[52]. Increasing the electrolyte-concentration would increase the current. The voltage applied was the same for all samples except Sample4. The ratio between the main solution of graphene + NMP and TBAPF₆ + NMP is also an important factor to consider. It was difficult to find the perfect ratio because oversaturation had to be taken into account as well. However, having a 1 M TBAPF₆ + NMP in a 1:1 relation with graphene + NMP was proven to be adequate for creating a conductive film of graphene.

5.1.2 Solvent comparison

The sonication of Benzylamine + graphene followed the standard procedure with 13 ml of the solution undergoing the sonication for 2 hours followed by 2 hours in a fume hood for cooling down. After the sonication, a centrifugation step was performed with the parameters 4000 RPM for 4 minutes. Just like with NMP, it was intended to make 1 M electrolyte solutions. However, due to the solubility restrictions of TBAPF₆ in benzylamine 0.1 M solutions were prepared instead. Attempts to make 0.5 M solutions also showed noticeable precipitation. the amperometer only showed a value of 89.8 μ A when 20 V was sent in. Thereby clearly indicating inadequate electrolyte concentration in the solution. After several attempts, it was concluded that Benzylamine alone was not possible to use with TBAPF₆ as the salt. It was impossible to get enough salt into the mixture and the small amount that was possible had too few electrolytes for the electrodeposition to work.

The solution to the problem was therefore to use a solvent mixture. It was tried with Benzylamine mixed with 10 percent NMP. Following this, it was necessary to use 2 ml NMP and 10 ml Benzylamine in a mixture to be able to dissolve 1 M salt. Then a little bit more Benzylamine was added to the solution in order to change the relation back to 1:10 again. The bath in the Electrodeposition process contained 13 ml Benzylamine + graphene, and it was added 9 Benzylamine + 10 percent NMP + TBAPF₆. This again resulted in too few electrolytes in the solution, so the last parameter was increased to 13 ml. The difference can be seen in the figure 5.3.

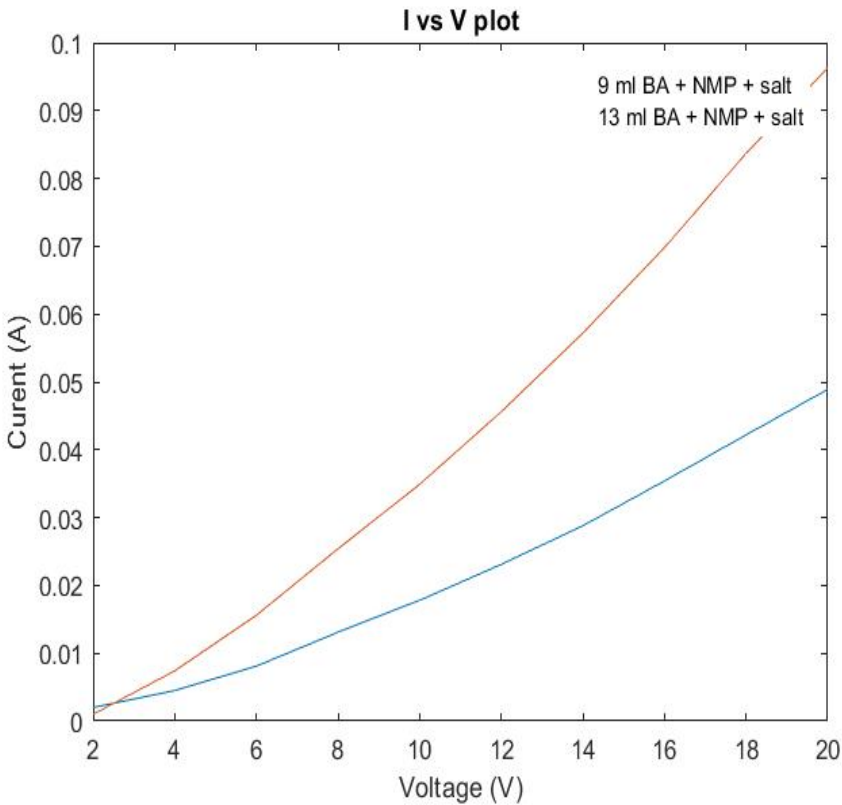


Figure 5.3: Plot of the difference in conductivity between 13 ml solution of Benzylamine + NMP + salt (red) and 9 ml of the same solution (blue).

By having the ratio between Benzylamine + graphene and the electrolyte-containing solution to 1:1, a doubling of the conductivity was achieved. And the behaviour became comparable to NMP alone as solvent. After an hour the current was measured to 0.124 A. Both samples developed showed resistance values at graphene level with 33.7 Ohm/square and 29.4 Ohm/square when the contact points were at a distance from each other and 15.5 Ohm/square and 18.6 Ohm/square when close proximity of the measurement points was measured.

Based on the parameters that were used in this experiment, a conclusion is quite straightforward. NMP is the superior solvent because of the salt solubility. Other salts would be worthwhile investigated in the future.

5.2 Doctor Blade, Drop Casting and Langmuir-Blodgett results

5.2.1 Doctor Blade

The Doctor Blade method had many parameters to consider. Attempting to vary all the parameters obviously led to a cornucopia of samples. The results presented in table 5.3 were given sample names based on how the films on the glass plates were fabricated. This can be found in the experimental section and appendix. From table 8.5 it was decided to include the conductivity of the following samples: Sample 2, Sample 4, Sample 6 and Sample 8. In addition to those, a simple glass plate was measured for reference. Included in the table was Doctor Blade applied on a FTO glass plate as well.

Sample name	Conductivity (in Ampere)
5 X FTO	0.2
Sample 2	0.5e-9
Sample 4	1e-9
Sample 6	54e-9
Sample 8	0.47e-6
Simple glass plate	0.4e-9

Table 5.3: Table of the samples chosen out from table 6.4 and their conductivity

From table 5.3, it can be seen that the measured conductivity-values were not very high. Except for the one obtained for the FTO glass plates. But that was as expected because of the choice of the substrate. The values for several of the methods were barely above the one for the reference, a simple glass plate not coated with anything. Although samples 6 and 8 showed promising results. Doctor Blade is often used to create a film of TiO₂[165][166]. However, TiO₂ is a starkly different material compared to exfoliated graphene. TiO₂ is much thicker and almost like a paste. Therein lies one of the biggest “limitations” of the Doctor Blade method, viscosity. In order for the deposition method to yield optimal results, the solution needs to be optimized towards its viscosity, solvent evaporation temperature etc.[167]. However, with exfoliated graphene both of these parameters are difficult to control due to the limitation of the material in efficient exfoliating agents and its limited dispersibility in them.

5.2.2 Drop Casting

The Drop Casting was done on both non-conductive simple glass and conductive FTO glass. Already during the first deposition it was noticed that the films were darker than the films created with other methods. As seen in the theory section, adding enough graphene stacks, inevitably, yields graphite rather than the intended graphene. More likely, the darker film color is the result of graphite/graphene aggregates.

Sample name	Current (in Ampere)
Sample 1	41e-9
Sample 2	104e-9
Sample 3	8e-9
Sample 4	1.6e-9
Reference	0.4e-9

Table 5.4: Table of the current measurements obtained on graphene films on simple glass deposited with the Drop Casting method

In table 5.4 several samples are presented. The centrifugation and sonication parts of the experiment had the same parameters. However, some changes in process could be found in the annealing. The films created with the Drop Casting method show better conductivity than the films developed with Doctor Blade. At the same time they are also more uniform and one can see a grey or dark film by the use of the optical method. The films created with Doctor Blade are more transparent. This indicates that the Drop Casting films contain more graphite than graphene. However, except for one film, none of the films actually showed any conductivity at the level of graphite. Drop Casting was also applied to coat an FTO glass. These films were also dark, but the resistance measured with a multimeter were close to graphene values but is more likely owed to the FTO substrate.

5.2.3 Langmuir-Blodgett

The Langmuir-Blodgett experiment was done with two set of input parameters. The annealing temperature was held constant at 100 °C, but the annealing time was different for the two sets. In the first set this time parameter was set as t=30 min and in the second it was set as t=60 min. In order to differentiate between them, the samples were named as G30 for those films obtained with the first experiment and the second as G60. In both setups one simple glass plate (SGP) and two FTO glass plates (named FTOI and FTOII) were used as substrates. The values of resistance and other experiment parameters for G30 can be seen in the table 5.5.

Number of immersions	SGP R (Ω)	FTOI R (Ω)	FTOII R (Ω)
0	0	21	22
1	0	21	22
2	0	21	22
3	0	21	22
4	0	21	22
5	0	140-152	29-41

Table 5.5: Table shows the parameters used in the G30 Langmuir-Blodgett experiment and the values of resistance obtained. The R in the names of the materials stands for resistance.

In table 5.5 it is seen that after 5 immersions different values for the two FTO glass plates are obtained, while the simple glass plate has no change in the resistance measured. The values in resistance obtained indicated that the coating on the surface of FTOI was pri-

marily graphite rather than graphene. Likewise, the values for the FTOII indicated that the coating was made up of graphene.

The G60 part of the experiment had a different time parameter compared to G30. This would mean less dipping and the intention was to compare the two experiments in order to see if there were any differences in when the desired values of resistance would be obtained. The measured values are found in table 5.6.

Number of immersions	SGP R (Ω)	FTOI R (Ω)	FTOII R (Ω)
0	0	25	25
1	0	35-40	100
2	0	35-40	100
3	0	35-40	150
4	0	35-40	135
5	0	35-40	40-50 one place and 150 other

Table 5.6: Table shows the parameters used in the G60 Langmuir-Blodgett experiment and the values of resistance obtained. The R in the names of the materials stands for resistance.

As can be seen in table 5.6 the measured values differed from the ones in the G30 experiment. With the FTOI the experiment was completed after just one dip. This was done because the graphene-values were achieved already then. Rest of the time was used for annealing. However, the resistance was still measured each hour for the FTOI despite no more dipping was done. It was quickly concluded that the coating was graphene and only one immersion was therefore done. For the FTOII a change in resistance was quickly obtained, however the value was closer to the literature value of graphite rather than graphene. It was therefore decided that more immersions followed by more annealing should be done. The values measured stayed the same until the fifth dipping. After 5-6 hours of subsequent annealing it was found that in some areas the resistance value was closer to the graphene value in some areas, while it was graphite in others. When it came to the simple glass plate, no difference in measured resistance was seen throughout the 9 hour experiment.

The Langmuir-Blodgett experiment looks to have the capability to create graphene thin films[168]. But because it is difficult to separate between a graphene or graphite film on the surface of the FTO glass[169], it is reasonable to conclude that the method is not optimal because it would require having a large surplus of FTO glass, or at least a larger quantity of FTO glass than that to be deposited on. The success rate was in both the G30 and G60 experiments only 50 percent for the FTO and no difference was seen at all compared to other methods when the deposition was done on simple glass plates. To be considered a reliable production method of graphene thin films, the method should have a higher success rate than 50 percent. Because of this, despite the small sample size, it is therefore concluded that the method has capability, but is too random in if whether one can get graphene or graphite coating on the substrate.

5.3 Morphological characterization

5.3.1 Deposition on simple glass plates

The Doctor Blade method was used to apply graphene on a simple glass plate. Figure 5.4 is representative of the coating morphology of the films obtained with the method.

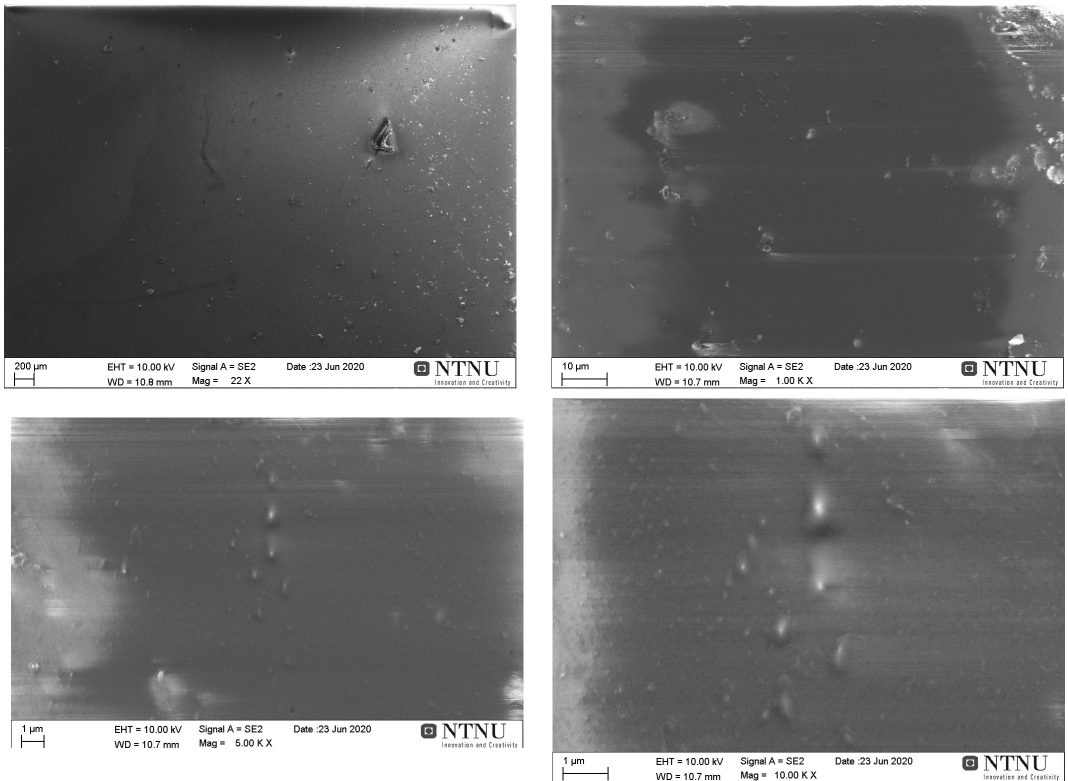


Figure 5.4: Image of the images taken with a SEM of the film obtained with the Doctor Blade method. The image on the upper left shows the 22x magnification, upper right shows the 1000x magnification, down left shows the 5000x magnification and down right shows the 10000x magnification

The $200 \mu\text{m}$ resolution shows a dark, non-transparent coating over the whole plate. With a single layer of graphene being almost completely transparent[18], and the transparency decreasing by the layer to the non-transparent graphite[34], an indication that the films are most likely graphene nanoplatelets. The $10 \mu\text{m}$ resolution shows two comparably different areas adjacent to each other. One area visibly darker than the other. This non-uniformity suggests the number of layers of graphene differ in the two areas. Some graphite aggregates can be observed on the $1 \mu\text{m}$ resolution images. These are likely to come from the blade's stakkato movement. With the reasoning for the hypothesis being the vertical line of the clumps.

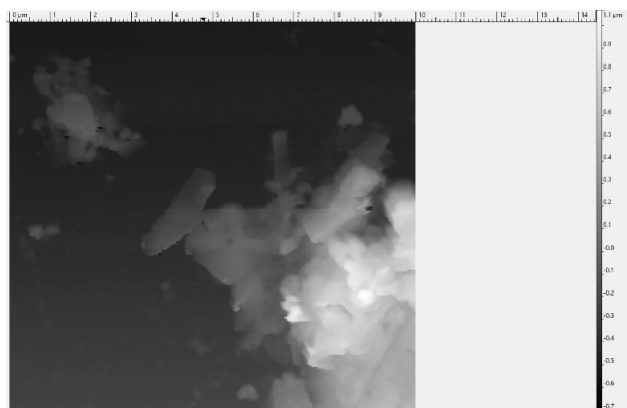


Figure 5.5: AFM image of the Doctor Blade sample

AFM of the graphene thin films fabricated with Doctor Blade, found on figure 5.5, shows a film thickness of $0.40 \mu\text{m}$, which again indicates close to 400 graphene layers. Meaning that it most likely is graphite. Furthermore, it can be seen that the film lacks uniformity and is non-coherent. Films that are not connected at the grain boundaries explain the limited conductivity measured at the macro-level [170, 171, 172].

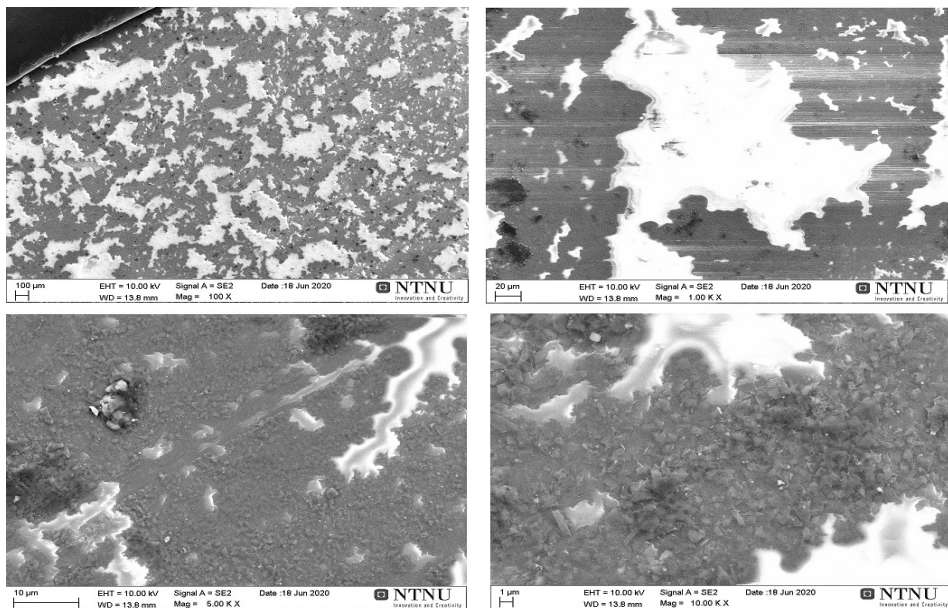


Figure 5.6: Image of the characterization done with the SEM tool on the films obtained by using the Drop Casting method. The upper left side shows the 100x magnification, the upper right side shows the 1000x magnification. While the two lower rows show the 5000x and 10000x magnifications respectively

The films obtained by the Drop Casting deposition method looked darker and more graphite-like when observed with an optical microscope. Figure 5.6 of the $100\ \mu\text{m}$ image shows a damascene[67] pattern. The pattern looks arbitrary, but is due to the reaggregation of graphene to graphite. LPE is a top-down production method where graphene is separated from graphite. A restacking commonly occurs when the material is dried out[173]. Drying is primarily done through temperature increase. Normally, the dispersed graphene flakes are stabilized against reaggregation by Coulomb repulsion due to the solvent[174]. Increasing the temperature over the boiling point of the solvent makes reaggregation the dominant mechanism[51]. This is further confirmed by the $10\ \mu\text{m}$ and $1\ \mu\text{m}$ resolution images where the grain boundaries of single crystal looks to have aggregated into graphite. The $20\ \mu\text{m}$ resolution showed that the film was non-uniform with large areas where coating had not occurred.

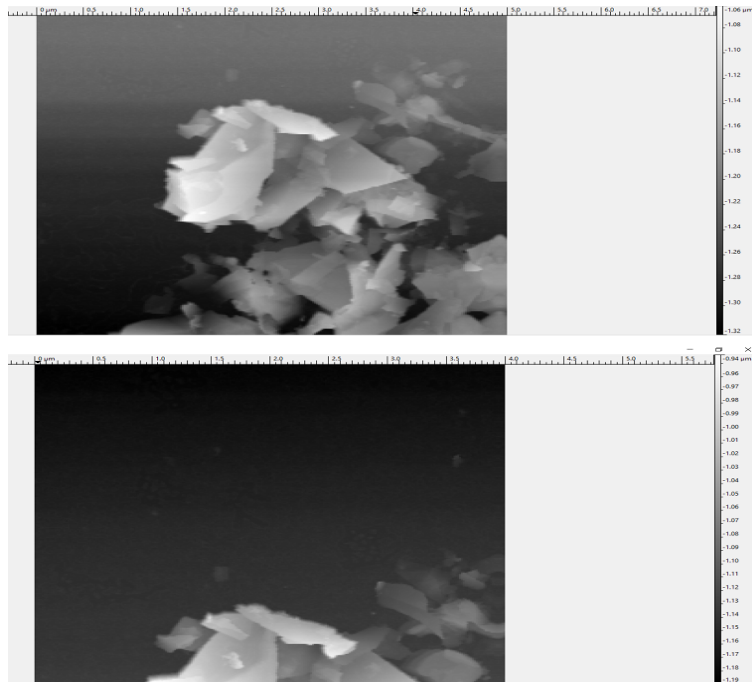


Figure 5.7: AFM image of the films obtained with the Drop Casting method. Both images show a film thickness of $0.25\ \mu\text{m}$. A aggregation of graphene layers can also be seen.

AFM was used on two separate areas of the film. These can be seen in figure 5.7. They both show film thickness of roughly $0.25\ \mu\text{m}$. This indicates some form of uniformity in the vertical dimension. However, as confirmed by the SEM images there is little uniformity in the lateral direction. A comparison between figures 5.5 and 5.7 shows that the single layers of graphene have restacked during the Drop Casting, while they were more dispersed when Doctor Blade was applied.

5.3.2 Deposition on conductive glass plates

An Electrodeposition on conductive glass was also performed. P13ED was, based on conductivity measurements, the sample that showed the highest promise. Figure 5.8 shows the SEM images of the sample with the $100\ \mu\text{m}$ and $10\ \mu\text{m}$ resolutions.

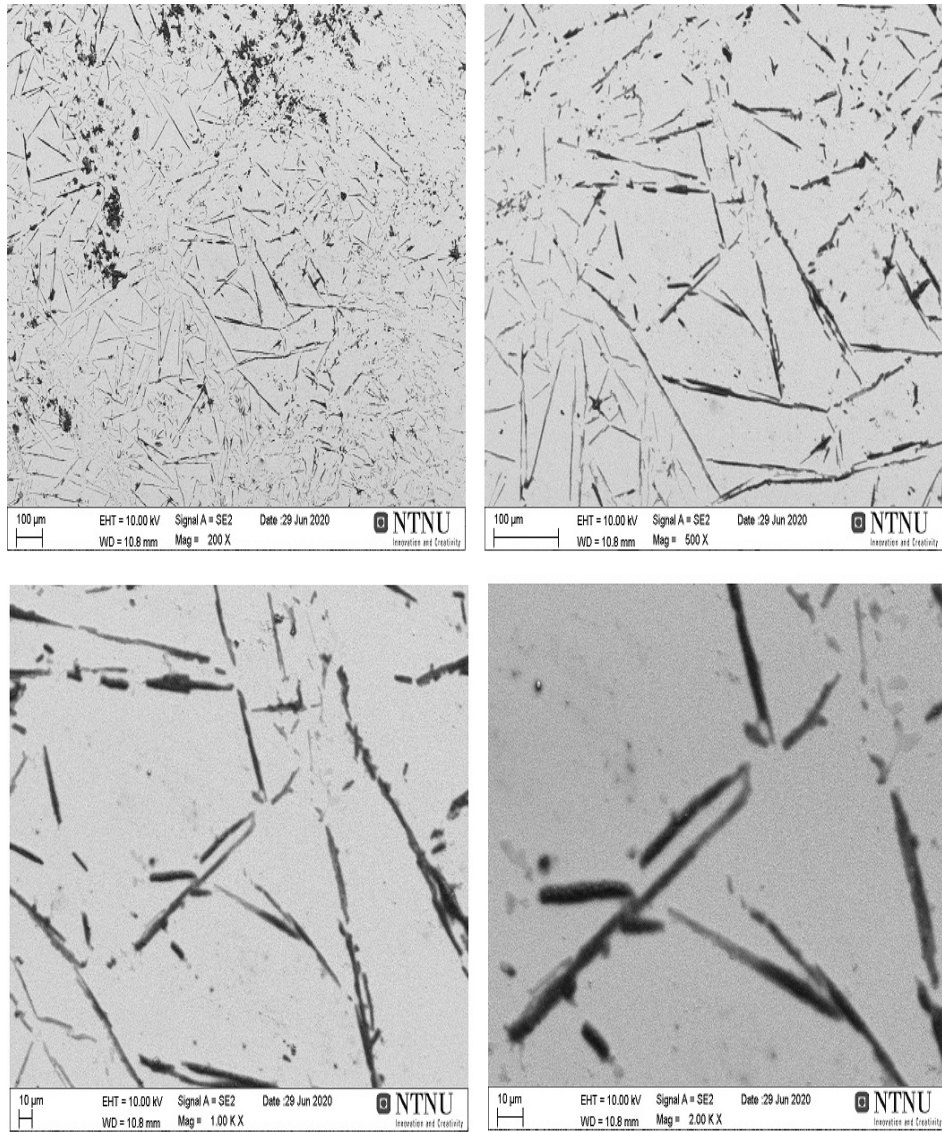


Figure 5.8: Shows the SEM images of sample P13ED at the magnifications 200x (upper left), 500x (upper right), 1000x (down left) and 2000x (down right)

Two areas can be discerned. The upper part shows puddles, while the lower part shows a

specific patterned film. Comparing this to figure 8.3 in the appendix, it can be seen that the graphene thin films deposited along the grain boundaries of F:SnO₂. Initially, this seems logical as the FTO pattern on the substrate is expected to conduct the electricity applied by the source meter and therefore promote the deposition. The magnifications further relay that the films surround an area or grain. Dong-Wook *et al.* have previously suggested a growth mechanism for TiO₂ nanorods on FTO glass[175]. It is believed that the grain boundaries act as nucleation sites during the early formation. Li *et al.* showed that the polycrystalline SnO₂ surface, with an isostructure with rutile TiO₂[176], provides favorable nucleation sites for the formation of nucleus. With solvent evaporation, it could be that Ostwald ripening could be a formation mechanism for graphene on the grain boundaries. The grain boundaries differentiate from the grains due to lower conductivity associated with it[177]. The dark complexion of the film indicates that some reaggregation has occurred. Because annealing was performed in this experiment, it could be that the conclusion found for Drop Casting, would be sufficient to explain the phenomenon. Because the film growth only occurs along the grain boundaries they are forced to reggregate due to space constraints.

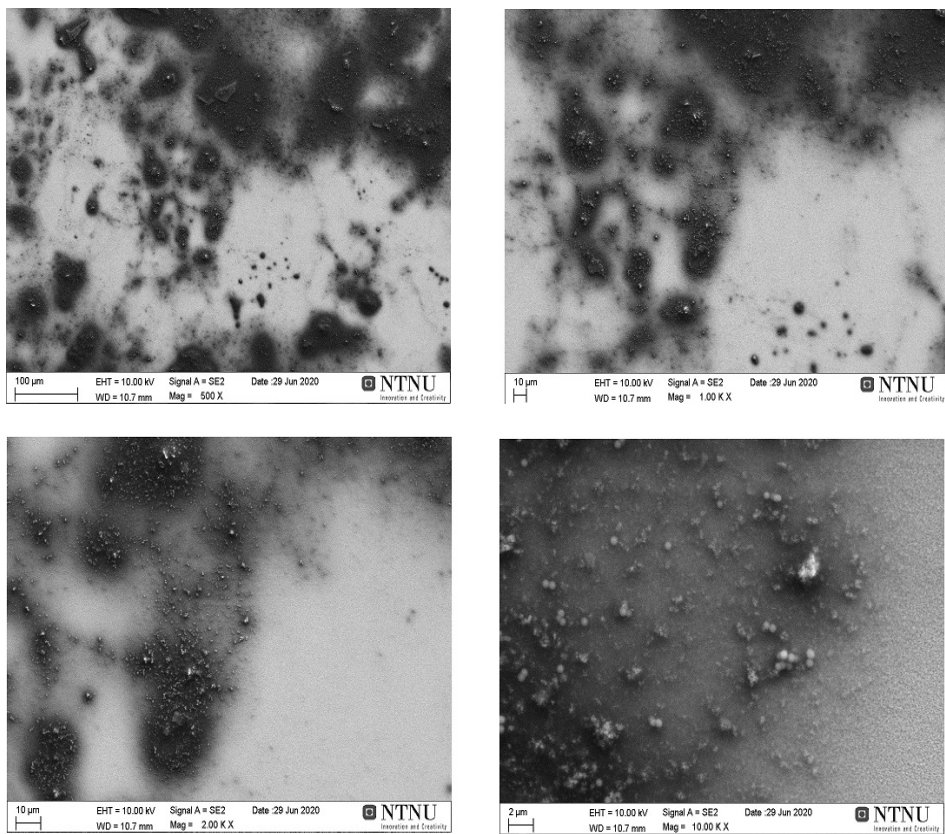


Figure 5.9: Shows the SEM images of sample P14ED at the magnifications 500x, 1000x, 2000x and 10000x

The characterization of sample P14ED was recorded on figure 5.9. The input voltage applied was +12 V rather than +20 V like for P13ED. A clear difference in film growth is seen. P14ED has many more puddles. Far fewer films growing along grain boundaries can be seen. Suggesting that the voltage applied was insufficient to produce a coating.

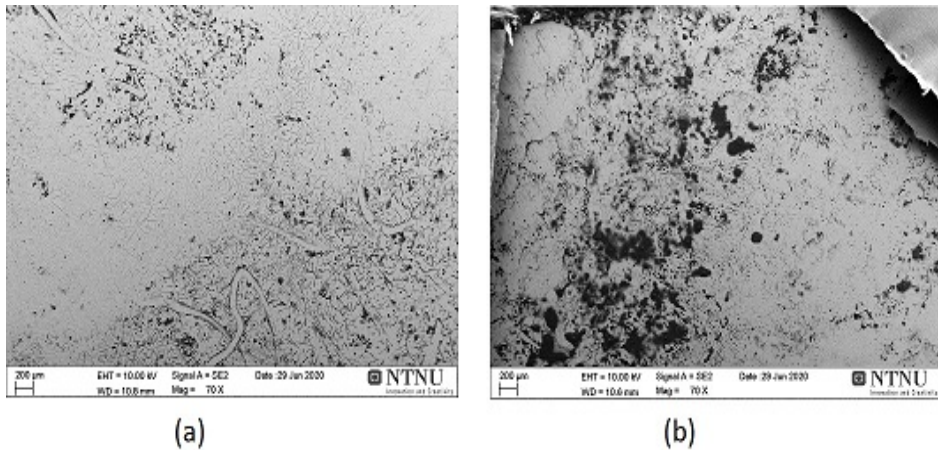


Figure 5.10: Image shows (a) P13ED with 70x magnification and (b) P14ED with 70x magnification

The differences can be clearly delineated on figure 5.10, where the same magnifications of the two samples are placed next to each other for comparison. Bereznev *et al.* listed how the films were interconnected, uniformity and adhesion to FTO as criteria for good deposition[178]. Based on that, P13ED showed good promise, while P14ED did not.

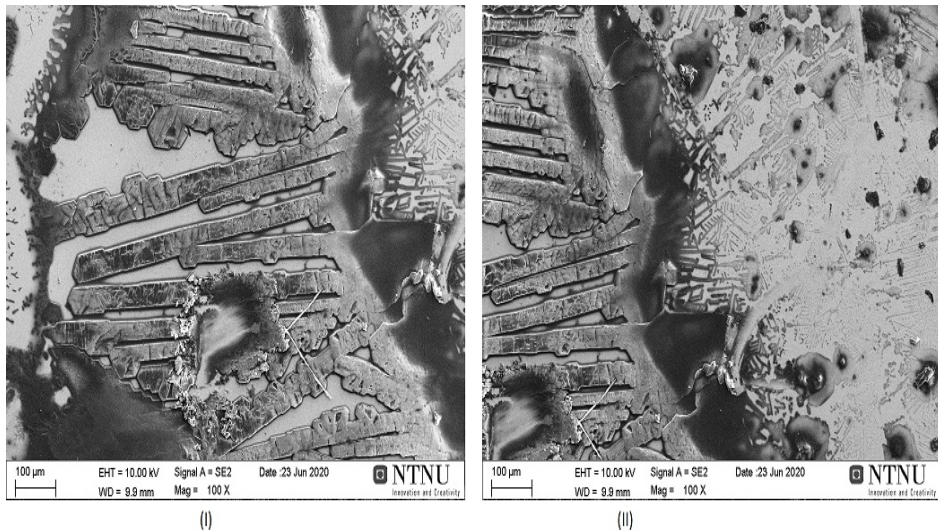


Figure 5.11: SEM image of two different areas on the P18ED sample with the 100x magnification

P18ED was a sample where the coating was produced by applying +20 V voltage for two hours. The SEM recording of two different areas with 100x magnification can be found on 5.11. Although, the areas are adjacent to each other, they both indicate a thicker film compared to P13ED and P14ED. The thicker films suggest that the growing has not occurred around the grain boundaries. This was investigated by taking a closer look at the two areas defined on figure 5.11, where the areas were denoted (I) and (II).

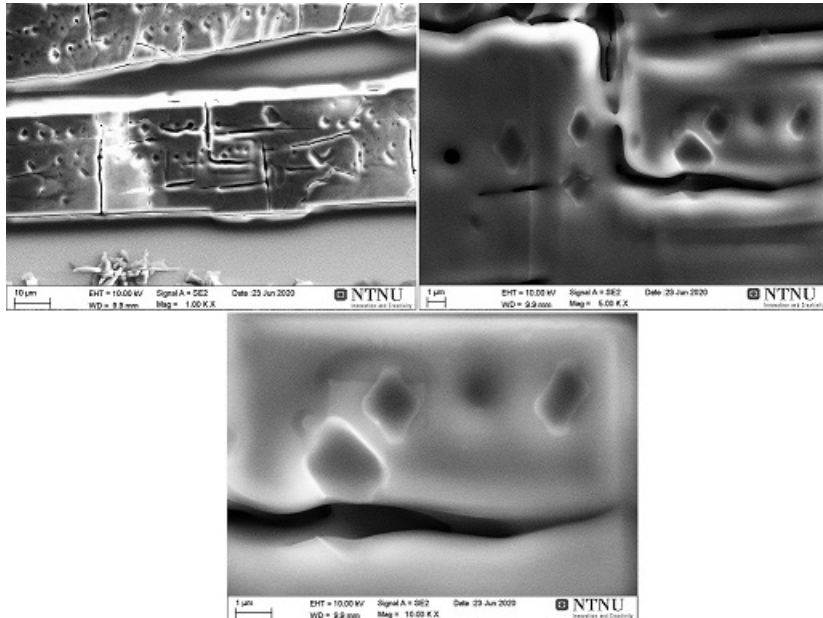


Figure 5.12: Recording of SEM images of the P18ED sample at the area denoted as area (I)

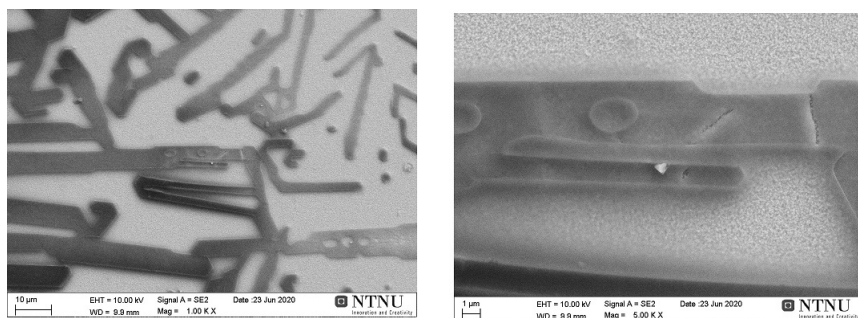


Figure 5.13: Recording of SEM images of the P18ED sample at the area denoted as area (II)

Recording of area (I) suggests that the film has advanced through the grain boundaries

because of reaggregation. However, the grains can be clearly identified. And, based on the conductivity measurements, it could have had adverse effect on the conductivity of the sample. Area (II) was comparable to the graphene thin films deposited on P13ED. Some defects like dislocations can be seen[51]. The next sample inspected was the P22ED. P22ED was made with Benzylamine instead of NMP. The electrolytes introduced to increase the conductivity in the film were composed of a solvent mixture. And the sample had big problems reaching the target current during measurements with the Four-point probe, and was a film considered to be less conductive than the samples made with NMP. The SEM recording with 70x and 200x magnifications can be found on figure 5.14.

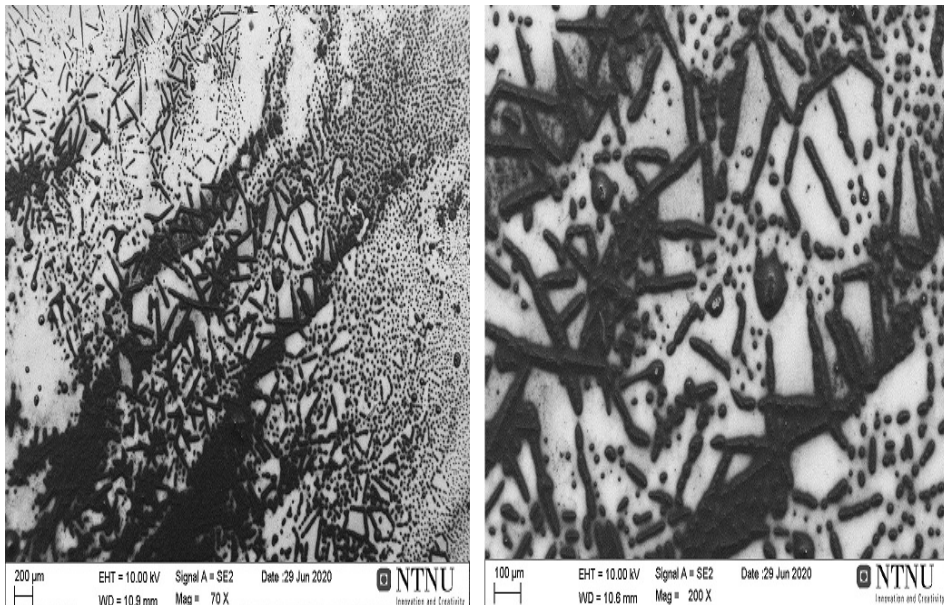


Figure 5.14: Recording of two SEM images of the surface of the P22ED taken with the 70x and 200x magnifications

SEM recordings of P22ED showed a film that nucleated and grew along the grain boundaries. Where it differentiated from P13ED was on the complexion of the films, which were clearly much darker in comparison. On the bottom layer of 70x, one can also see large puddles of film not deposited along the FTO layer. Having in mind that there were big problems with achieving the proper conductivity of the film, a possible explanation could be that the a certain conductivity is necessary to do the Electrodeposition process. Likewise, the quality (as defined by Bereznev *et al.*) of the graphene thin films was dependent on having the correct ratio of electrolyte and voltage applied in order for the deposition method to succeed.

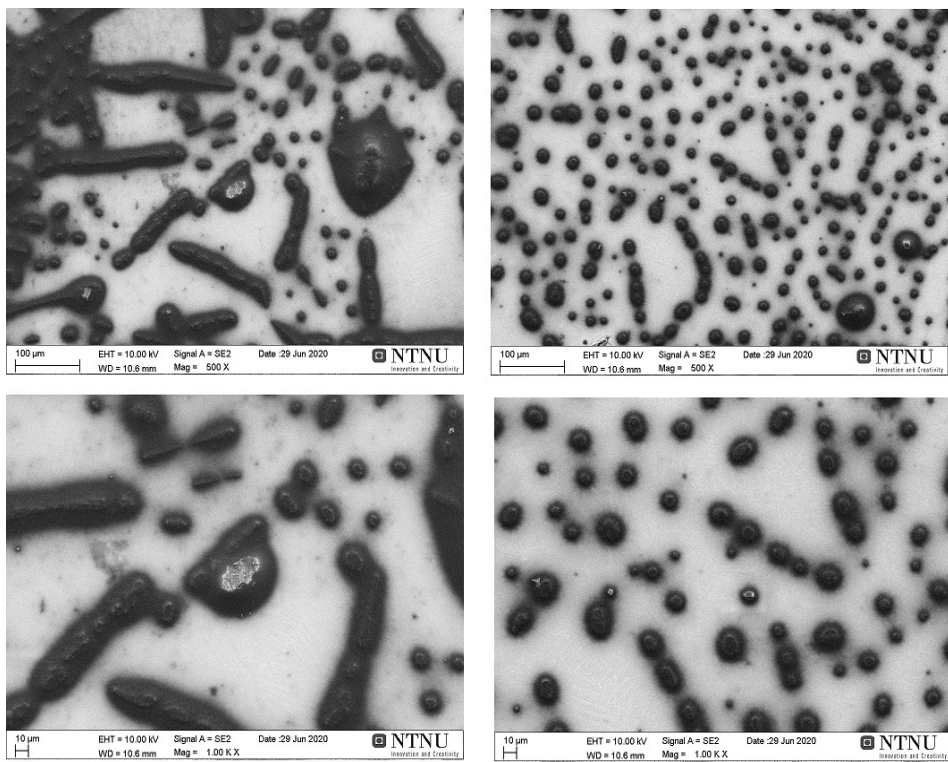


Figure 5.15: SEM recordings of four images of the P22ED sample. They show two different areas on the surface at two magnifications, 500x and 1000x. The upper image is 500x and the image immediately below it, represents the 1000x magnification

Figure 5.15 of the P22ED with stronger magnifications showed interrupted graphene thin film growth. The films have formed as a nucleus at the grain boundaries, but because of insufficient voltage/electrolyte have not grown along the boundary to become an interconnected film.

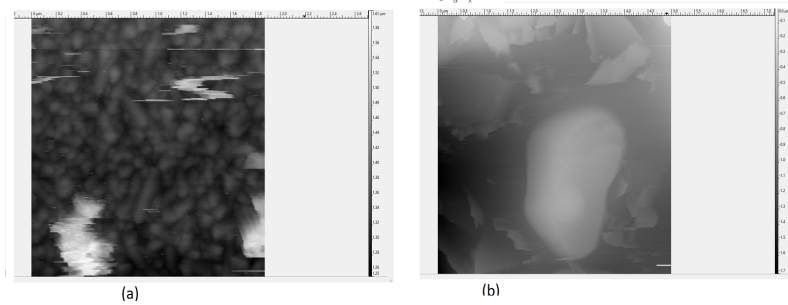


Figure 5.16: Recordings of the AFM of (a) P22ED and (b) P13ED

AFM images of the P13ED and P22ED were included to compare the film thickness. This was done on figure 5.16. The respective film thickness of the P13ED was $1.7 \mu\text{m}$ and P22ED was $0.4 \mu\text{m}$. The thicker film on P13ED meant that Electrodeposition had worked for a longer deposition time. On (a) one could see grain boundaries indicating several graphene monolayers aggregated into a graphite film. On (b) far fewer grain boundaries and thereby fewer graphene layers packed into the image. This was in line with the images from the SEM recordings.

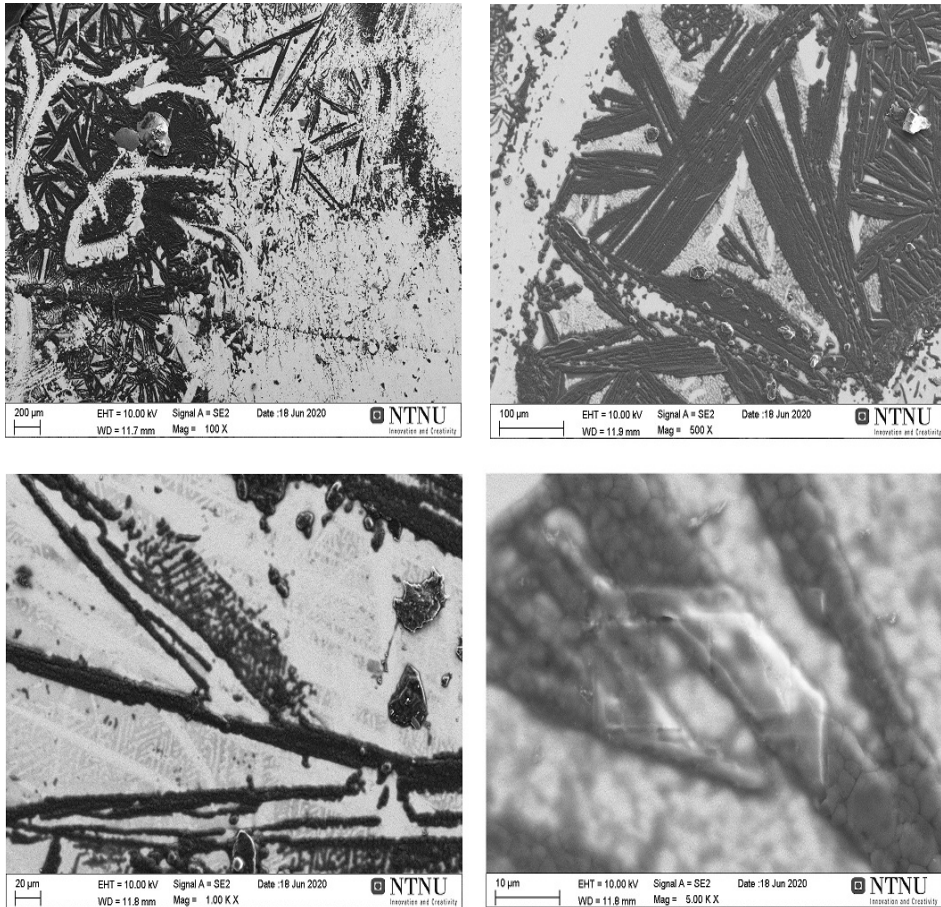


Figure 5.17: Four SEM images of a sample where negative current was applied. Upper left is 100x magnification, the upper right is 500x, the down left is 1000x and the down right is 5000x

The sample on figure 5.17 had -10 mA current applied for one hour. The films are grown in the characteristic pattern around a grain. However, the films are thick. Which suggests long enough deposition time to have negative effect on the conductivity.

5.4 Implementation of the graphene thin films in a DSSC

The J-V characteristics of the DSSC were measured with a Keithley 2450 under a Scientech SP300B solar simulator with a AM1.5 G filter, calibrated to $\frac{mW}{cm^2}$ with a Newport Reference Solar Cell and Meter (91150 V). All the cells were masked with a 0.159 cm² black mask before characterization. IPCE measurements were obtained from a device fabricated with a halogen lamp (Ocean Optics HL-2000), a monochromator (Spectral Products CM110), corrected to the Keithley 2450. The light intensity was determined using a NIST traceable photodiode (Thorlabs, FDS100-CAL). To characterize the graphene counter-electrode in a DSSC J-V plot was done on figure 5.18.

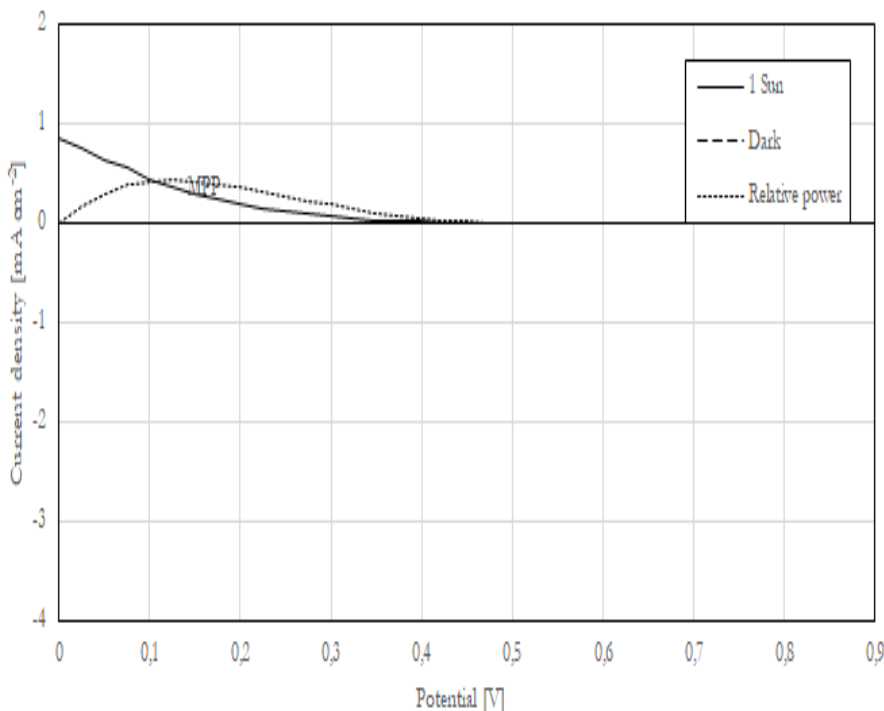


Figure 5.18: The J-V plot for the DSSC with graphene used as a counter-electrode

The J-V plot exhibits clear deviations from the “ideal J-V curve”. Examining characteristics (Table 5.7) we can clearly see a severely limited FF of 0.114 which indicates several competing (unwanted) processes taking place in the solar cell. Lowered values of J_{sc} (compared to reference solar cells) suggest that the photogenerated charges are lost in the closed solar cell circuit. This is in line with what we would expect to be caused by a bottleneck at the catalytic sites of the CE, which underperform with graphene instead of the reference Pt layer. Lower V_{oc} values are strange, since the change in the catalyst should not, in principle, affect the open circuit voltage. The only logical explanation

is perhaps that graphene nanoparticles have detached themselves from the CE and have circulated through the electrolyte to the active layer of N719 on TiO_2 , thus affecting the V_{oc} . This is therefore a clear indication of something going wrong, or that the graphene counter-electrode did not work as it was supposed to. To further investigate this, the EQE vs wavelength is presented in figure 5.19.

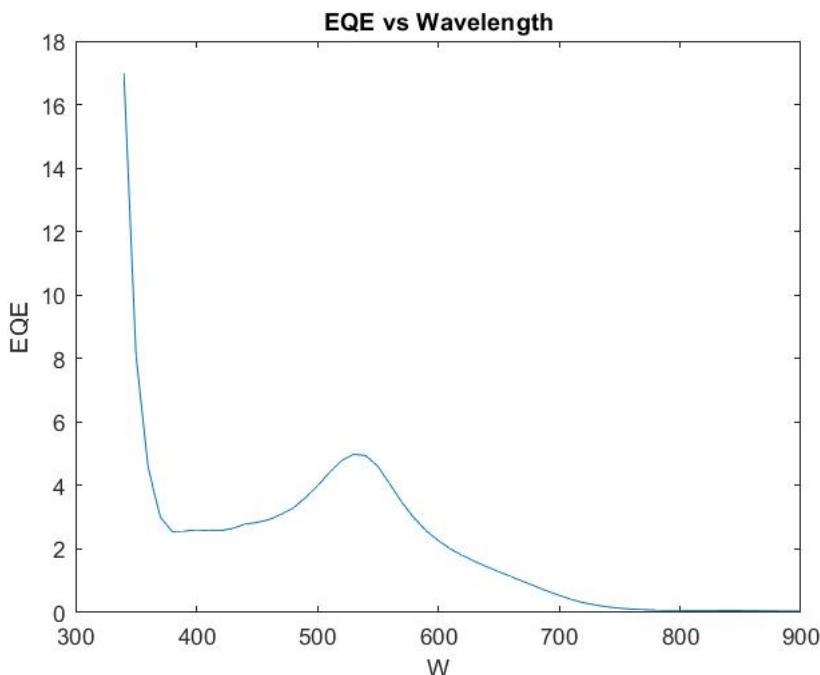


Figure 5.19: Plot of the EQE vs wavelength for the DSSC.

External quantum efficiency (EQE) measurements provide an quantifiable way to calculate the number of photogenerated electrons per number of incident photons. The EQE plot is presented in Figure 5.19 and revealed a maximum of 5% at 540 nm. This value is extremely low compared to typical values of 60-80% for the reference DSSC. This provides additional evidence that there are severe limitations to the flow of electrons in the solar cell.

Parameters	Graphene	Pt
V_{MPP}	0.125 V	0.450 V
J_{MPP}	0.366 mA/cm ²	6.329 mA/cm ²
$Power_{out}$	0.046 mW/cm ²	2.848 mW/cm ²
Total power _{out}	0.288 mW	17.912 mW
J_{SC}	0.864 mA/cm ²	7.136 mA/cm ²
V_{OC}	0.463 V	0.573 V
FF	0.114	9.697
Efficiency	0.046 %	2.848 %
Cell active area	0.159 cm ²	0.159 cm ²

Table 5.7: Table shows the different values obtained for the different parameters when the DSSC was tested with a graphene counter electrode and a Pt counter electrode.

Based on the plots and the results achieved, where especially the efficiency is given particular importance, it was concluded that the graphene thin films that were manufactured were not capable of functioning as a counter electrode in a DSSC. The reasons for the failure could be several. A credible theory could be that the films on the sample had reaggregated to graphene nanoplatelets[108] and thereby lacked both the necessary conductivity[31] and transparency to function as intended. All indications suggested single layers of graphene would work[179]. It should also be mentioned that during the testing the Pt did not provide a very good power conversion efficiency at only 2.8 percent. But the measured value at 0.046 percent is still far away from achieving that result. A second attempt was made later, but the results did not improve.

5.5 The absorbance of the graphene thin films

The absorption was measured with a U-1900 Spectrophotometer from Hitachi. In circumstances involving vertical incident light, there should be expected an optical absorption of approximately 2.3 percent for single layer graphene[18]. In agreement with the literature, the expectation was an absorption peak on the UV-Vis plot at around 300 nm. The sample that was investigated was P13ED. Only one sample is presented in order to avoid repetitive paragraphs since the results were almost identical. An ultraclean blank FTO glass plate was used as a baseline, in accordance with standard procedure.

The only sample investigated in this section was the P13ED, assumed to be the best sample based on conductivity measurements and material characterization. P13ED showed an absorption peak at 300 nm and a wide absorption peak can be seen. The rest of the line follows the baseline of the FTO glass plate unpatterned.

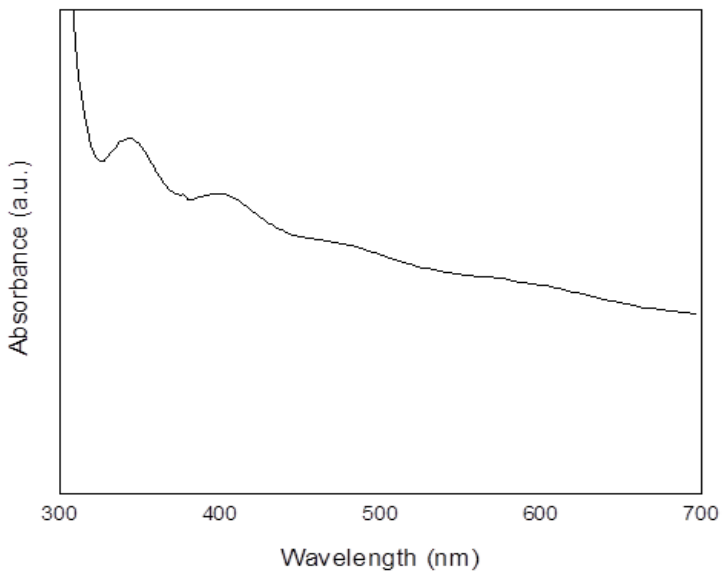


Figure 5.20: Plot of the absorbance spectrum for the P13ED sample.

The absorption spectrum for the samples was as anticipated. A single layer of graphene has 98 percent transmission[18], suggesting very little absorption. Implying that the absorption spectrum seen in the plot reflects FTO with a transmission closer to 80 percent with an absorption peak at 300 nm[180]. This was confirmed. Lalasari *et al.* found that thicker film on F:SnO₂ resulted in less light passing through[181]. Comparing P13ED and P14ED (found in the appendix) in this regard, and by referring to the morphology section, it is seen that adding a layer of graphene to FTO films either suggests this to not be true or, the deposited material is in fact a single layer graphene. The absorbance spectrum of P14ED is skewed, meaning that the Electrodeposition was not complete and the film is graphitic in nature. This was also indicated by the SEM images.

Conclusion and Future Work

This thesis presented a project where the intention was to develop conductive graphene thin films through various deposition techniques. Although the conductivity varied greatly in the numerous samples prepared, there were still conductivity in all of them (with the exception of those developed with the Spin Coating method).

By using several characterization tools, like SEM, AFM and Four point probe, an experimental procedure was developed towards a deposition of exfoliated graphene. The characterization tools were used to differentiate between conductivity, film morphology and absorbance. With that in mind, it was concluded that Electrodeposition gave the highest quality graphene thin films when all variables were taken into consideration.

It is concluded that the most important factor for obtaining a good film was the combined factor of applied voltage and number of electrolytes in the solution. The time parameter that gave the best result at +20 V applied voltage was decided to be one hour.

Of the other methods, the Langmuir-Blodgett was the closest to achieve conductivity comparable to the one obtained with the Electrodeposition. The three other methods, Drop Casting, Spin Coating and Doctor Blade were less successful. Despite that, some minor conductivity was observed. Low conductivity in the films was more likely the result of lack of connectivity/coherency/uniformity in the films. Morphological characterization of the films proved that initial explanation. Morphological study of the electrodeposited thin films showed graphene forming along the grain boundaries of the FTO patterned substrate. Increasing the deposition time led to films that crossed the boundaries on to the grain-areas. This had a negative effect on the conductivity of the sample.

P13ED was the sample that looked to overall have the best properties with, conductivity values high as 1.333e5 S/m. Material characterization showed that the films looked to have the best adhesion to the pattern on the conductive FTO surface. The absorbance was also satisfactory. From this it was inferred that the process of +20 V voltage sent in for

an hour in an Electrodeposition was the best method to achieve the desired graphene thin films.

A secondary objective of the work on this thesis was to try out the graphene thin films coated on a FTO glass plate as a counter electrode in a DSSC. This was not considered a success. Graphene as a transparent conducting layer with these methods was tested in a UV-Vis Spectrophotometer. The result from both conductivity tests and absorbance spectrum indicates that the graphene thin films have considerable potential in future applications. Both conductivity and absorbance showed optimal values in accordance with the expected literature values. However, it must be emphasized that more work is needed. Examples of such work would be trying out a different electrolyte/salt, an attempt at finding out the optimal deposition time for patterning the FTO glass with graphene, a graphene-solvent solution more suited to the task at hand and perfecting the mechanism of the film growth along the grain boundaries.

Experimental section

7.1 Chemicals and Materials

All the chemicals were used as received. The product specification of the graphite used to create graphene is: flakes, 99 percent carbon basis, -325 mesh particle size (\geq 99 percent), natural. Graphite grade 230 U, 808067-2.5 KQ, Lot # MKBX6591V, Sigma Aldrich, produced in the USA.

The FTO glass plates were of the type TEC10 from Sigma Aldrich. Dimensions varied after what use they were for. The simple glass plates had the dimensions 25mm*75mm. These substrates were cleaned by ultra sonication in acetone, isopropanol alcohol (IPA) and methanol for 10 min each, followed by rinsing in de-ionized (DI) water and drying in N2 gas before use. The chemicals used were the solvents N-methyl-2-pyrrolidone (NMP) and Benzylamine.

7.2 Production of exfoliated graphene

50 mg/ml of graphite were added to 10 ml of Benzylamine or NMP. The solution was then placed in a tip horn sonicator with a corresponding 300 ml ice bath placed beneath it to keep the sonicating mixture from overheating. The duration of sonication was 30 minutes followed by 30 minutes in a fume hood. Following the sonication, the mixture was centrifuged at 4000 RPM for 4 minutes. This parameter was held fixed throughout the experiment. The centrifugation was done by a Heraeus Labofuge 300. Only the supernatant was used for all deposition techniques.

7.3 Methods used to fabricate the films

7.3.1 Electrodeposition experimental procedure

Pt and FTO were used as electrodes. Optimal size dimension of the electrodes was 10 mm * 10 mm. The amount of NMP and salt (electrolyte) is measured out. Graphene and NMP was used as electrolytic bath in the 30 ml beaker. A ratio of NMP and salt and NMP and graphene at 1:1 showed efficiency. The voltage applied was +20 V. Deposition time was one hour. This time was decided after careful consideration and multiple attempts with other deposition times.

7.3.2 Langmuir-Blodgett experimental procedure

A FTO glass plate was slowly immersed in small 30 ml beaker containing centrifuged exfoliated graphene. Then it was slowly pulled out. A tweezer was used for this task. The glass plate was put on a hot plate with a temperature of 100 °C. The conductivity was measured after the annealing. If desired conductivity was reached, the experiment was aborted. If not, the glass plate is immersed in the beaker again.

7.3.3 Drop Casting experimental procedure

The hotplate used was a Corning PC-400. The experimental procedure consisted of taking the supernatant parts of the solution containing graphene with a pipette and depositing it on a glass plate. Then different parameters of annealing were used. One example was first hour at 100 °C, second hour held fixed at 200 °C and final hour at 300 °C.

7.3.4 Doctor Blade experimental procedure

Doctor Blade procedure was done on a MSK-AFA II. The coating was performed with a glass that holds the substrate on a fixed position when the blades crosses it. The equipment was cleaned with acetone before and after the experiment. The glass substrate to be coated is filled with exfoliated graphene on it. The filling is done according to the amount of film coating wanted.

7.4 Characterization Methods

AFM images were recorded by the BioScope Catalyst AFM from Bruker. The tool is integrated with an inverted Axio observer. No sample preparation, like glass cutting or similar procedures, was needed because the dimensions of the glass plates was appropriate for insertion in to the equipment. Included in the AFM equipment was an optical microscope, thereby giving the ability to investigate the samples with it in addition.

SEM images were recorded by a Fe-SEM (Zeiss Ultra 55 LE). The SEM was of the thermal field emission type. Because the samples were dry, not much preparation was needed. However, it was mandatory to store them at the EMLab facility the day before a sample

investigation. They were stored in a refrigerator and packed in a Al-foil. The foil packaging was limited to the parts that were not inspected with the SEM.

UV-inspection was done with a U-1900 from Hitachi. The samples were first cleaned with acetone and then taped firmly to the sensing element on the equipment with ordinary scotch tape.

Electrical conductivity measurements were done with a Four-point probe from Ossila and a multimeter. A Keithley 2450 was also employed for this task on samples that could not reach the target current of the Four point probe.

7.5 Fabrication of the Solar Cell

The method used on fabricating the Solar Cell is based on previously reported procedures by Buene *et al.* and Hora *et al.*[182, 183]. The anodes were prepared from FTO glass (TEC10, Sigma Aldrich), which was cleaned in a KOH-solution (150 g/L) in 70 wt% ethanol under sonication for 45 minutes. Immersion of the glass in aqueous TiCl_4 -solution (40 mM) at 70 °C for 2 × 45 minutes followed by rinsing with deionized water and ethanol was carried out to deposit a blocking layer on the FTO-sample. The layer of TiO_2 formed was sintered at 500 °C for an hour.

Pastes of TiO_2 were screen printed onto the FTO (mesh count 54, thread diameter 64 mm, area 0.2826 cm²), first two active layers (18NR-T, Dyesol) were printed, with 10 minutes heating on a hotplate at 120 °C after each layer. A scattering layer (WER2-O, Dyesol) was ultimately printed, and the TiO_2 was sintered in a programmable furnace (Nabertherm LT 9/12) at set temperatures of 125, 250, 325, 450, and 500 °C for 5, 5, 5, 15, and 15 minutes with a ramping time of 10 minutes. Before staining the electrodes were annealed at 500 °C for 30 minutes, using a hot air gun.

The counter electrodes were prepared from TEC10 FTO glass supplied by Sigma Aldrich. Holes were drilled into the electrodes from the FTO-side using a diamond drill bit, this procedure was carried out under water. The glass plates were then cleaned using Deconex 21 (aq., 2 g/L), deionized water, ethanol, and acetone, in a ultrasonic bath for 15 minutes for each. A solution of H_2PtCl_6 (10 mM in 2-propanol) was dropcast (5 $\mu\text{L}/\text{cm}^2$) on the FTO before heating at 400 °C for 15 minutes with a hot air gun formed the catalytic layer of Pt.

The photoanodes were placed in the dye bath while still holding 80 °C from the annealing-procedure and stored in an oven at 30 °C overnight. The dye baths were prepared using a mixture of acetonitrile and THF (43/57, v/v) to make a solution of dye and co-adsorbent CDCA, at concentrations of 0.5 mM and 5 mM respectively. The staining of the reference N719 was done similarly, but the solvent used was in this case ethanol. Following 15 hours of staining the electrodes were rinsed in acetonitrile for 2 minutes, then sealed to the counter electrode using Surlyn (25 μm , Solaronix) in a drybox. A 4 * 20 second treatment of the cell using a 50 W PTC heat element was sufficient to seal the cells. The electrolyte

was vacuum backfilled into the device, the filling-hole was sealed with Surlyn and a glass cover disk, then to complete the devices the electrodes were painted with silver conducting paint (Electrolube, SCP). The electrolyte employed was the A6141 electrolyte, consisting of butylmethylimidazolium iodide (0.60 M), I₂ (0.03 M), guanidinium thiocyanate (0.1 M), and t-butylpyridine (0.50 M) dissolved in acetonitrile/valeronitrile (85/15, v/v)[184].

Bibliography

- [1] Randviir, E. P.; Brownson, D. A.; Banks, C. E. *Materials Today* **2014**, *17*, 426–432.
- [2] Spyrou, K.; Rudolf, P. *Functionalization of Graphene*, 1st ed.; Wiley: Hoboken, New Jersey, 2014; Chapter Introduction to Graphene.
- [3] Novoselov, K. S.; Falko, V. I.; Colombo, L.; Gellert, P. R.; Schwab, M. G.; Kim, K. *Nature* **2012**, *490*, 192–200.
- [4] Katsnelson, M. I. *Materials Today* **2007**, *10*, 20–27.
- [5] Geim, A. K.; Novoselov, K. S. The rise of graphene. 2007.
- [6] Clegg, B. *The Graphene Revolution - The weird science of the ultra-thin*; Hotscience: London, 2018.
- [7] Castro Neto, A. H.; Guinea, F.; Peres, N. M. R.; Novoselov, K. S.; Geim, A. K. *Rev. Mod. Phys.* **2009**, *81*, 109–162.
- [8] Li, B.; Ou, P.; Wei, Y.; Zhang, X.; Song, J. *Materials (Basel)* **2018**, *11*.
- [9] Dash, S.; Patnaik, A. *IEEE International Conference on Antenna Innovations Modern Technologies for Ground, Aircraft and Satellite Applications (iAIM)* **2017**, 2017, 1–4.
- [10] Landau, L. D. *Phys. Z. Sowjetunion* **11**, 26–35.
- [11] Peierls, R. *Annales de l'institut Henri Poincaré* **1935**, *5*, 177–222.
- [12] Mermin, N. D. *Phys. Rev.* **1968**, *176*, 250–254.
- [13] Kittel, C. *Introduction to Solid State Physics*; John Wiley and Sons, Inc, 1953.
- [14] Nelson, D.; Piran, T.; Weinberg, S. *Statistical Mechanics of Membranes and Surfaces*; Default Book Series, 2004.
- [15] Nelson, D.; Peliti, L. *J. Phys. France* **1987**, *48*, 1085–1092.

-
- [16] Gui, G.; Zhong, J.; Ma, Z. *Journal of Physics Conference Series* **2012**, *402*, 2004.
 - [17] Manchala, S.; Tandava, V. S. R. K.; Jampaiah, D.; Bhargava, S.; Shanker, V. *ACS Sustainable Chemistry Engineering* **2019**, *7*, 11612–11620.
 - [18] Sang, M.; Shin, J.; Kim, K.; Yu, K. *Nanomaterials (Basel)* **2019**, *9*, 374.
 - [19] Yin, L.-J.; Li, S.-y.; Qiao, J.; Nie, J.; He, L. *Physical Review B* **2015**, *91*.
 - [20] Zhang, Y.; Tan, Y.; Stormer, H.; Kim, P. *Nature* **2005**, *438*, 201–204.
 - [21] Novoselov, K. S.; Jiang, Z.; Zhang, Y.; Morozov, S. V.; Stormer, H. L.; Zeitler, U.; Maan, J. C.; Boebinger, G. S.; Kim, P.; Geim, A. K. *Science* **2007**, *315*, 1379–1379.
 - [22] Das, S.; Pandey, D.; Thomas, J.; Roy, T. *Advanced Materials* **2018**, *31*, 1802722.
 - [23] McCann, E. *NanoScience and Technology* **2011**, 237–275.
 - [24] Kogan, E.; Nazarov, V.; Silkin, V.; Kaveh, M. *PHYSICAL REVIEW B* **2013**, *89*, 165430.
 - [25] Wallace, P. R. *Phys. Rev.* **1947**, *71*, 622–634.
 - [26] Wang, H.; Zhao, H.; Hu, G.; Li, S.; Su, H.; Zhang, J. *Scientific Reports* **2015**, *5*, 18258.
 - [27] Shaw, G.; Mandl, F. *Quantum Field Theory, Second Edition*; Wiley, 2010.
 - [28] Thomson, M. *Modern Particle Physics*; University of Cambridge University Printing House: Cambridge, 2013.
 - [29] Sahu, S.; Rout, G. *International Nano Letters* **2017**, *7*, 81–89.
 - [30] Ariel, V. *arXiv: General Physics* **2012**, 1–5.
 - [31] Mousavi, H.; Khodadadi, J. *TheScientificWorldJournal* **2014**, *2014*, 581478.
 - [32] Balandin, A.; Ghosh, S.; Bao, W.; Calizo, I.; Teweldebrhan, D.; Miao, F.; Lau, J. *Nano letters* **2008**, *8*, 902–907.
 - [33] Tian, M.; Huang, Y.; Wang, W.; Li, R.; Liu, P.; Liu, C.; Zhang, Y. *Journal of Materials Research* **2014**, *29*, 1288–1294.
 - [34] Ma, Y.; Zhi, L. *Small Methods* **2019**, *3*, 1800199.
 - [35] Lee, S.; Jo, Y.; Hong, S.; Kim, D.; Lee, H. W. *Current Optics and Photonics* **2017**, *1*, 7–11.
 - [36] Fasolino, A.; Los, J.; Katsnelson, M. *Nature materials* **2007**, *6*, 858–61.
 - [37] Lee, S.; Zhong, Z. *Nanoscale* **2014**, *6*, 13283–13300.
 - [38] Zhu, Y.; Murali, S.; Cai, W.; Li, X.; Suk, J. W.; Potts, J. R.; Ruoff, R. S. *Advanced Materials* **2010**, *22*, 3906–3924.
-

-
- [39] Lourtioz, J.-M.; Lahmani, M.; Dupas-Haeberlin, C.; Hesto, P. *Nanosciences and Nanotechnology*; Springer, 2016.
- [40] Wang, X.; Shi, Y. *RSC Nanoscience and Nanotechnology* **2014**, *32*, 1–30.
- [41] Picraux, S. T. *Encyclopedia Britannica* **2020**,
- [42] Rudrapati, R. *Graphene: Fabrication Methods, Properties, and Applications in Modern Industries*; InTechOpen, 2020; pp 9–22.
- [43] Zhu, Y.; Ji, H.; Cheng, H.-M.; Ruoff, R. *National Science Review* **2018**, *5*, 90–101.
- [44] Habiba, K.; Makarov, V.; Weiner, B.; Morell, G. *Fabrication of Nanomaterials by Pulsed Laser Synthesis*; 2014; pp 263–291.
- [45] Hummers, W. S.; Offeman, R. E. *Journal of the American Chemical Society* **1958**, *80*, 1339–1339.
- [46] Stankovich, S.; Dikin, D.; Dommett, G.; Kohlhaas, K.; Zimney, E.; Stach, E.; Piner, R.; Nguyen, S.; Ruoff, R. *Nature* **2006**, *442*, 282–286.
- [47] Moon, I.; Junghyun, L.; Ruoff, R.; Lee, H. *Nature communications* **2010**, *1*, 73.
- [48] Boukhvalov, D.; Katsnelson, M. *Journal of the American Chemical Society* **2008**, *130*, 10697–701.
- [49] Gao, W.; Alemany, L.; Ci, L.; Ajayan, P. *Nature chemistry* **2009**, *1*, 403–408.
- [50] Said, M.; Hidayah, N.; Liu, W. W.; Lai, C. w.; Zulkepli, N. N.; Khe, C.-S.; Hashim, U.; Lee, H. C. *AIP Conference Proceedings* **2017**, *1892*, 150002.
- [51] Callister, W. D.; Rethwisch, D. G. *Material Science and Engineering*; Wiley, 2011.
- [52] Xu, Y.; Cao, H.; Xue, Y.; Li, B.; Cai, W.-H. *Nanomaterials* **2018**, *8*, 942.
- [53] Radamson, H. H. *Springer Handbooks* ; Springer, 2017; QC 20200624.
- [54] Ciesielski, A.; Samori, P. *Chem.Soc.Rev* **2014**, *43*, 381–398.
- [55] Lucasen, S. M. Synthesis and evaluation of nanohybrid materials for the solid-phase extraction of trace organic pollutants from water samples. 2020.
- [56] Bhoria, R. *Enhancing Liquid Phase Exfoliation of Graphene in Organic Solvents with Additives*; InTechOpen, 2019; pp 1–15.
- [57] Khan, U.; Gallagher, A.; Lotya, M.; De, S.; Coleman, J. *Small (Weinheim an der Bergstrasse, Germany)* **2010**, *6*, 864–71.
- [58] Economopoulos, S.; Rotas, G.; Miyata, Y.; Shinohara, H.; Tagmatarchis, N. *ACS Nano* **2010**, *4*, 7499–7507.
- [59] Sharma, V.; Garg, A.; Sood, S. C. *International Journal of Engineering Trends and Technology (IJETT)* **2015**, *26*, 38–42.

-
- [60] Solomons, G.; Fryhle, C.; Snyder, S. *Organic Chemistry*; Wiley, 2014.
- [61] Qiu, X.; Bouchiat, V.; Colombet, D.; Ayela, F. *RSC Advances* **2019**, *9*, 3232–3238.
- [62] Liangchuan, L.; Ming, Z.; Long, J.; Lincong, L.; Youtang, M.; Xiao, L.; Zhaoyou, M.; Zhenzhao, L.; Shengli, Y.; Hongwei, Z. *Frontiers in Materials* **2019**, *6*, 325.
- [63] Coello Fiallos, D. LOW DIMENSIONAL MATERIALS. Ph.D. thesis, University of Calabria, 2017.
- [64] Krane, N.; Krane, N. K. Preparation of Graphene Selected Topics in Physics: Physics of Nanoscale Carbon. 2011.
- [65] Bonaccorso, F.; Lombardo, A.; Hasan, T.; Sun, Z.; Colombo, L.; Ferrari, A. C. *Materials Today* **2012**, *15*, 564–589.
- [66] Costa, M.; Ribeiro, H.; Kessler, F.; Souza, E.; Fechine, G. J. M. *Materials Research Express* **2016**, *3*, 025303.
- [67] Quirk, M.; Serda, J. *Semiconductor Manufacturing Technology*; Prentice Hall: Taiwan, 2001.
- [68] Yang, X.; Zhang, G.; Prakash, J.; Chen, Z.; Gauthier, M.; Sun, S. *International Reviews in Physical Chemistry* **2019**, *38*, 149–199.
- [69] Martin, P. *Handbook of Deposition Technologies for Films and Coatings*; Elsevier, 2010.
- [70] Zhang, Y.; Zhang, L.; Zhou, C. *Accounts of chemical research* **2013**, *46*, 2329–2339.
- [71] Munoz, R.; Gomez-Aleixandre, C. *Chemical Vapor Deposition* **2013**, *19*, 297–322.
- [72] Pessoa, R.; Fraga, M.; Vieira, L.; Galvão, N.; Maciel, H.; Massi, M. *Plasma-assisted techniques for growing hard nano-structured coatings: An overview*; 2014; pp 455–479.
- [73] Kalita, G.; Tanemura, M. *Fundamentals of Chemical Vapor Deposited Graphene and Emerging Applications*; InTechOpen, 2017.
- [74] Li, X.; Cai, W.; An, J.; Kim, S.; Nah, J.; Yang, D.; Piner, R.; Velamakanni, A.; Jung, I.; Tutuc, E.; Banerjee, S.; Colombo, L.; Ruoff, R. *Science (New York, N.Y.)* **2009**, *324*, 1312–4.
- [75] Hansora, D.; Shimpi, N.; Mishra, S. *JOM* **2015**, *67*, 2855–2868.
- [76] Eigler, S.; Hirsch, A. *Angewandte Chemie International Edition* **2014**, *53*, 7720–7738.
- [77] Simpson, C.; Brand, J.; Berresheim, A.; Przybilla, L.; Räder, H.; Müllen, K. *Chemistry (Weinheim an der Bergstrasse, Germany)* **2002**, *8*, 1424–1429.

-
- [78] Choucair, M.; Thordarson, P.; Stride, J. *Nature nanotechnology* **2009**, *4*, 30–33.
- [79] Speyer, L.; Fontana, S.; Cahen, S.; Ghanbaja, J.; Medjahdi, G.; Hérold, C. *Solid State Sciences* **2015**, *50*, 42–51.
- [80] Yazdi, G.; Iakimov, T.; Yakimova, R. *Crystals* **2016**, *6*, 53.
- [81] Heer, W.; Berger, C. *Journal of Physics D Applied Physics* **2012**, *45*, 150301.
- [82] Richter, N.; Hernandez, Y. R.; Schweitzer, S.; Kim, J.-S.; Patra, A. K.; Englert, J.; Lieberwirth, I.; Liscio, A.; Palermo, V.; Feng, X.; Hirsch, A.; Müllen, K.; Kläui, M. *Phys. Rev. Applied* **2017**, *7*, 024022.
- [83] Yazdi, G.; Vasiliauskas, R.; Iakimov, T.; Zakharov, A.; Syväjärvi, M.; Yakimova, R. *Carbon* **2013**, *57*, 477–484.
- [84] Emtsev, K.; Bostwick, A.; Horn, K.; Jobst, J.; Kellogg, G.; Ley, L.; Mcchesney, J.; Ohta, T.; Reshanov, S.; Rohrl, J.; Rotenberg, E.; Schmid, A.; Waldmann, D.; Weber, H.; Seyller, T. *Nature materials* **2009**, *8*, 203–207.
- [85] Li, X.; Cai, W.; Colombo, L.; Ruoff, R. *Nano Lett.* **2009**, *9*, 4268–4272.
- [86] Li, X.; Zhu, Y.; Cai, W.; Borysiak, M.; Han, B.; Chen, D.; Piner, R.; Colombo, L.; Ruoff, R. *Nano letters* **2009**, *9*, 4359–63.
- [87] Krebs, H.-U.; Weisheit, M.; Faupel, J.; Süske, E.; Scharf, T.; Fuhse, C.; Störmer, M.; Sturm, K.; Seibt, M.; Kijewski, H.; Nelke, D.; Panchenko, E.; Buback, M. *Pulsed Laser Deposition (PLD) – A Versatile Thin Film Technique*; 2003; Vol. 43; pp 101–107.
- [88] Nelson, J. *The Physics of Solar Cells*; Imperial College Press: London, 2008.
- [89] Bazylewski, P.; Akbari-Sharraf, A.; Ezugwu, S.; Ouyang, T.; Park, J.; Fanchini, G. *Crystalline and non-crystalline Solids*; InTechopen.com, 2016; Chapter Graphene Thin Films and Graphene Decorated with Metal Nanoparticles.
- [90] Liu, Z. In *Laser Applied Coatings*; Cottis, B., Graham, M., Lindsay, R., Lyon, S., Richardson, T., Scantlebury, D., Stott, H., Eds.; Elsevier, 2010; pp 2622–2635.
- [91] Yang, Z.; Hao, J. *J. Mater. Chem. C* **2016**, *4*, 8859–8878.
- [92] Parasuraman, K.; Raghunathan, V. *Surface Engineering* **2006**, *22*, 81–83.
- [93] Bleu, Y.; Bourquard, F.; Tite, T.; Loir, A.-S.; Maddi, C.; Donnet, C.; Garrelie, F. *Frontiers in Chemistry* **2018**, *6*, 572.
- [94] Koh, A.; Foong, Y.; Chua, D. *Diamond and Related Materials* **2012**, *25*, 98–102.
- [95] Maddi, C. et al. *Diamond and Related Materials* **2016**, *65*, 17–25.
- [96] Kumar, I.; Khare, A. *Applied Surface Science* **2014**, *317*, 1004–1009.

-
- [97] Hemani, G.; Quevedo-Lopez, M.; Fischetti, M. *Bulletin of the American Physical Society* **2013**, 6013.
- [98] Wang, J.; Xiong, Z.; Yu, J.; Yin, H.; Wang, X.; Peng, L.; Wang, Y.; Wang, X.; Jiang, T.; Cao, L.; Wu, W.; Wang, C.; Zhang, L. *Micro Nano Letters* **2015**, 10, 649–652.
- [99] Hirsch, A. *Angewandte Chemie (International ed. in English)* **2015**, 54, 9132–9133.
- [100] Xiao, X.; Li, Y.; Liu, Z. *Nature Materials* **2016**, 15, 697–698.
- [101] Cataldi, P.; Athanassiou, A.; Bayer, I. *Applied Sciences* **2018**, 8, 1438.
- [102] Kong, W.; Kum, H.; Bae, S.-H.; Shim, J.; Kim, H.; Kong, L.; Meng, Y.; Wang, K.; Kim, C.; Kim, J. *Nature Nanotechnology* **2019**, 14, 927–938.
- [103] Shapira, P.; Gok, A.; Salehi, F. *Journal of Nanoparticle Research* **2016**, 18, 269.
- [104] Yan, M. *Journal of Physics: Conference Series* **2018**, 1143, 012012.
- [105] Shuaiwei, W.; Yang, B.; Yuan, J.; Si, Y.; Chen, H. *Scientific Reports* **2015**, 5, 14957.
- [106] Lindsay, L.; Broido, D.; Mingo, N. *Phys. Rev. B* **2010**, 82, 115427.
- [107] Ghosh, S.; Bao, W.; Nika, D. L.; Subrina, S.; Pokatilov, E. P.; Lau, C. N.; Balandin, A. A. *Nature Materials* **2010**, 9, 555–558.
- [108] Kauling, A.; Seefeldt, A.; Pisoni, D.; Pradeep, R.; Bentini, R.; Oliveira, R.; Novoselov, K.; Castro Neto, A. *Advanced Materials* **2018**, 30, 1803784.
- [109] Leng, Y. *Materials Characterization: Introduction to Microscopic and Spectroscopic Methods*, 2nd ed.; Wiley-VCH Verlag GmbH: Singapore, 2013.
- [110] Malard, L.; Pimenta, M.; Dresselhaus, G.; Dresselhaus, M. *Physics Reports* **2009**, 473, 51–87.
- [111] Childres, I.; Jauregui, L.; Park, W.; Cao, H.; Chena, Y. *New Developments in Photon and Materials Research* **2013**, 49, 403–418.
- [112] Garside, M. *Statista* **2019**, 1–78.
- [113] Gomez, L.; Zhang, Y.; Zhou, C. *Large Scale Graphene by Chemical Vapor Deposition: Synthesis, Characterization and Applications*; 2011; pp 161–184.
- [114] Vlassiouk, I.; Fulvio, P.; Meyer, H.; Lavrik, N.; Dai, S.; Datskos, P.; Smirnov, S. *Carbon* **2013**, 54.
- [115] Begg, D.; Fischer, S.; Dornbusch, R. *Economics - 8th Edition*; McGraw-Hill Education, 2005.
- [116] Petridis, L. V.; Kokkinos, N. C.; Mitropoulos, A. C.; Kyzas, G. Z. *Interface Science and Technology* **2019**, 30, 173–197.

-
- [117] Zhang, S. Study of fluorine-dope tin oxide (FTO) thin films for photovoltaics applications. Ph.D. thesis, TU Darmstadt, 2017.
- [118] Woo, Y. *Micromachines* **2018**, *10*, 13.
- [119] Lopez-Naranjo, E.; Gonzalez-Ortiz, L.; Apatiga, L.; Rivera-Munoz, E.; Ramirez, A. *Journal of Nanomaterials* **2016**, *2016*, 1–12.
- [120] Cao, W.; Li, J.; Chen, H.; Xue, J. *Journal of Photonics for Energy* **2014**, *4*, 040990.
- [121] Layani, M.; Kamyshny, A.; Magdassi, S. *Nanoscale* **2014**, *6*, 5581–5591.
- [122] Shanthi, E.; Banerjee, A.; Dutta, V.; Chopra, K. L. *Journal of Applied Physics* **1982**, *53*, 1615–1621.
- [123] Grundmann, M. *The Physics of Semiconductors*; Springer-Verlag: Berlin, 2010; Vol. 19.
- [124] Burstein, E. *Physical Review* **1954**, *93*, 632–633.
- [125] Rey, G. Nanostructured metallic oxides (ZnO, SnO₂) for photovoltaics applications particularly transparent conductive oxides and dye-sensitized solar cells. Ph.D. thesis, University of Grenoble, 2012.
- [126] Liu, J.; Yi, Y.; Zhou, Y.; Cai, H. *Nanoscale research letters* **2016**, *11*, 108.
- [127] Yoo, D.; Kim, J.; Kim, J. *Nano Research* **2014**, *7*, 717–730.
- [128] Harindu, N.; Kim, J.-K.; Lee, J.-M. *Nano-Micro Letters* **2018**, *10*, 18.
- [129] An, S. J.; Zhu, Y.; Lee, S.; Stoller, M.; Emilsson, T.; Park, S.; Velamakanni, A.; An, J.; Ruoff, R. *Journal of Physical Chemistry Letters - J PHYS CHEM LETT* **2010**, *1*, 1259–1263.
- [130] Schlesinger, M. *Electroplating*; Wiley: Windsor, 2004.
- [131] Ray, A. *Electroplating of Nanostructures*, 1st ed.; InTech: Gujarat, India, 2015; Chapter Electrodeposition of Thin Films for Low-cost Solar Cells.
- [132] Sun, J.; Chen, Y.; Cai, X.; Ma, B.; Chen, Z.; Priydarshi, M.; Chen, K.; Gao, T.; Song, X.; Ji, Q.; Guo, X.; Zou, D.; Zhang, Y. F.; Liu, Z. *Nano Research* **2015**, *8*, 1–13.
- [133] Xiong, W.; Zhou, Y. S.; Jiang, L. J.; Sarkar, A.; Mahjouri-Samani, M.; Xie, Z.; Gao, Y.; Ianno, N.; Jiang, L.; Lu, Y. *Advanced materials (Deerfield Beach, Fla.)* **2013**, *25*, 630–634.
- [134] Yan, Z.; Peng, Z.; Sun, Z.; Yao, J.; Zhu, Y.; Liu, Z.; Ajayan, P.; Tour, J. *ACS nano* **2011**, *5*, 8187–92.

-
- [135] Eggenhuisen, T.; Galagan, Y.; Biezemans, A.; Slaats, T.; Voorthuijzen, P.; Kommeren, S.; Shanmugam, S.; Teunissen, P.; Hadipour, A.; Verhees, W.; Veenstra, S.; Coenen, M.; Gilot, J.; Andriessen, R.; Groen, P. *Journal of Materials Chemistry A* **2015**, *3*, 7255–7262.
- [136] Galagan, Y.; Mescheloff, A.; Veenstra, S.; Andriessen, R.; Katz, E. *Physical chemistry chemical physics : PCCP* **2015**, *17*, 3891–3897.
- [137] Arsalis, A.; Alexandrou, A.; Georghiou, G. *Renewable Energy* **2018**, *126*, 354–369.
- [138] Alhelal, A. *International Journal of Inventive Engineering and Sciences (IJIES)* **2015**, *3*, 11–14.
- [139] Majewski, A. *Dieselnet Technology Guide* **2019**, 1–30.
- [140] Schroder, K. *Semiconductor material and device characterization*; John Wiley Sons, Inc.: Hoboken, New Jersey., 2006.
- [141] Peng, L.; Sun, Y.; Meng, Z.; Wang, Y.; Xu, Y. *Journal of Power Sources* **2013**, *227*, 131–136.
- [142] Bartesaghi, D.; Pérez, I.; Knipepert, J.; Roland, S.; Turbiez, M.; Neher, D.; Koster, L. *Nature communications* **2015**, *6*, 7083.
- [143] Sharma, K.; Sharma, V.; Sharma, S. *Nanoscale Research Letters* **2018**, *13*, 1–46.
- [144] Kumar, R.; Sahajwalla, V.; Bhargava, P. *Nanoscale Advances* **2019**, *1*, 3192–3199.
- [145] Yun, S.; Hagfeldt, A. *Counter Electrodes for Dye-Sensitized and Perovskite Solar Cells*; Wiley: Weinheim, 2018.
- [146] Roy-Mayhew, J.; Aksay, I. *Chemical reviews* **2014**, *114*, 6323–6348.
- [147] Zhu, G.; Wang, H.; Xu, H.; Zhang, Q.; Sun, H.; Zhang, L. *RSC Adv.* **2016**, *6*, 58064–58068.
- [148] Bourget, C. *HortScience* **2008**, *43*, 1944–1946.
- [149] Morkoc, H. *Handbook of Nitride Semiconductors and Devices: Electronic and Optical Processes in Nitrides* **2009**, *2*, 1–846.
- [150] Nakamura, S.; Iwasa, N.; Senoh, M.; Mukai, T. *Japanese Journal of Applied Physics* **1992**, *31*, 1258.
- [151] Uchida, Y.; Taguchi, T. *Optical Engineering* **2005**, *44*, 124003.
- [152] Jiang, G.; Tian, H.; Wang, X.; Hirtz, T.; Wu, F.; Yancong, Q.; Gou, G.; Wei, Y.-H.; Yang, J.-M.; Yang, S.; Yang, Y.; Ren, T. *Nanoscale Advances* **2019**, *1*, 4745–4754.
- [153] Huang, Y.; Huang, Z.; Zhong, Z.; Yang, X.; Hong, Q.; Wang, H.; Huang, S.; Gao, N.; Chen, X.; Cai, D.; Kang, J. *Scientific Reports* **2018**, *8*, 13721.

-
- [154] Kawamoto, H. *IEEE Proceedings* **2002**, *90*, 1–41.
- [155] Beeckman, J.; Neyts, K.; Vanbrabant, P. *OPTICAL ENGINEERING* **2011**, *50*, 081202.
- [156] Walton, H. G.; Dunmur, D. *Encyclopedia Britannia* **2020**,
- [157] Castellano, J. *Liquid Crystals Today* **1991**, *1*, 4–6.
- [158] Vaan, A. *Journal of The Society for Information Display - J SOC INF DISP* **2007**, *15*, 274–279.
- [159] Luo, Z.; Wu, S.-T. *Optics and Photonics News* **2015**, *26*, 19–21.
- [160] Chae, G. *Japanese Journal of Applied Physics* **2001**, *40*, 1282–1286.
- [161] Oh, B.-Y.; Jeong, M.-C.; Moon, T.-H.; Lee, W.; Myoung, J.-M.; Hwang, J.-Y.; Seo, D.-S. *Journal of Applied Physics* **2006**, *99*, 124505–124505.
- [162] Chung, S.-H.; Noh, H. *Optics Express* **2015**, *23*, 32149.
- [163] Walker, G. *Journal of the Society for Information Display* **2012**, *20*, 413–440.
- [164] Cai, W.; Zhu, Y.; Li, X.; Piner, R.; Ruoff, R. *Applied Physics Letters* **2009**, *95*, 123115–123115.
- [165] Meen, T.; Tsai, J.-K.; Tu, Y.; Wu, T.-C.; Hsu, W. *Nanoscale research letters* **2014**, *9*, 523.
- [166] Huynh, T.-P.; Hoang, T.-T.; Nguyen, P.; Tran, T.-N.; Nguyen, T.-V. *IEEE Photovoltaic Specialists Conference (PVSC)* **2009**, *34*, 002168–002171.
- [167] Berni, A.; Mennig, M.; Schmidt, H. *Sol-Gel Technologies for Glass Producers and Users*, 1st ed.; Springer-Verlag: New York, 2004; Chapter 2.
- [168] Li, X.; Zhang, G.; Bai, X.; Sun, X.; Wang, X.; Wang, E.; Dai, H. *Nature nanotechnology* **2008**, *3*, 538–42.
- [169] Zheng, Q.-b.; Shi, L.-f.; Yang, J. *Transactions of Nonferrous Metals Society of China* **2012**, *22*, 2504–2511.
- [170] Koga, H.; Nogi, M.; Komoda, N.; Nge, T.; Sugahara, T.; Saganuma, K. *NPG Asia Materials* **2014**, *6*, 93.
- [171] Davis, B.; Hussein, M. *Physical review letters* **2014**, *112*, 055505.
- [172] Kang, S.; Yoo, J.; Lyeo, H.-K.; Song, J.; Lee, S.; Yu, J. *Journal of Applied Physics - J APPL PHYS* **2011**, *110*, 023506.
- [173] Sole, C.; Drewett, N.; Liu, F.; Abdelkader, A.; Kinloch, I.; Hardwick, L. *Journal of Electroanalytical Chemistry* **2015**, *1*, 35–41.

-
- [174] Lotya, M.; Hernandez, Y.; King, P.; Smith, R.; Nicolosi, V.; Karlsson, L.; Blighe, F.; De, S.; Wang, Z.; McGovern, I.; Duesberg, G.; Coleman, J. *Journal of the American Chemical Society* **2009**, *131*, 3611–20.
- [175] Xianhui, M.; Shin, D.-W.; Yu, S. M.; Park, M.-H.; Yang, C.; Lee, J. H.; Yoo, J. *Journal of Nanoscience and Nanotechnology* **2014**, *14*, 8839–8844.
- [176] Chen, S.; Li, Z.; Zhang, Z. *Journal of Nanomaterials* **2011**, *2011*, 1–8.
- [177] Tan, A.; Kuo, C. K.; Nicholson, P. S. *Solid State Ionics* **1991**, *45*, 137–142.
- [178] Bereznov, S.; Kocharyan, H.; Maticiu, N.; Revathi, N.; Volobujeva, O.; Tverjanovich, A.; Kois, J. *Applied Surface Science* **2017**, *425*, 722–727.
- [179] Capasso, A.; Bellani, S.; Palma, A. L.; Najafi, L.; Del Rio Castillo, A. E.; Currel, N.; Cinà, L.; Miseikis, V.; Coletti, C.; Calogero, G.; et al., *2D Materials* **2019**, *6*, 035007.
- [180] Vinutha, K.; Naveen, K. B.; Tejas, K.; Jai, K. B.; Sumanth, K. D.; Mahesh, M. "Imperial Journal of Interdisciplinary Research (IJIR)" **2016**, *2*, 1011–1016.
- [181] Lalasari, L.; Arini, T.; Andriyah, L.; Firdiyono, F.; Yuwono, A. H. Electrical, optical and structural properties of FTO thin films fabricated by spray ultrasonic nebulizer technique from SnCl₄ precursor. 2018; p 020001.
- [182] Buene, A.; Economopoulos, S.; Uggerud, N.; Gautun, O.; Hoff, B. *Dyes and Pigments* **2018**, *151*, 263–271.
- [183] Hora, C.; Santos, F.; Sales, M.; Ivanou, D.; Mendes, A. *ACS Sustainable Chemistry Engineering* **2019**, *7*, 13464–13470.
- [184] Nazeeruddin, M.; De Angelis, F.; Fantacci, S.; Selloni, A.; Viscardi, G.; Liska, P. e. a. *Journal of the American Chemical Society* **2005**, *127*, 16835–16847.
- [185] Saukkonen, Z.; Huaijin, P.; Lund, G.; Hashmi, K.; Miettunen, J.; Halme, I.; Asghar, H.; Vahlman, T. *Journal of The Electrochemical Society* **2012**, *159*, 656–661.

Appendix

8.1 Multimeter measurements of the Electrodeposition samples

Multimeter measurements are not considered to be scientific, however they are included to provide a more in-depth look at the samples obtained with the Electrodeposition method. Some of the resistance values were slightly skewed because of a heat wave during the measurements. Two classifications can be seen in table 8.1: KD and LD. KD represents the shortest possible distance between two measuring points. LD represents the ambiguously termed longer distance.

Sample name	KD Resistance (Ohm/square)	LD Resistance (Ohm/square)
Blank Uclean	15.7	25.9
Blank reg	15.5	25.4
P4ED	17.0	28.4
P5ED	22.1	53.1
P11ED	0	0
P18ED	16.8	41.2
P20ED	14.6	25
P13ED	18.6	32.1
P10ED	18.0	33.7
P22ED	15.5	29.4
P21ED	18.6	31.4
P23ED	18.4	35
P15ED	16.2	125.6
P14ED	19.0	35.1

Table 8.1: Table of the measured conductivity with a multimeter.

In addition to the samples already mentioned in the Results and Discussion chapter, other

samples were also included in table 8.1. P4ED and P5ED had -10 mA sent in for an hour. While P11ED had -10 mA sent in for three hours straight. The process of P20ED had also +20 V for one hour, but the annealing was only two hours rather than the recommended three hours. With P21ED the solvent was changed. Benzylamine + graphene and Benzylamine + TBAPF₆ as electrolyte. +20 V sent in for one hour. P22ED followed the same procedure as P21ED, but a solvent mixture of Benzylamine and NMP + TBAPF₆ was used instead of Benzylamine + TBAPF₆ alone. P23ED is the same as P22ED and used as a control group.

8.2 The failure of the Spin Coating method

Spin Coating is a method widely used in the Semiconductor industry. Because of this, it was decided to have Spin Coating as one of the methods to deposit graphene thin films. Both modes, static and dynamic, were tried. But it was found that without photoresist, too much graphene would fly off the substrate for a film to be created. A photoresist was not included in order to limit the process steps. Initial attempts quickly showed that the static mode was not usable. The viscosity of the solution was very low since very little graphene was used and the solution's viscosity was highly dependent on the viscosity of the solvent. Suggesting that it was very liquid. Because of that a quasi-dynamic mode was devised. The new quasi-dynamic method composed of several static modes done after each other without any long stretches of breaks. The Spin Coating experiment lasted three full days, and the process parameters are given in the tables below. SCP1 indicates the first day, SCP2 the second day, and finally SCP3 represents the third day. Step 1 represents Spin-up, step 2 was Spin-off and step 3 was the solvent evaporation.

Step	1	2	3
RPM	1000	2000	3000
Acceleration (RPM)	1000	1000	1000
time (s)	2	2	30
Step	1	2	3
RPM	1000	1500	2000
Acceleration (RPM)	1000	500	500
time (s)	2	2	30
Step	1	2	3
RPM	1000	2000	4000
Acceleration (RPM)	1000	1000	2000
time (s)	2	2	30

Table 8.2: Shows the parameters for SCP1

Step	1	2	3
RPM	500	1500	2500
Acceleration (RPM)	500	1000	1000
time (s)	2	3	35

Table 8.3: Shows the parameters for SCP2

Step	1	2	3
RPM	500	1500	3000
Acceleration (RPM)	500	1000	1500
time (s)	2	2	30

Table 8.4: Shows the parameters used in SCP3

8.3 Doctor Blade parameters and samples

The Doctor Blade method had many parameters that could be varied. Below, in table 8.5 of the samples that were considered best by optical characterization are presented:

Sample name	film deposited	time blade is used	Speed	Annealing	Vertical distance
Sample 1	one time	one roll	010	5 hours	5
Sample 2	one time	two rolls	015	5 hours	1
Sample 3	3 times	3 rolls	098	5 hours	5
Sample 4	one time	one roll	019	3.5 hours	3
Sample 5	one time	10 rolls	038	3.5 hours	3
Sample 6	one time	3 rolls	059	3.5 hours	3
Sample 7	one time	15 rolls	075	3.5 hours	3
Sample 8	one time	10 rolls	019	4 hours	3
Sample 9	10 times	30 rolls	019	4 hours	3
Sample 10	one time	50 rolls	019	4 hours	3

Table 8.5: Table shows the samples and the parameter used when film was deposited with Doctor Blade method. In the Vertical distance we have used number to show the vertical distance of the blade. This number does not mean the distance in meter, but instead show a defined distance where 5 means a vertical distance as high as possible and means that the blade will take as little film as possible, while 1 means that the blade is at its lowers and will take as much film as possible.

Rolls was how many times the blade would roll across the sample. The annealing with annealing time showing integer values was increased 100 °C each hour. Except for those with half-integer, for those the temperature was increased each half an hour.

8.4 Absorbance of other samples

Because the text was edited with a view to brevity and clarity, the absorbance was limited to only one figure. The other figures were comparable to the one presented in absorption spectrum, and they were therefore included in the appendix. The other samples investigated with the UV-Vis equipment were the P14ED and P22ED. On P14ED the first peak looks to be slightly skewed to the right. It begins at 310 nm rather than 300 nm. Besides that, the plot looks to follow the baseline, although looks to have higher absorbance throughout. The figure for the absorbance of P14ED can be seen on figure 8.1.

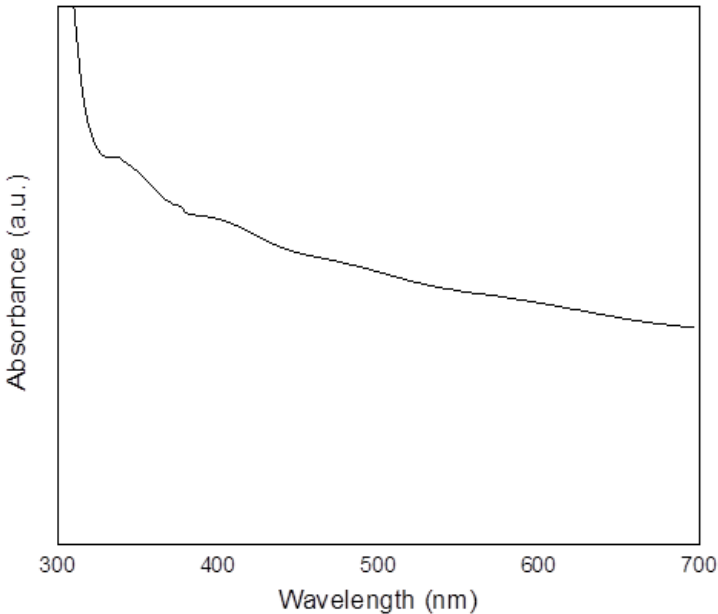


Figure 8.1: Plot of the absorbance spectrum for the P14ED sample.

P22ED was developed by using a solvent mixture of NMP and Benzylamine. The conductivity was poorer than in the other samples. The plot looks to have properties with similarities to both P13ED and P14ED. First peak begins at around 350 nm like for P14ED and the second absorbance peak is wide like that one of P13ED.

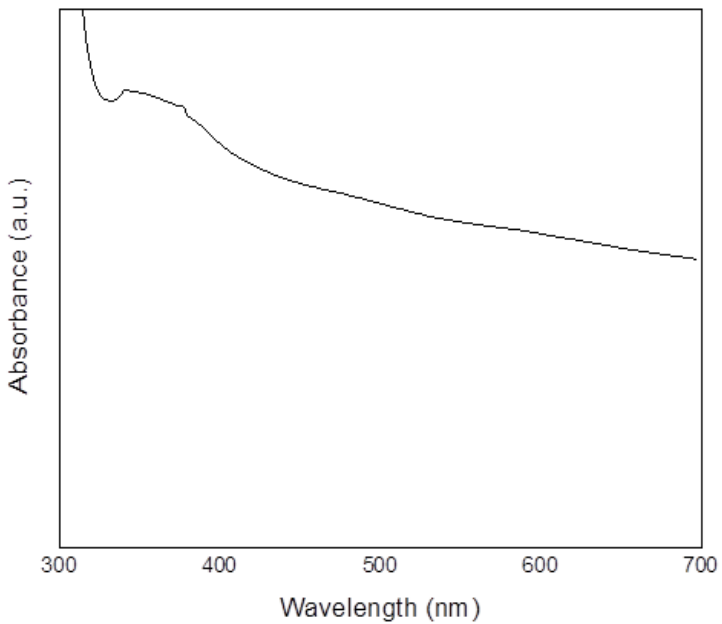


Figure 8.2: Plot of the absorbance spectrum for the P22ED sample

8.5 SEM image of bare FTO

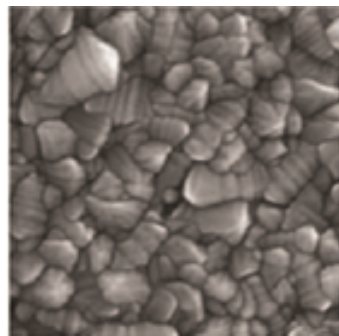


Figure 8.3: SEM image of a bare FTO glass plate[185].

8.6 50000x magnification SEM images

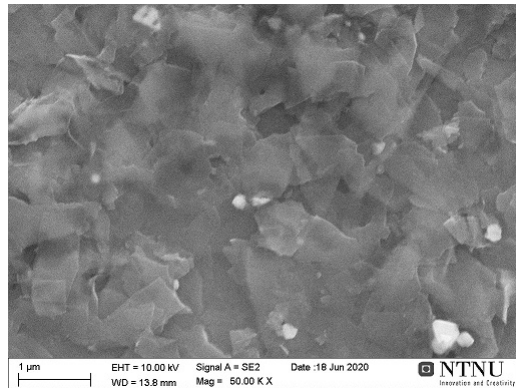


Figure 8.4: Image of the 50000x magnification of Drop Casting film

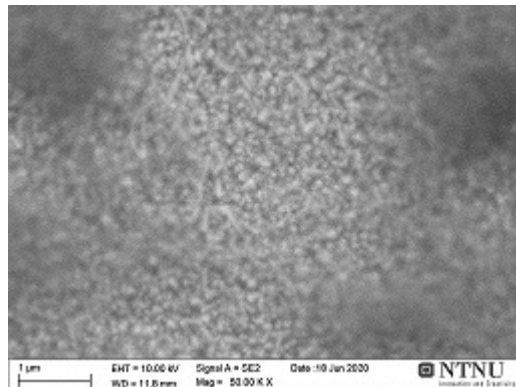
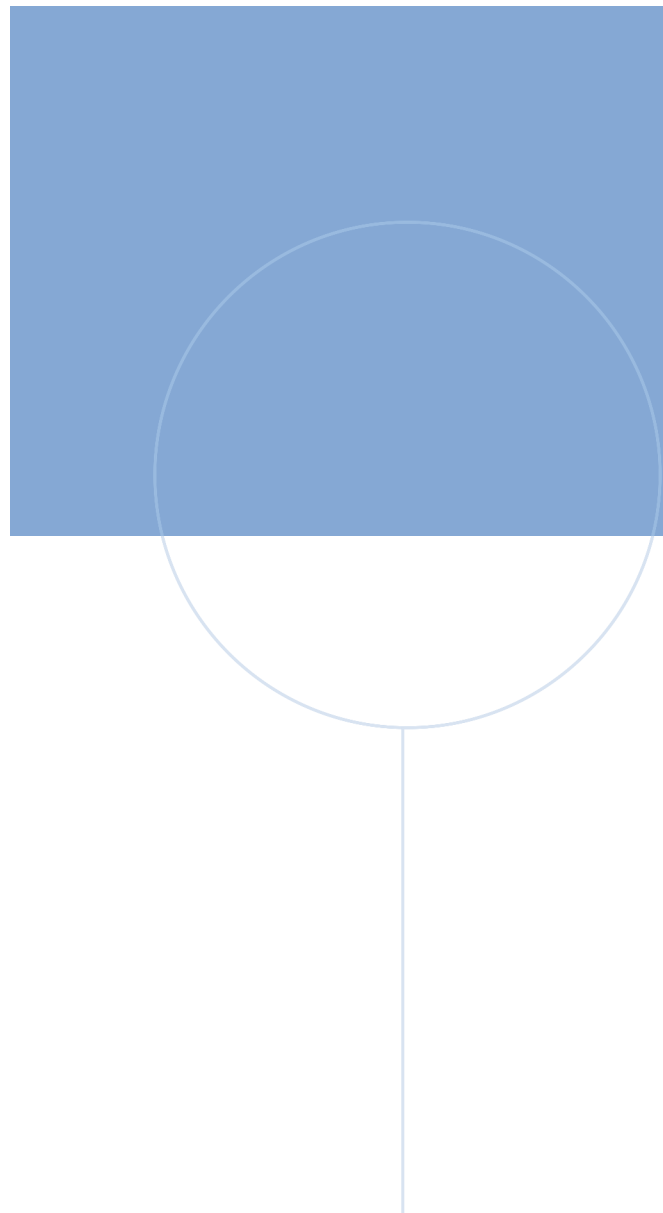


Figure 8.5: Image of the 50000x magnification of the sample on figure 5.17



NTNU

Norwegian University of
Science and Technology